ELECTROCHEMICAL AND SPECTROELECTROCHEMICAL STUDIES ON BIS-PORPHYRINS, PORPHYRINS WITH CHARGED SUBSTITUENTS AND WATER-SOLUBLE PORPHYRAZINES

_____

A Thesis

Presented to

The Faculty of the Department of Chemistry

University of Houston

_____

In Partial Fulfillment

Of the Requirements for the Degree

Master of Science

_____

By

Lihan Zeng

August 2015

ELECTROCHEMICAL AND SPECTROELECTROCHEMICAL STUDIES ON BIS-PORPHYRINS, PORPHYRINS WITH CHARGED SUBSTITUENTS AND WATER-SOLUBLE PORPHYRAZINES

_____

Lihan Zeng

APPROVED**:**

_____

Dr. Karl M. Kadish, Chairman

_____

Dr. John L. Bear

_____

Dr. Steven Baldelli

_____

Dr. Jakoah Brgoch

_____

Dr. Eric Van Caemelbecke
Houston Baptist University

_____

Dean, College of Natural Sciences and Mathematics

Dedication

This Thesis is dedicated to

my parents, Zhong Zeng and Liyi Li

and

my loved Yan Cui

Acknowledgements

I would like to express my deepest appreciation to my advisor, Dr. Karl M. Kadish for his excellent guidance, caring, patience, and providing me with a unique atmosphere for doing research with him.

I would also express my gratitude to my committee members, Dr. John L. Bear, Dr. Eric Van Caemelbecke, Dr. Steven Baldelli and Dr. Jakoah Brgoch for their precious comments and suggestions on my research projects and scientific writings.

I also appreciate Dr. Zhen Fu and Dr. Yuanyuan Fang for kindly and patiently sharing their valuable knowledge and giving me helpful advice within countless times of discussion.

Finally, I want to thank Dr. Roberto Paolesse, Dr. Claudio Ercolani, Dr. Maria Pia Donzello and Dr. Claude P. Gros for kindly providing the compounds and important suggestions on this thesis.

ELECTROCHEMICAL AND SPECTROELECTROCHEMICAL STUDIES ON BIS-PORPHYRINS, PORPHYRINS WITH CHARGED SUBSTITUENTS AND WATER-SOLUBLE PORPHYRAZINES

_____

An Abstract of a Thesis

Presented to

The Faculty of the Department of Chemistry

University of Houston

_____

In Partial Fulfillment

Of the Requirements for the Degree

Master of Science

_____

By

Lihan Zeng

August 2015

Abstract

In this thesis, the electrochemical and spectral properties of a series of bis-porphyrins, porphyrins with charged subsituents and water-soluble porphyrazines are investigated in aqueous or non-aqueous media. Bis-porphyrins containing a β,β'-fused pyrazino (Pz) linking group were examined by electrochemistry and thin-layer UV-visible spectroelectrochemistry in PhCN containing 0.1 M tetra-n-butylammonium perchlorate (TBAP) as supporting electrolyte. The investigated compounds are represented as M(TPP)-Pz-(TPP)M, where TPP is the dianion of tetraphenylporphyrin and M = Zn^{II}, Cu^{II} or Ag^{II}. The effect of the linking Pz group on the redox potentials and UV-visible spectra of the neutral, electroreduced and electrooxidized bis-porphyrins is discussed. Electrochemical and spectral properties of a new class of water-soluble porphyrazine complexes are characterized in pyridine, DMSO, DMF and water media. The investigated compounds are represented as [{$Pd(OAc)_2$}$_4$LM] (L = tetrakis-2,3-[5,6-di(2-pyridyl)pyrazino]porphyrazinato dianion; M = $Mg^{II}(H_2O)$, Zn^{II}, Cu^{II}, Co^{II}, Pd^{II}, Pt^{II}) and bear four $Pd(OAc)_2$ units, each externally coordinated at the vicinal pyridine N atoms of a single dipyridinopyrazine fragment of the porphyrazine macrocycle ("py-py" coordination). The electrochemistry and spectroelectrochemistry of a series of tetra-*N*-alkylpyridyl and tetrasulfonato manganese porphyrins are studied in DMSO and DMF. The mixture of tetra-*N*-alkylpyridyl and tetrasulfonato manganese porphyrins with 1:1 molar ratio in DMF solution is also studied by electrochemistry and spectroelectrochemistry and is described in this thesis.

Table of Contents

Title		Page
List of Abbreviations		x
List of Charts		xii
List of Figures		xiii
List of Tables		xvii
List of Schemes		xviii
Chapter One	**Introduction**	1
1.1	Outline of Research in This Thesis	2
1.2	Use of Electrochemistry and Spectroelectrochemistry to Study Model Compounds	2
1.3	Porphyrins and Ring-Extended Porphyrins	3
1.4	Porphyrazines and Phthalocyanines	7
1.5	Positively and Negatively Charged Porphyrins	12
1.6	References	15
Chapter Two	**Experimental Methods**	19
2.1	Electrochemical Methods	20
2.1.1	Cyclic Voltammetry Experimental Conditions	20
2.1.2	Cyclic Voltammetry Analytical Theory	23
2.1.3	UV-visible Spectroelectrochemistry Methods	25
2.2	Other Experimental Procedures for Electrochemistry	26

2.2.1 Degassing the Solution..... 26

2.2.2 Temperature Control..... 26

2.3 Chemicals and Investigated Compounds..... 26

2.3.1 Chemicals..... 30

2.3.2 Investigated Compounds..... 30

2.4 References..... 32

Chapter Three **Electrochemistry and Spectroelectrochemistry of *β*-Pyrazino-Fused Tetraarylporphyrins in Nonaqueous Media**..... 33

3.1 Introduction..... 34

3.2 Results and Discussion..... 38

3.2.1 UV-vis Absorption Spectra of Neutral Compounds..... 38

3.2.2 Electrochemistry..... 41

3.2.3 Spectroelectrochemical Monitoring of Reduction and Oxidation Products..... 47

3.3 Conclusions..... 52

3.4 References..... 56

Chapter Four **A Rare Class of Uncharged Highly Water-Soluble Hom/Heteropentametallic Porphyrazine Macrocycles: Electrochemistry and Spectroelectrochemistry**..... 59

4.1 Introduction..... 60

4.2 Results and Discussion..... 62

4.2.1 Synthetic Aspects and Properties..... 62

4.2.2 UV-visible Spectra..... 66

4.2.3 Electrochemical and Spectroelectrochemical Measurements..... 76

4.2.4 Singlet Oxygen Quantum Yield Measurements..... 84

4.3 Conclusions..... 90

4.4 References..... 91

Chapter Five **Tetraanionic and Tetracationic Water-Soluble Manganese Porphyrins: Electrochemical and Spectroelectrochemical Characterization**..... 95

5.1 Introduction..... 96

5.2 Results and Discussion..... 99

5.2.1 Synthesis of PEG Derivatives..... 99

5.2.2 Electrochemical Measurements..... 102

5.2.3 Reduction of Interacting and Non-Interation *N*-Alkyl Substituents..... 108

5.2.4 Influenece of Central Metal Ion on Ease of Macrocycle and *N*-Alkylpyridyl Reduction..... 109

5.2.5 Spectrochemical Measurements..... 109

5.2.6 Spectral Properties of Highly Reduced *N*-Alkyl Derivatives..... 113

5.2.7 Can Potentials for Reduction of *N*-Alkylpyridyl of Compound **1** Be Changed..... 117

5.3 Conclusions..... 125

5.4 References..... 126

List of Abbreviations

Abbreviation	Meaning
A	absorbance
CE	counter electrode
CH_2Cl_2	dichloromethane
CV	cyclic voltammetry
DMF	N,N'-dimethylformamide
DMSO	dimethylsulfoxide
$\Delta E_{1/2}$	different in half-wave potential
$E_{1/2}$	half-wave potential
E_p	peak potential (by cyclic voltammetry)
E_{pa}	anodic peak potential (by cyclic voltammetry)
E_{pc}	cathodic peak potential (by cyclic voltammetry)
ε	molar absorptivity
ESR	electron spin resonance
FTIR	fourier transform infrared
HOMO	highest occupied molecular orbital
i_{pa}	anodic peak current (by cyclic voltammetry)
i_{pc}	cathodic peak current (by cyclic voltammetry)
LUMO	lowest unoccupied molecular orbital
λ_{max}	wavelength at a specific peak maximum
OEP	2, 3, 7, 8, 12, 13, 17, 18-octaethylporphyrin dianion
py	pyridine

PhCN	benzonitrile
Q	quinoxaline
RE	reference electrode
SAR	structure-activity relationships
SCE	saturated calomel electrode
SOD	Superoxide dismutase
TA	tetraazaanthracene
TBAP	tetra-*n*-butylammonium perchlorate
TMPyP	tetra-*N*-methylpyridylporphyrin
TPP	5,10,15,20-tetraphenylporphyrin dianion
TPPS	tetrasulfonatoporphyrin
WE	working electrode

List of Charts

Chart		Page
Chart 1-1.	Structures of free-base porphin, tetraphenylporphyrin (H_2TPP) and octaethylporphyrin (H_2OEP).....	5
Chart 1-2.	Structures of a) metalloporphyrin with *β*,*β*′-fused quinoxaline (Q) or tetraazaanthracene (TA) groups and b) *β*,*β*′-fused tetraazaanthracene bis-porpoyrins.....	6
Chart 1-3.	Strucutes of porphyrazine and phthalocyanine.....	10
Chart 1-4.	Strucutes of a) [LM] and and b) [$(PdCl_2)_4$LM] porphyrazine complexes.....	11
Chart 1-5.	Structures of positively charged tetra-*N*-methylpyridylporphyrin (TMPyP) and negatively charged tetrasulfonatoporphyrin (TPPS).....	14
Chart 3-1.	Structures of (a) investigated bis-porphyrins with Zn(II), Cu(II) and Ag(II) central metal ions and (b) related reference compounds where R is a tri-*t*-butylphenyl group.....	37
Chart 4-1.	Schematic formulations of the Zn^{II} octacation $[(CH_3)_8LZn]^{8+}$ and the Zn^{II}/Pt^{II} hexacation $[(PtCl_2)(CH_3)_6LZn]^{6+}$ (both neutralized by I^- ions)	63
Chart 4-2.	Structures of [{$Pd(OAc)_2$}$_4$LM] (M = $Mg^{II}(H_2O)$, Zn^{II}, Cu^{II}, Co^{II}, Pd^{II}, Pt^{II})	64
Chart 5-1.	Structures of the investigated Manganese TMPyP and TPPS derivatives.....	97
Chart 5-2.	Structures of the TMPyP(PEG)M derivatives, M = Cu(II), Pd(II) and 2H.....	98

List of Figures

Figure		Page
Figure 2-1.	Schematic illustration of the utilized electrochemical cell with glassy carbon (or platinum) working, platinum counter electrode and saturated calomel reference electrode (SCE).....	21
Figure 2-2.	Cyclic voltammetry waveform showing reduction scan between 0.0 to -1.0 V.....	22
Figure 2-3.	Schematic illustration of a cyclic voltammogram.....	24
Figure 2-4.	Schematic illustration of the thin-layer UV-visible spectroelectrochemical cell.....	27
Figure 2-5.	Schematic illustration of UV-visible spectroelectrochemical setup.....	28
Figure 2-6.	UV-visible spectral changes of $(NO_2TdmPP)Co^{II}$ during controlled potential oxidations in CH_2Cl_2 containing 0.1 M TBAP. Figure is reproduced from publication by Sun, B.; etc.....	29
Figure 3-1.	UV-vis spectra of M(TPP) and M(TPP)-Pz-(TPP)M in PhCN.....	40
Figure 3-2.	Cyclic voltammograms of M(TPP) and M(TPP)-Pz-(TPP)M in PhCN containing 0.1 M TBAP where M equals (a) Cu(II), (b) Zn(II) and (c) Ag(II).....	42
Figure 3-3.	UV-visible spectral changes during the controlled potential reduction of (a) Zn(TPP)-Pz-(TPP)Zn and (b) Zn(TPP) in PhCN, 0.1 M TBAP.....	49
Figure 3-4.	UV-visible spectral changes during the controlled potential oxidation of (a) Zn(TPP)-Pz-(TPP)Zn and (b) Zn(TPP) in PhCN, 0.1 M TBAP.....	50

Figure 3-5. UV-visible spectral changes for Ag(TPP)-Pz-(TPP)Ag during controlled potential (a) reduction and (b) oxidation in PhCN, 0.1 M TBAP..... 51

Figure 3-6. Measured HOMO-LUMO gap for related Cu(II) porphyrins in PhCN, containing 0.1 M TBAP..... 54

Figure 3-7. Correlation of reduction potential between M(TPP) and M(TPP)-Pz-(TPP)M..... 55

Figure 4-1. IR spectra in KBr of A) [{$Pd(OAc)_2$}$_4$LZn], B) [($PdCl_2$)$_4$LZn], C) [LZn]..... 67

Figure 4-2. UV-visible spectra of A) [{$Pd(OAc)_2$}$_4$LZn] in DMSO (red line, c = 9.55 x 10^{-6} M) and in H_2O (black line, c = 1.06 x 10^{-5} M); B) $[(CH)_8LZn]^{8+}$ in H_2O (c = 4.09 x 10^{-6} M); C) $[(PtCl_2)(CH_3)_6LZn]^{6+}$ in H_2O (c = 1.18 x 10^{-5} M)..... 71

Figure 4-3. Cyclic voltammograms of [{$Pd(OAc)_2$}$_4$LM] in DMSO, 0.1 M TBAP..... 80

Figure 4-4. Cyclic voltammograms of [{$Pd(OAc)_2$}$_4$LCu] in DMSO containing 0.1 M TBAP..... 81

Figure 4-5. Cyclic voltammograms of [{$Pd(OAc)_2$}$_4$LM] (M = Mg^{II}, Zn^{II}) in H_2O with 0.1 M a) KCl and b) NaOAc..... 82

Figure 4-6. UV-visible spectral changes in DMSO containing 0.2 M TBAP during first reduction of a) [{$Pd(OAc)_2$}$_4$LPd] at E_{app} = -0.55 V and b) [($PdCl)_2$)$_4$LPd] at E_{app} = -0.20 V..... 85

Figure 4-7. a) UV-visible spectra of a DMF/HCl solution ([HCl] = 1 x 10^{-4} M) containing [{$Pd(OAc)_2$}$_4$LZn] and DPBF before (red line) and after (black line) laser irradiation; b) Stern-Volmer data analysis of the DPBF photooxidation (shown in the inset)..... 88

Figure 5-1. Cyclic voltammograms of investigated manganese TMPyP and TPPS derivatives in DMSO, 0.1 M TBAP. Scan rate of 0.1 V/s... 104

Figure 5-2. Cyclic voltammograms of investigated manganese TMPyP and TPPS derivatives in DMF, 0.1 M TBAP. Scan rate of 0.1 V/s..... 105

Figure 5-3. Cyclic voltammograms illustrating the three types of redox behaviors for TMPyPM derivatives: a) M = Mn(III), b) M = Cu(II), Pd(II) and c) M= 2H in DMSO, 0.1 M TBAP. Scan rate of 0.1 V/s..... 110

Figure 5-4. Cyclic voltammograms illustrating the stepwise reductions for TMPyP(PEG)H_2 derivative, in DMSO, 0.1 M TBAP. Scan rate of 0.1 V/s..... 111

Figure 5-5. Correlation between ring-centered reduction potentials between TPPM and TMPyPM in DMSO, 0.1 M TBAP. The value of $E_{1/2}$ for TPP(VO) were taken from ref 29..... 112

Figure 5-6. UV-visible changes for the Mn^{III}/Mn^{II} process of investigated compounds in DMSO, containing 0.1 M TBAP. A summary of the spectral data is given in Table 5-2..... 114

Figure 5-7. UV-visible changes for reductions on the macrocycle of TMPyP(PEG)M where M = Mn(III), Cu(II), Pd(II) or H_2 in DMSO, containing 0.1 M TBAP..... 116

Figure 5-8. Cyclic voltammograms of 1:1 mixture (mole ratio) of compound **1** and compound **2** in DMF, 0.1 M TBAP. Scan rate of 0.1 V/s.... 119

Figure 5-9. First scan of UV-visible spectral changes of 1:1 mixture (mol ratio) of compound **1** and compound **2** during reductions in DMF, 0.1 M TBAP, containing 0.1 M TBAP..... 123

Figure 5-10. Second scan of UV-visible spectral changes of 1:1 mixture (mol ratio) of compound **1** and compound **2** during reductions in DMF, 0.1 M TBAP, containing 0.1 M TBAP..... 124

List of Tables

Table		Page
Table 3-1.	UV-visible spectra data ($\lambda_{max,}$ nm) of investigated M(TPP)-Pz-(TPP)M and related compounds in PhCN.....	39
Table 3-2.	Half-wave potentials (V vs SCE) of porphyrins M(TPP)-Pz-(TPP)M, M(P)-TA-(P)M, M(P-TA) and M(TPP), where M = Zn, Cu, Ag and Co in different solvents containing 0.1 M TBAP.....	43
Table 4-1.	UV-visible spectral data of the species [{$Pd(OAc)_2$}$_4$LM] and the related compounds [LM] and [($PdCl_2$)$_4$LM], (M = $Mg^{II}(H_2O)$, Zn^{II}, Cu^{II}, Co^{II}, Pd^{II}, Pt^{II}) in different solvents.....	73
Table 4-2.	Molar concentration of saturated solutions in water of [{$Pd(OAc)_2$}$_4$LM] complexes (M = $Mg^{II}(H_2O)$, Zn^{II}, Cu^{II}, Co^{II}, Pd^{II}, Pt^{II}).....	76
Table 4-3.	Half-wave potentials of reductions ($E_{1/2}$, V vs. SCE) of [{$Pd(OAc)_2$}$_4$LM], [LM] and [($PdCl_2$)LM] in DMSO and H_2O (0.1M KCl or 0.1M NaOAc).....	80
Table 4-4.	Singlet Oxygen Quantum Yields (Φ_Δ) in DMF and/or DMF preacidified with HCl (1÷2 x 10^{-4} M) of [{$Pd(OAc)_2$}$_4$LM] (M = Zn^{II}, $Mg^{II}(H_2O)$, Pd^{II}, Pt^{II}) and related species.....	90
Table 5-1.	Reduction potentials ($E_{1/2}$ V vs SCE) of investigated TMPyP and TPPS complexes in DMF and DMSO, 0.1 M TBAP.....	108
Table 5-2.	UV-visible spectral data λ_{max} (nm) of investigated manganese porphyrins in DMSO and DMF, containing 0.1 M TBAP. Shoulder bands can be seen in Figure 5-3.....	116

List of Scheme

Scheme		Page
Scheme 5-1.	Synthesis route for free-base TMPyP(PEG) complex.....	101
Scheme 5-2.	Synthesis route for TPPS(PEG)H_2 complex.....	102
Scheme 5-3.	Proposed Reduction mechanism of Compounds **1-4** in DMF or DMSO, containing 0.1 M TBAP. The listed potentials were recorded in DMSO for compounds **1** and **2**.....	107
Scheme 5-4.	Proposed conformation for the 1:1 mixture of compounds **1** and **2** in DMF or DMSO solution.....	121

Chapter One

Introduction

1.1 Outline of Research

In this thesis, Chapter One gives a general introduction of the investigated compounds and utilized techniques included in this work, while the detailed experimental techniques including instrumental methods and chemicals are described in Chapter Two. In the following three chapters, the investigation of three different kinds of metal complexes is discussed, one of which is the macrocyles involving porphyrin, porphyrazine and corrole, respectively. In Chapter Three, electrochemistry and spectroelectrochemistry of β-pyrazino-fused bis-tetraarylporphyrins in nonaqueous media are investigated. This is then followed by the electrochemical study of a rare class of uncharged highly water-soluble homo/heteropentametallic porphyrazine macrocycles in Chapter Four. Chapter Five mainly focuses on the electrochemical and spectroelectrochemical characterization of tetracationic and tetraanionic water-soluble manganese porphyrins.

1.2 Use of electrochemistry and spectroelectrochemistry to study model compounds

The use of cyclic voltammetry and spectroelectrochemistry can help to elucidate the redox properties of metalloporphyrins and metallocorroles containing both main group and transition metal ions.

Cyclic voltammetry is utilized to study the redox potentials and electron transfer mechanisms as a function of solvent and supporting electrolytes, type and oxidation state of central metal ion, axial coordination of the metal ions and macrocyclic structures.

Spectroelctrochemisty, which is the technique of combining UV-visible spectroscopy and electrochemistry allows for the rapid acquisition of data which is then used in elucidating both kinetic and thermodynamic aspects of the various electron transfer reactions, as well as site of electron transfer reaction.

1.3 Porphyrins and Ring-Extended Porphyrins

Porphyrins are a group of heterocyclic macrocycle organic compounds, composed of four modified pyrrole subunits interconnected at their α carbon atoms via methine bridges (=CH−). The parent porphyrin is a porphin (shown in Char 1-1) and substituted porphines are called porphyrins, of which examples are given by metal-free tetraphenyl porphyrin (H_2TPP) and octaethylporphyrin (H_2OEP). The porphyrin macrocycle is aromatic by (Hückel's rule), possessing 4n+2 π electrons (n=4, for the shortest cyclic path). Thus porphyrin macrocycles are highly conjugated systems and consequently they typically have very intense absorption bands in the visible region and may be deeply colored.

Porphyrins and porphyrin-like compounds have unique physical and photochemical properties, suggesting their use for diverse applications in the fields of biology, medicine and material science.[1-3] In this regard a number of ring-extended porphyrins have been synthesized for use as molecular wires and switches.[4-13] Examples of "Simple" ring-extended derivatives among these compounds are the 5,10,15,20-tetrakis(3,5-di-*tert*-butylphenyl)-porphyrins containing a β,β'-fused quinoxaline (Q) or tetraazaanthracene (TA) group, whose structures are shown in Chart 1-2a and are

represented as (PQ)M and (PTA)M, where PQ = the dianion of 5,10,15,20-tetrakis(3,5-di-tert -butylphenyl)quinoxalino-porphyrin and PTA = the dianion of 5,10,15, 20-tetrakis(3,5-di-*tert*-butylphenyl)-6′,7′-dimethyl-1′,4′,5′,8′-tetraazaanthraceno porphyrin.

Extensive research has been undertaken in understanding the electronic character of the porphyrin bridge interaction in quinoxalinoporphyrins where delocalization of electron density upon electrochemical reduction has been demonstrated.[7] A positive linear shift in reduction potentials with an increase in the number of fused quinoxaline (Q) groups has been well-documented upon going from simple metalloporphyrins to derivatives of mono- and "linear" bis-quinoxalinoporphyrins, with the magnitude of the shift depending upon the type and oxidation state of the central metal ion and the specific site of electron transfer.[3-5,7,8,10-12,14-16]

The linking of porphyrins at their β, β'-pyrrole positions is the first step in preparing porphyrin modular units as building blocks towards a porphyrinbased molecular wire[4,14,15]. The synthetic flexibility afforded by functionalizing the porphyrin β-pyrrolic periphery as well as the ability to selectively metalate constituent macrocycles[4,17-21] offers the possibility to creating molecules with pre-designed molecular functionality. β,β'-appended and linked porphyrins have been proposed as key components for applications in the area of molecular switches,[16] rectifiers,[22] solar cells[23] and in long-distance electron-transfer.[24,25]

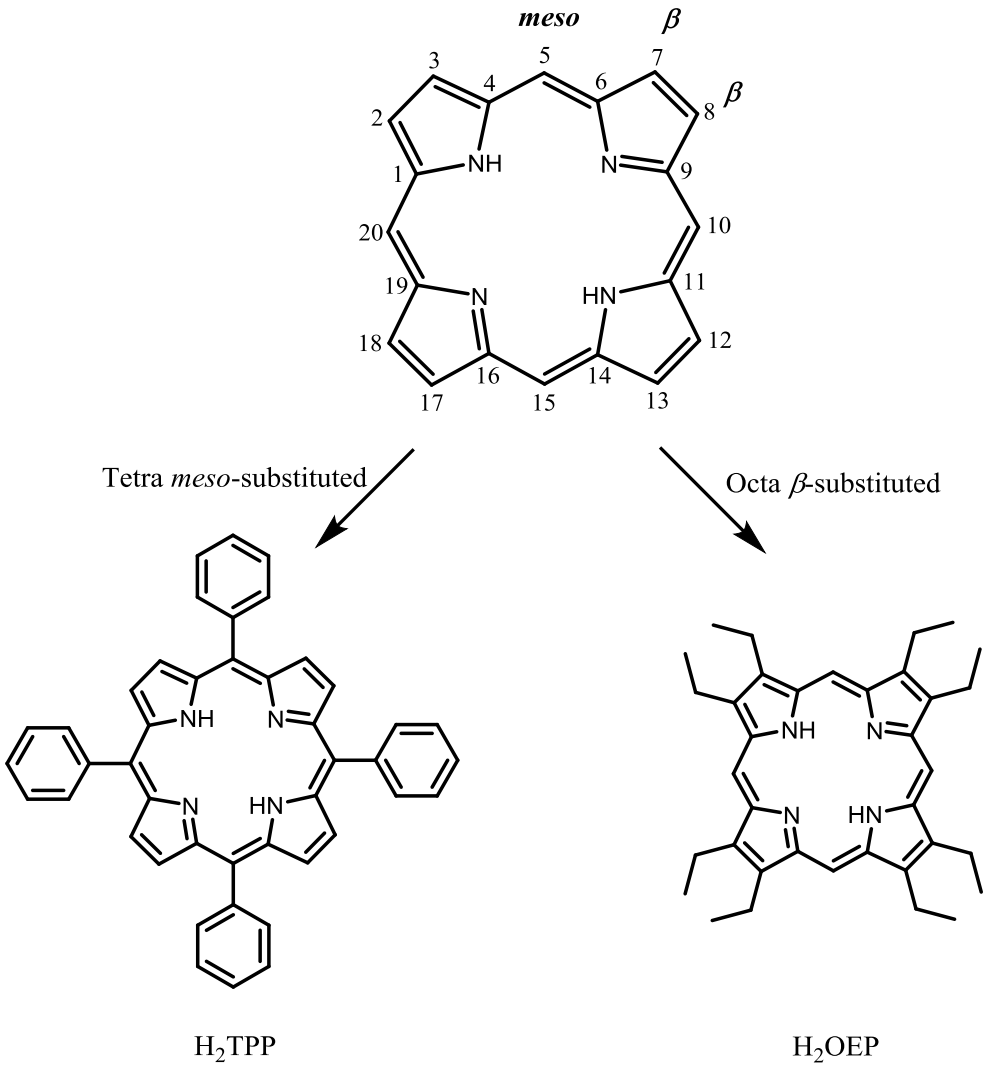

Chart 1-1. Structures of free-base porphin, tetraphenylporphyrin (H_2TPP) and octaethylporphyrin (H_2OEP).

a)

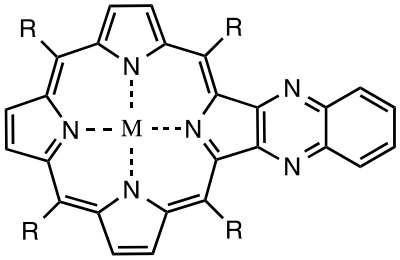

(PQ)M

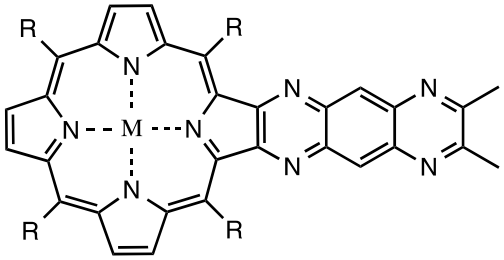

(PTA)M

---

b)

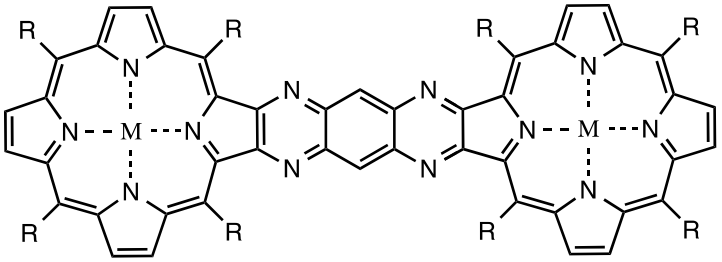

M(P)-TA-(P)M

Chart 1-2. Structures of a) metalloporphyrin with β, β'-fused quinoxaline (Q) or tetraazaanthracene (TA) groups and b) β,β'-fused tetraazaanthracene bis-porphyrins.

One type of examples are *β,β′*-fused tetraazaanthracene porpoyrins where tetraazaanthracene (TA) is fused to two porphyrin macrocycles, linking them in a linear fashion. Recently, our laboratory has studied these TA-linked bis-porphyrins shown in Chart 1-2b on their electrochemical and spectroelectrochemical properties.[26] A strong interaction between the two electroactive macrocycles of the bis-porphyrin was reported, as well as the effect of the fused electroactive TA group on the redox potentials and UV-visible spectra.

In order to compare the effect of linking groups on porphyrin dyads, *β,β′*-pyrazino-fused tetraarylporphyrins were studied in Chapter Three by electrochemistry and thin-layer UV-visible spectroelectrochemistry in non-aqueous media.

1.4 Porphyrazines and Phthalocyanines

As shown in Chart 1-3, porphyrazines have a symmetrical 18π-electron conjugated cyclic tetrapyrrole structure similar to porphyrins being with the difference of having four meso-nitrogen atoms on the macrocyle instead of four carbon atoms in the case of porphyrins.[40,41]

Similar to porphyrazines (see Chart 1-3), phthalocyanines are "extended porphyrines" by β-pyrrole positions being fused by for benzo groups, leading to an expanded π-ring conjugated system.[40,41] These differences include physical properties that are distinct from both porphyrins and porphyrazines.

Porphyrins are active photosensitizers, able to absorb light in the visible region and generate singlet oxygen, $^1O_2$, the main cytotoxic agent in photodynamic therapy

(PDT), a nowadays widely used anticancer curative modality.[42-46] Porphyrins, howeverexhibit weak absorptions in the phototherapeutic spectral window (600− 850 nm), this requiring high dosages in PDT; in addition, they induce long-lasting skin photosensitivity. Unlike the porphyrins, phthalocyanines, typical porphyrin-like macrocycles, and porphyrazines in general, normally show intense absorption bands in the therapeutic window. Thus, phthalocyanines[45,46] and various types of porphyrazine macrocycles, that is, tetrapyrazinoporphyrazines,[47-50] secoporphyrazines,[51,52] and benzonaphthoporphyrazines[53] have been actively considered as promising photosensitizers in PDT.

In previous studies, our lab investigated the spectral, electrochemical and spectroelectrochemical behaviors of metalloporphyrazine derivatives which are represented as [LM][54-56] and [$(PdCl_2)_4$LM][54,57] shown in Chart 1-4a and Chart 1-4b, respectively, where L = tetrakis-2,3-[5,6-di(2-pyridyl)pyrazino]porphyrazinato dianion, M = $Mg^{II}(H_2O)$, Mn^{II} , Co^{II} , Cu^{II}, Pd^{II} or Zn^{II}, and $PdCl_2$ are units coordinated to the pyridine N atoms of the four external dipyridinopyrazine fragments ("py-py" coordination).[54,56,58]

Electrochemical and spectroelectrochemical studies conducted in non-aqueous media indicated that the series of neutral [LM] complexes[54-56] undergo stepwise one-electron reductions with formation of -1, -2, -3, and -4 charged species at potentials significantly shifted in a positive direction with respect to $E_{1/2}$ values for reduction of a related series of phthalocyanines, due to their remarkable electron-deficient properties induced by the presence of the strongly electron-withdrawing "dipyridinopyrazine"

fragments,[56,57] while [$(PdCl_2)_4$LM] complexes can be stepwise reduced via two one-electron reversible or quasi-reversible processes which are easier to reduce than the [LM] complexes with same central metal ions, and be followed by an irreversible electroreduction of external $PdCl_2$ groups leading to the loss of $PdCl_2$ groups and the formation of $[LM]^{2-}$, which can further be reduced to $[LM]^{3-}$ and $[LM]^{4-}$ at the electrode surface.[54,56,59]

But these compounds, as well as related phthalocyanine and porphyrazine complexes, are normally only soluble in nonaqueous media and are virtually insoluble in water. This lack of solubility has presented a serious drawback to characterizing the compounds in water solution and has also limited their use for applications in the fields of biochemistry and medicine.[40,42-46,56]

In Chapter Four, the electrochemical and spectroelectrochemical properties of a new class of water-soluble homo/heteropentanuclear porphyrazine complexes are studied. The investigated compounds are represented as [$\{Pd(OAc)_2\}_4$LM] (L = tetrakis-2,3-[5,6-di(2-pyridyl)pyrazino]porphyrazinato dianion, M = $Mg^{II}(H_2O)$, Zn^{II}, Cu^{II}, Co^{II}, Pd^{II}, Pt^{II}) and bear four $Pd(OAc)_2$ units, each externally coordinated at the vicinal pyridine N atoms of a single dipyridinopyrazine fragment of the porphyrazine macrocycle (“py-py” coordination).

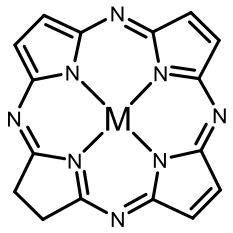

porphyrazine

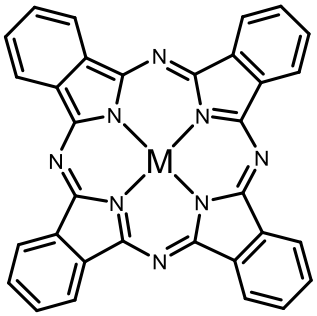

phthalocyanine

Chart 1-3 Structures of porphyrazine and phthalocyanine.

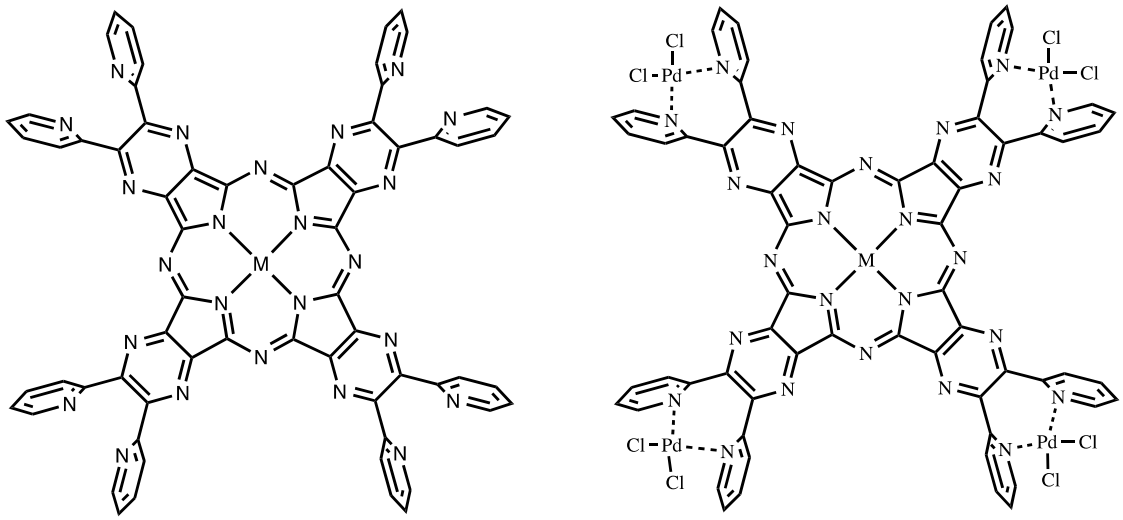

(a) [LM] (b) [$(PdCl_2)$LM]

Chart 1-4 Structures of a) [LM] and and b) [$(PdCl_2)_4$LM] porphyrazine complexes.

1.5 Positively and Negatively Charged Porphyrins

The positively and negatively charged porphyrins also belonging to water-soluble porphyrins were first introduced by Hambright with quaternizing *N*-methylpyridylporphyrin[27] in the early 1970s along with the first relevant data on the aqueous chemistry of these system, which has a profound impact on their use in biological and medical settings.[28-32] Structures of positively charged (tetra-*N*-methylpyridylporphyrin) and negatively charged (tetrasulfonatoporphyrin) porphyrins are shown in Chart 1-5. Several cationic substituted Mn(III) *N*-pyridylporphyrins and the anionic Mn(III) caboxylatophenylporphyrins were described in a first publication by the Fridocih group on SOD (superoxide dismutase) mimics as an important medical application.[33] Meanwhile, the first structure-activity relationships (SAR) between the SOD activity of the compounds and the metal-centered reduction potential were established.[34] The relationships were later refined to include electrostatic contributions,[35,36] but paved the way to guide the design of these SOD mimics and redox modulators.

More than 35 different metal ions have been reported to incorperted into the central cavity of H_2TMPyP.[27] The electrochemical behaviors of the TMpyP derivatives in have been studied in non-aqueous media.[37,38] In nonaqueous media, redox behaviors of four *meso*-*N*-pyridyl substituents on TMPyP macrocycles are related to the type of central metal ions and counter anions in the solution.[38,39]

In Chapter Five, redox behavior of newly synthesized tetracationic and tetraanionic water-soluble manganese porphyrins represented as TMPyP(PEG)Mn and

TPPS(PEG)Mn are characterized by electrochemistry and spectroelectrochemistry in DMF and DMSO with the comparison of TMPyPMn and TPPSMn. In addition, the electrochemistry and spectroelectrochemistry of “raft” of TMPyPMn and TPPSMn is studied in Chapter Four.

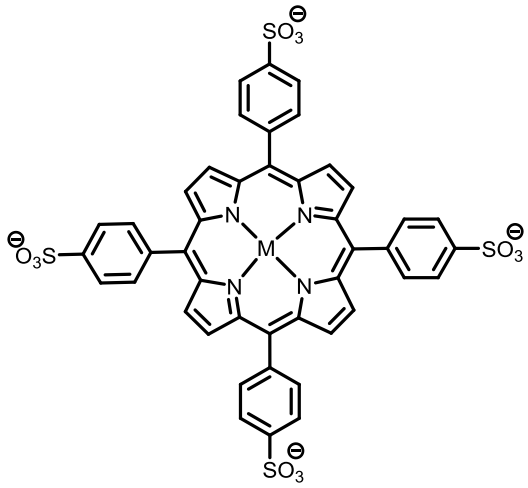

TPPSM

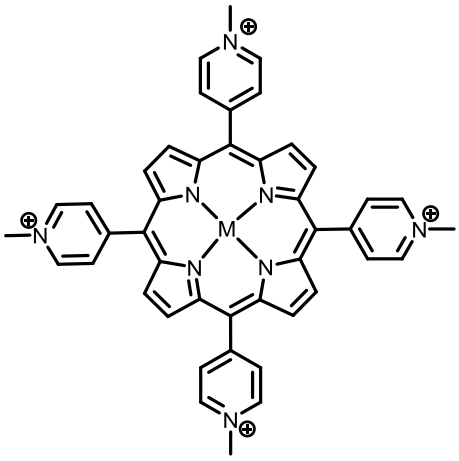

TMPyPM

Chart 1-5. Structures of positively charged tetra-*N*-methylpyridylporphyrin (TMPyP) and negatively charged tetrasulfonatoporphyrin (TPPS).

1.6 References

(1) Martinez-Diaz, M. V.; Torres, T.; World Scientific Publishing Co. Pte. Ltd.: 2010; Vol. 10, p 141.

(2) Duclairoir, F.; Marchon, J.-C.; World Scientific Publishing Co. Pte. Ltd.: 2010; Vol. 10, p 245.

(3) Ethirajan, M.; Patel, N. J.; Pandey, R. K.; World Scientific Publishing Co. Pte. Ltd.: 2010; Vol. 4, p 249.

(4) Crossley, M. J.; Burn, P. L. *J. Chem. Soc., Chem. Commun.* **1987**, 39.

(5) Lu, T. X.; Reimers, J. R.; Crossley, M. J.; Hush, N. S. *J. Phys. Chem.* **1994**, *98*, 11878.

(6) Crossley, M. J.; Sintic, P. J.; Walton, R.; Reimers, J. R. *Org. Biomol. Chem.* **2003**, *1*, 2777.

(7) Ou, Z.; E, W.; Shao, J.; Burn, P. L.; Sheehan, C. S.; Walton, R.; Kadish, K. M.; Crossley, M. J. *J. Porphyrins Phthalocyanines* **2005**, *9*, 142.

(8) Armstrong, R. S.; Foran, G. J.; Hough, W. A.; D'Alessandro, D. M.; Lay, P. A.; Crossley, M. J. *Dalton Trans.* **2006**, 4805.

(9) Zhu, W.; Sintic, M.; Ou, Z.; Sintic, P. J.; McDonald, J. A.; Brotherhood, P. R.; Crossley, M. J.; Kadish, K. M. *Inorg. Chem.* **2010**, *49*, 1027.

(10) Flamigni, L.; Marconi, G.; Johnston, M. R. *Phys. Chem. Chem. Phys.* **2001**, *3*, 4488.

(11) Hutchison, J. A.; Bell, T. D. M.; Ganguly, T.; Ghiggino, K. P.; Langford, S. J.; Lokan, N. R.; Paddon-Row, M. N. *J. Photochem. Photobiol., A* **2008**, *197*, 220.

(12) Sintic, P. J.; E, W.; Ou, Z.; Shao, J.; McDonald, J. A.; Cai, Z.-L.; Kadish, K. M.; Crossley, M. J.; Reimers, J. R. *Phys. Chem. Chem. Phys.* **2008**, *10*, 515.

(13) Beavington, R.; Burn, P. L. *Perkin 1* **2000**, 1231.

(14) Crossley, M. J.; Govenlock, L. J.; Prashar, J. K. *J. Chem. Soc., Chem. Commun.* **1995**, 2379.

(15) Crossley, M. J.; Burn, P. L. *J. Chem. Soc., Chem. Commun.* **1991**, 1569.

(16) Sendt, K.; Johnston, L. A.; Hough, W. A.; Crossley, M. J.; Hush, N. S.; Reimers, J. R. *J. Am. Chem. Soc.* **2002**, *124*, 9299.

(17) Crossley, M. J.; Burn, P. L.; Langford, S. J.; Pyke, S. M.; Stark, A. G. *J. Chem. Soc., Chem. Commun.* **1991**, 1567.

(18) Crossley, M. J.; King, L. G.; Newsom, I. A.; Sheehan, C. S. *J. Chem. Soc., Perkin Trans. 1* **1996**, 2675.

(19) Crossley, M. J.; Sheehan, C. S.; Khoury, T.; Reimers, J. R.; Sintic, P. J. *New J. Chem.* **2008**, *32*, 340.

(20) Kadish, K. M.; E, W.; Sintic, P. J.; Ou, Z.; Shao, J.; Ohkubo, K.; Fukuzumi, S.; Govenlock, L. J.; McDonald, J. A.; Try, A. C.; Cai, Z.-L.; Reimers, J. R.; Crossley, M. J. *J. Phys. Chem. B* **2007**, *111*, 8762.

(21) Crossley, M. J.; Harding, M. M.; Tansey, C. W. *J. Org. Chem.* **1994**, *59*, 4433.

(22) E, W.; Kadish, K. M.; Sintic, P. J.; Khoury, T.; Govenlock, L. J.; Ou, Z.; Shao, J.; Ohkubo, K.; Reimers, J. R.; Fukuzumi, S.; Crossley, M. J. *J. Phys. Chem. A* **2008**, *112*, 556.

(23) Eu, S.; Hayashi, S.; Umeyama, T.; Matano, Y.; Araki, Y.; Imahori, H. *J. Phys. Chem. C* **2008**, *112*, 4396.

(24) Crossley, M. J.; Sintic, P. J.; Hutchison, J. A.; Ghiggino, K. P. *Org. Biomol. Chem.* **2005**, *3*, 852.

(25) Hutchison, J. A.; Sintic, P. J.; Crossley, M. J.; Nagamura, T.; Ghiggino, K. P. *Phys. Chem. Chem. Phys.* **2009**, *11*, 3478.

(26) Ou, Z.; Zhu, W.; Sintic, P. J.; Fang, Y.; Crossley, M. J.; Kadish, K. M. *J. Porphyrins Phthalocyanines* **2012**, *16*, 674.

(27) Hambright, P.; Academic Press: 2000; Vol. 3, p 129.

(28) Faraggi, M.; Peretz, P.; Weinraub, D. *Int. J. Radiat. Biol. Relat. Stud. Phys., Chem. Med.* **1986**, *49*, 951.

(29) Weinraub, D.; Peretz, P.; Faraggi, M. *J. Phys. Chem.* **1982**, *86*, 1839.

(30) Ilan, Y.; Rabani, J.; Fridovich, I.; Pasternack, R. F. *Inorg. Nucl. Chem. Lett.* **1981**, *17*, 93.

(31) Pasternack, R. F.; Banth, A.; Pasternack, J. M.; Johnson, C. S. *J Inorg Biochem* **1981**, *15*, 261.

(32) Weinraub, D.; Levy, P.; Faraggi, M. *Int. J. Radiat. Biol. Relat. Stud. Phys., Chem. Med.* **1986**, *50*, 649.

(33) Faulkner, K. M.; Liochev, S. I.; Fridovich, I. *J Biol Chem* **1994**, *269*, 23471.

(34) Kachadourian, R.; Batinic-Haberle, I.; Fridovich, I. *Inorg. Chem.* **1999**, *38*, 391.

(35) Spasojevic, I.; Batinic-Haberle, I.; Reboucas, J. S.; Idemori, Y. M.; Fridovich, I. *J. Biol. Chem.* **2003**, *278*, 6831.

(36) Reboucas, J. S.; DeFreitas-Silva, G.; Spasojevic, I.; Idemori, Y. M.; Benov, L.; Batinic-Haberle, I. *Free Radical Biol. Med.* **2008**, *45*, 201.

(37) Kadish, K. M.; Sazou, D.; Liu, Y. M.; Saoiabi, A.; Ferhat, M.; Guilard, R. *Inorg. Chem.* **1988**, *27*, 686.

(38) Kadish, K. M.; Araullo, C.; Maiya, G. B.; Sazou, D.; Barbe, J. M.; Guilard, R. *Inorg. Chem.* **1989**, *28*, 2528.

(39) Van Caemelbecke, E.; Derbin, A.; Hambright, P.; Garcia, R.; Doukkali, A.; Saoiabi, A.; Ohkubo, K.; Fukuzumi, S.; Kadish, K. M. *Inorg. Chem.* **2005**, *44*, 3789.

(40) Leznoff, C. C.; Lever, A. B. P.; Editors *Properties and Applications. [In: Phthalocyanines, 1993; 2]*; VCH, 1993.

(41) L'Her, M.; Pondaven, A.; Elsevier Science: 2003; Vol. 16, p 117.

(42) Ethirajan, M.; Chen, Y.; Joshi, P.; Pandey, R. K. *Chem. Soc. Rev.* **2011**, *40*, 340.

(43) Celli, J. P.; Spring, B. Q.; Rizvi, I.; Evans, C. L.; Samkoe, K. S.; Verma, S.; Pogue, B. W.; Hasan, T. *Chem. Rev. (Washington, DC, U. S.)* **2010**, *110*, 2795.

(44) Moreira, L. M.; dos Santos, F. V.; Lyon, J. P.; Maftoum-Costa, M.; Pacheco-Soares, C.; da Silva, N. S. *Aust. J. Chem.* **2008**, *61*, 741.

(45) O'Connor, A. E.; Gallagher, W. M.; Byrne, A. T. *Photochem. Photobiol.* **2009**, *85*, 1053.

(46) Szacilowski, K.; Macyk, W.; Drzewiecka-Matuszek, A.; Brindell, M.; Stochel, G. *Chem. Rev. (Washington, DC, U. S.)* **2005**, *105*, 2647.

(47) Zimcik, P.; Novakova, V.; Miletin, M.; Kopecky, K. *Makrogeterotsikly* **2008**, *1*, 21.

(48) Zimcik, P.; Miletin, M.; Novakova, V.; Kopecky, K.; Nejedla, M.; Stara, V.; Sedlackova, K. *Aust. J. Chem.* **2009**, *62*, 425.

(49) Novakova, V.; Morkved, E. H.; Miletin, M.; Zimcik, P. *J. Porphyrins Phthalocyanines* **2010**, *14*, 582.

(50) Mitzel, F.; FitzGerald, S.; Beeby, A.; Faust, R. *Eur. J. Org. Chem.* **2004**, 1136.

(51) Baum, S. M.; Trabanco, A. A.; Montalban, A. G.; Micallef, A. S.; Zhong, C.; Meunier, H. G.; Suhling, K.; Phillips, D.; White, A. J. P.; Williams, D. J.; Barrett, A. G. M.; Hoffman, B. M. *J. Org. Chem.* **2003**, *68*, 1665.

(52) Sakellariou, E. G.; Montalban, A. G.; Meunier, H. G.; Rumbles, G.; Phillips, D.; Ostler, R. B.; Suhling, K.; Barrett, A. G. M.; Hoffman, B. M. *Inorg. Chem.* **2002**, *41*, 2182.

(53) Michelsen, U.; Kliesch, H.; Schnurpfeil, G.; Sobbi, A. K.; Woehrle, D. *Photochem. Photobiol.* **1996**, *64*, 694.

(54) Donzello, M. P.; Viola, E.; Cai, X.; Mannina, L.; Rizzoli, C.; Ricciardi, G.; Ercolani, C.; Kadish, K. M.; Rosa, A. *Inorg. Chem.* **2008**, *47*, 3903.

(55) Donzello, M. P.; Viola, E.; Ercolani, C.; Fu, Z.; Futur, D.; Kadish, K. M. *Inorg. Chem.* **2012**, *51*, 12548.

(56) Bergami, C.; Donzello, M. P.; Monacelli, F.; Ercolani, C.; Kadish, K. M. *Inorg. Chem.* **2005**, *44*, 9862.

(57) Clack, D. W.; Hush, N. S.; Woolsey, I. S. *Inorg. Chim. Acta* **1976**, 129.

(58) Donzello, M. P.; Viola, E.; Bergami, C.; Dini, D.; Ercolani, C.; Giustini, M.; Kadish, K. M.; Meneghetti, M.; Monacelli, F.; Rosa, A.; Ricciardi, G. *Inorg. Chem.* **2008**, *47*, 8757.

(59) Donzello, M. P.; Viola, E.; Cai, X.; Mannina, L.; Ercolani, C.; Kadish, K. M. *Inorg. Chem.* **2010**, *49*, 2447.

Chapter Two

Experimental Methods

2.1 Electrochemical Methods

2.1.1 Cyclic Voltammetry Experimental Conditions

Cyclic voltammetry was carried out at 298 K by using an EG&G Princeton Applied Research (PAR) 173 potentiostat/galvanostat. Measurements were conducted in a homemade "three-electrode" setup (show in Figure 2-1), which includes a glassy carbon working electrode with a diameter of 3 mm (WE), a platinum counter electrode (CE) and a saturated calomel reference electrode (SCE). Materials for the working electrode can also be platinum. The SCE was separated from the bulk of the solution by a fritted bridge of low porosity, which contained the solvent/supporting electrolyte mixture. In some measurements, ferrocene (Fc) was used as an internal standard.

In cyclic voltammetry, the potential of the working electrode ramps linearly versus as shown in Figure 2-2. During the initial forward scan (from t_0 to t_f) an increasingly reducing potential is applied from 0.00 V to -1.00 V. Once the desired potential is reached, which is -1.00 V at t_f in this case, the direction of scan is reversed and is towards back to the initial potential (0.00 V). The cycles of scan can be repeated as many times as desired.

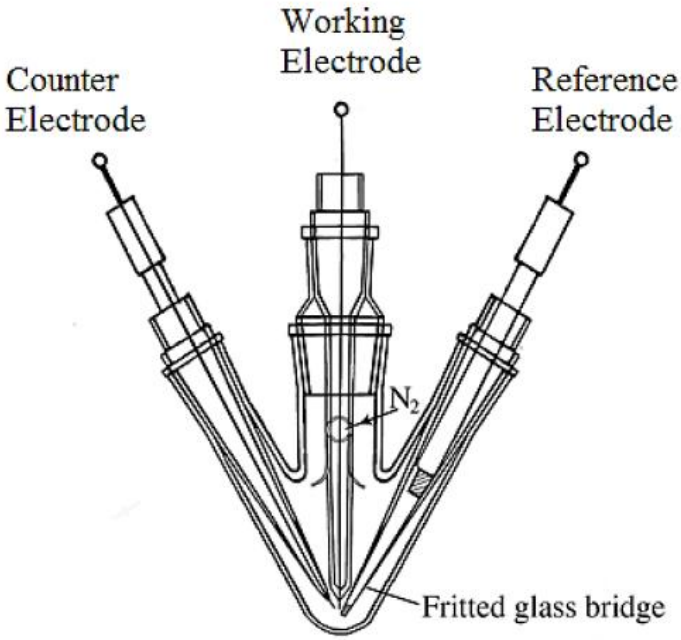

Figure 2-1. Schematic illustration of the utilized electrochemical cell with glassy carbon (or platinum) working, platinum counter electrode and saturated calomel reference electrode (SCE).

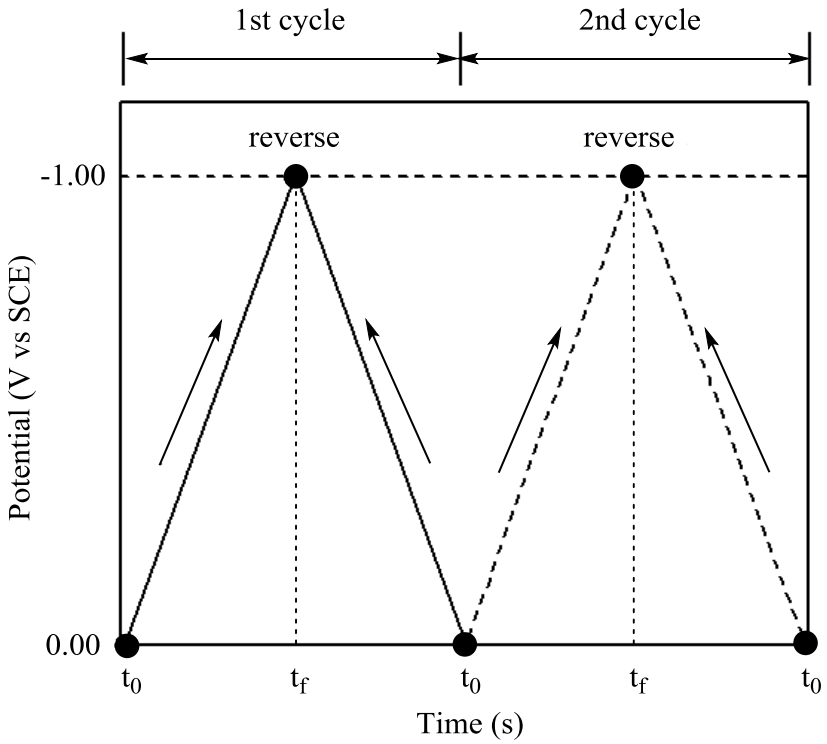

Figure 2-2. Cyclic voltammetry waveform showing reduction scan between 0.0 to -1.0 V.

2.1.2 Cyclic Voltammetry Analytical Theory

The potential is applied between the working electrode and the reference electrode while the current is measured between the working electrode and the counter electrode. The plot of the current-voltage curve is called cyclic voltammogram. A typical cyclic voltammogram example is given in Figure 2-3, where the initial forward scan is from 0.00 V to -1.00 V, and the peak current for reduction (cathodic current) is given by i_{pc}, and the peak potential for reduction is given by E_{pc}. The reverse peak potential for oxidation is given by E_{pa}. The magnitude of the peak current is defined by the Randles-Sevcik equation[1-3] given in Equation 2-1,

$$i_p = (2.69 \times 10^5) n^{3/2} A C D^{1/2} v^{1/2} \quad (2\text{-}1)$$

where i_p is peak current (μA), n is number of electrons transferred, A the area of the electrode surface (cm^2), D the diffusion coefficient of analyte in the solution (cm^2/s), C the the concentration of the analyte (mol/cm^3), and v the the scan rate (V/s).

If the redox couple is reversible, during the reverse scan (t_1 to t_0) the reoxidation process will give rise to an oxidation peak, which has a shape similar to that of reduction. On the other hand, if the redox couple is irreversible, the oxidation peak current may be smaller than that for the reduction or in some cases no oxidation peak will be observed during the reverse scan, due to the chemical reaction following electron transfer process. Thus, cyclic voltammetry can provide information about reversibility of the electron transfer and the stability of the electrogenerated product.

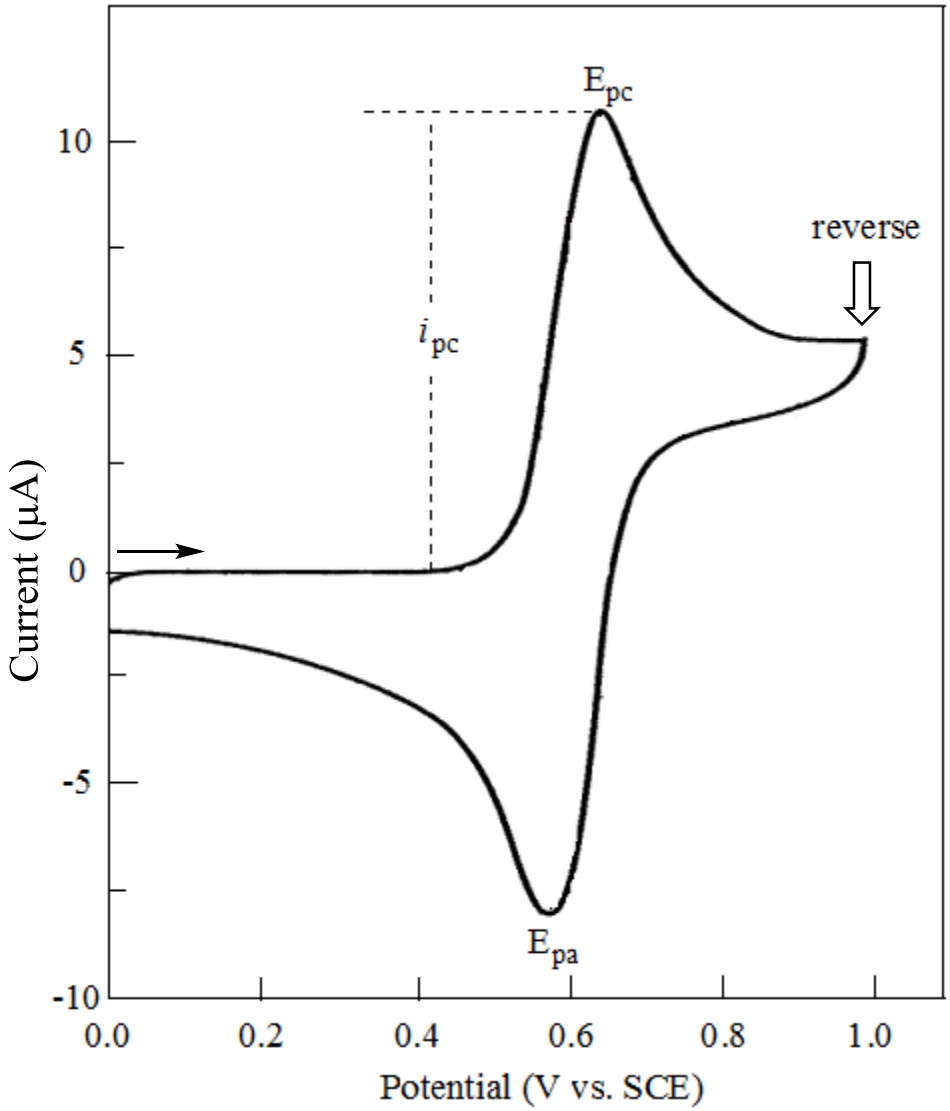

Figure 2-3. Schematic illustration of a cyclic voltammogram.

When the redox process is reversible, the half-wave potential $E_{1/2}$ is defined by Equation 2-2, which is the average value of the cathodic (E_{pc}) and anodic (E_{pa}) peak potentials (Figure 2-3). For reversible reactions the difference between (ΔE_p) should be 59/n mV at 25 ^oC according to the Nernst Equation where n is the number of electrons transferred.[1] Thus, the number of electron transferred during the redox process can be determined.

$$E_{1/2} = \frac{|E_{pa} + E_{pc}|}{2} \qquad (2\text{-}2)$$

2.1.3 UV-visible Spectroelectrochemistry Methods

UV-visible spectroelectrochemical experiments were performed with a home-built thin-layer cell[4,5] that has a light transparent platinum net working electrode (Figure 2-4). Potentials were applied and monitored with an EG&G PAR Model 173 potentiostat. Time-resolved UV-visible spectra were recorded with a Hewlett-Packard Model 8453 diode array spectrophotometer. The combination of electrochemistry and spectroscopy allows for a determination of the spectrum of the species formed in solution during the time of the elctron transfer.[6] The use of spectroelectrochemistry may help to determine the specific site of electron transfer. One example of typical metal-centered and macrocycle-centered spectral changes is given by $(NO_2TdmPP)Co^{II}$ during a controlled potential oxidations,[7] which is shown in Figure 2-6 with the structure of compound inserted in the figure. During the first one-electron abstraction at applied potential of E_{app} = 0.95 V, the Soret band at 427 nm decreases in intensity with formation of a new Soret band at 445 nm. This spectral change indicates the metal-centered electron transfer

leading to the conversion of Co^{II} to Co^{III}. The second electron abstraction at E_{app} = 1.20 V results in the decrease of Soret band at 445 nm, while a new broad band grows in at 675 nm, which is the typical spectral change for macrocycle-centered electron transfer reaction.

2.2 Other Experimental Procedures for Electrochemistry

2.2.1 Degassing the Solution

High-purity nitrogen from Trigas was used to deoxygenate the solution for five to ten minutes before each electrochemical experiment and a positive pressure was maintained above the solution throughout the experiment.

2.2.2 Temperature Control

All electrochemical experiments were performed at room temperature ($22 \pm 1\ ^{o}C$) unless otherwise noted. However, low temperature and variable temperature electrochemistry were also carried out. A dry ice/acetone mixture (2 was used to prepare a slush bath, whose temperature ramped from 22 to -75 ^{o}C. The exact temperature was monitored using a mercury thermometer and the cell was centered in the slush bath containing the dry ice and acetone mixture.

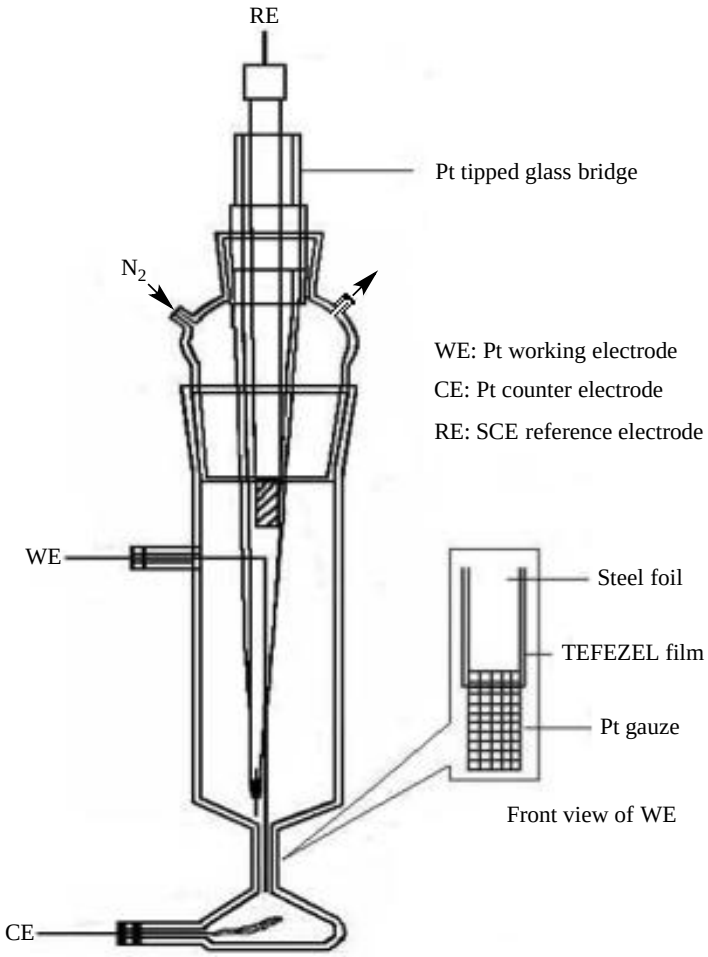

Figure 2-4. Schematic illustration of the thin-layer UV-visible spectroelectrochemical cell.

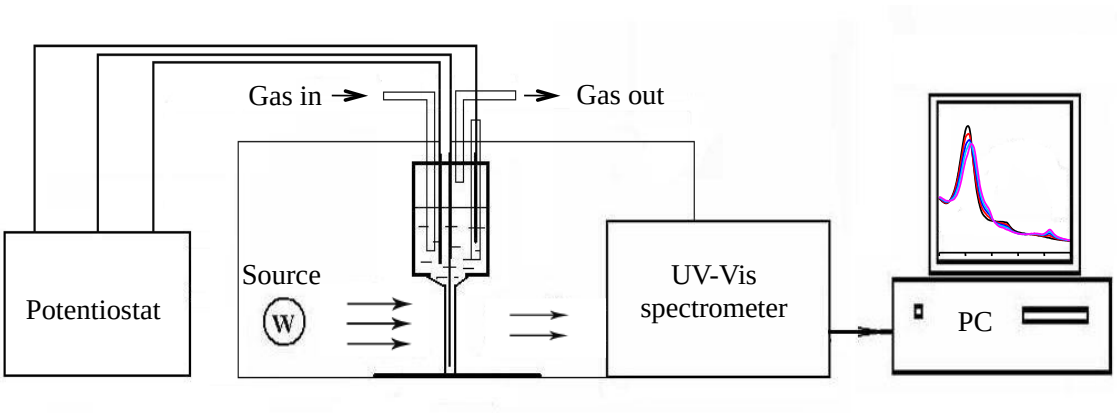

Figure 2-5. Schematic illustration of UV-visible spectroelectrochemical setup.

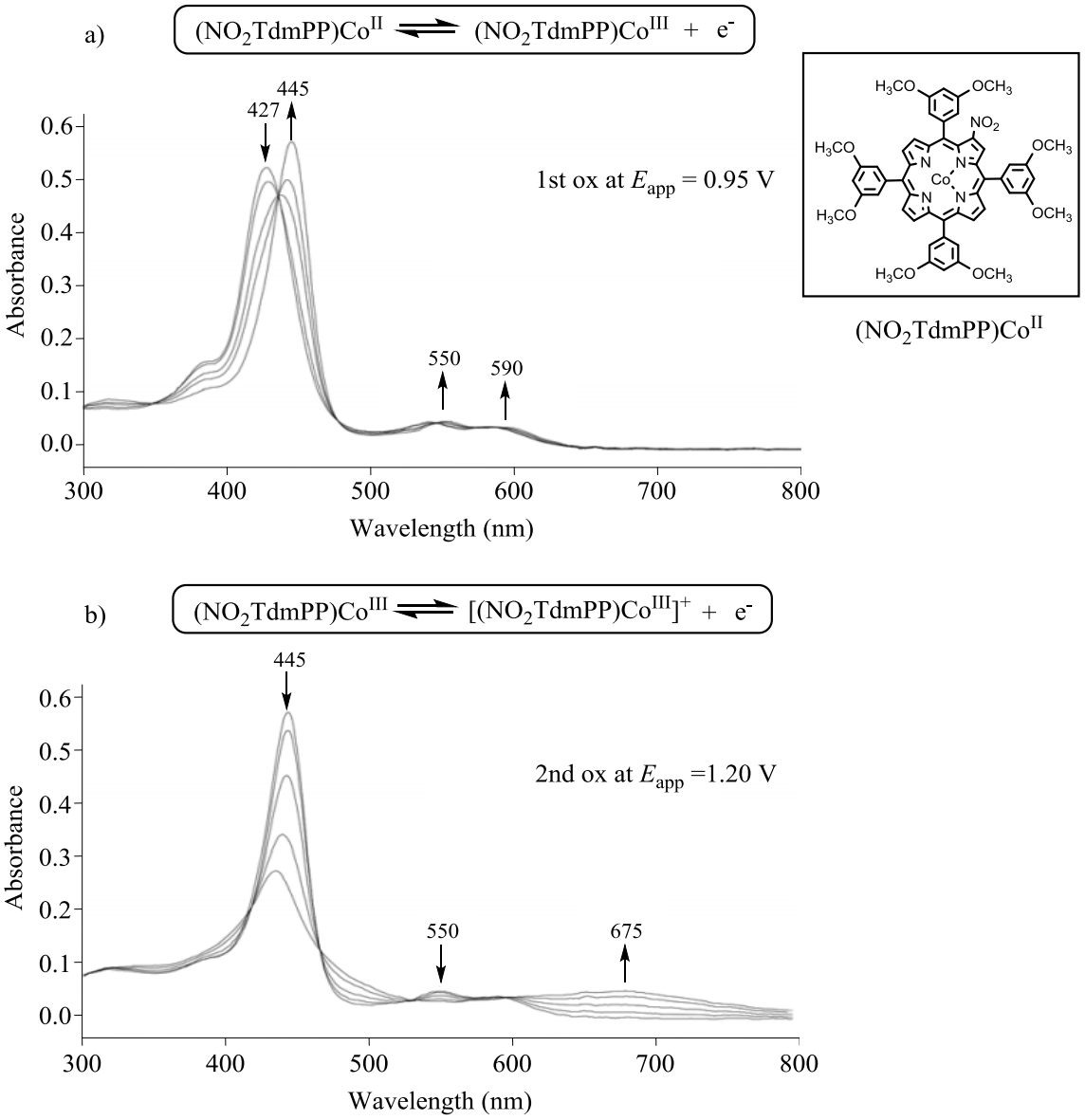

Figure 2-6. UV-visible spectral changes of $(NO_2TdmPP)Co^{II}$ during controlled potential oxidations in CH_2Cl_2 containing 0.1 M TBAP. Figure is reproduced from publication by Sun, B.; etc.[7]

2.3 Chemicals and Examined Compounds

2.3.1 Chemicals

Absolute dichloromethane (CH_2Cl_2, 99.8%) from EMD Chemicals Inc. was used for electrochemistry without further purification. *N,N'*-dimethylformamide (DMF), dimethyl sulfoxide (DMSO) were purchased from Sigma-Aldrich Chemical Co.. Benzonitrile (PhCN) was purchased from Sigma-Aldrich Chemical Co. and distilled over P_2O_5 under vacuum prior to use. High purity N_2 from Matheson-Trigas was used to deoxygenate the solution before each electrochemical experiment. Tetra-*n*-butylammonium perchlorate (TBAP), tetra-*n*-butylammonium chloride > 97% (TBACl), tetra-*n*-butylammonium bromide > 98% (TBABr) and tetra-*n*-butylammonium iodide > 99% (TBAI), used as supporting electrolyte, were purchased from Sigma-Aldrich. For the electrochemical measurements in water the supporting electrolyte was KCl (0.1 M) or sodium acetate (NaOAc, 0.1 M).

2.3.2 Investigated Compounds

All compounds studied in the thesis were commercially available or were prepared by our collaborators. The Zn, Cu and Ag *β*-pyrazino-fused tetraarylporphyrins complexes described in Chapter Three were prepared and provided by group of Dr. Roberto Paolesse at the University of Rome in Italy.[8] The water-soluble porphyrazins $\{Pd(OAc)_2\}_4LM$, where M = $Mg^{II}(H_2O)$, Zn^{II}, Cu^{II}, Co^{II}, Pd^{II}, Pt^{II} described in Chpater Four were made by Dr. Maria Pia Donzello and Dr. Claudio Ercolani in Italy.[9] Synthesis of the tetraanionic and tetracationic water-soluble manganese porphyrins and related

compounds in Chapter Five is completed by Dr. Claude Gros's group in Dijon, France.[10] All of the investigated complexes were stored in the dark and in some cases under vacuum conditions. The UV-visible spectrum of each compound was measured before carrying out experiments in Houston and our spectral data was compared to the spectra provided by our collaborators or published in the literature. If the spectra were different, as happened in a few instances, we identified the reason for the difference or informed by collaborator of the problem so that our collaborators could resynthesize the compound if needed. In this way, we could be assured that the examined compound was in the same form as provided by our collaborators who had characterized the compounds by a number of standard methods (NMR, mass spectroscopy, elemental analysis, ESR, etc) prior to sending samples to Houston.

2.4 References

(1) *Electrochemical Methods : Fundamentals and Applications*; Bard, A. J.; Faulkner, L. R., Eds.; John Wiley & Sons, Inc.: New York, 2001.

(2) Nicholson, R. S.; Shain, I. *Anal. Chem.* **1964**, *36*, 706.

(3) Heinze, J. *Angew. Chem.* **1984**, *96*, 823.

(4) Lin, X. Q.; Kadish, K. M. *Anal. Chem.* **1985**, *57*, 1498.

(5) Kadish, K. M.; Mu, X. H.; Lin, X. Q. *Electroanalysis (N. Y.)* **1989**, *1*, 35.

(6) Kaim, W.; Fiedler, J. *Chem. Soc. Rev.* **2009**, *38*, 3373.

(7) Sun, B.; Ou, Z.; Yang, S.; Meng, D.; Lu, G.; Fang, Y.; Kadish, K. M. *Dalton Trans.* **2014**, *43*, 10809.

(8) Fang, Y.; Mandoj, F.; Zeng, L.; Pudi, R.; Stefanelli, M.; Paolesse, R.; Kadish, K. M. *J. Porphyrins Phthalocyanines.* **2015**, *19*, 388.

(9) Donzello, M. P.; Vittori, D.; Viola, E.; Zeng, L.; Cui, Y.; kadish, K. M.; Ercolani, C. *J. Porphyrins Phthalocyanines.* **2015**, (in press).

(10) Laguerre, A.; Chang, Y.; Pirrotta, M.; Desbois, N.; Gros, C. P.; Lesniewska, E.; Monchaud, D. *Org. Biomol. Chem.* **2015**, *13*, 7034.

Chapter Three

Electrochemistry and Spectroelectrochemistry of β-Pyrazino-Fused Tetraarylporphyrins in Nonaqueous Media

3.1 Introduction

Extended porphyrinoid molecules have attracted much attention because of their fundamental, theoretical interest, and their use for diverse applications in the fields of biology, technology and medicine.[1-4] *β*,*β*'-Appended and linked porphyrins have been proposed as key components for applications in building electron- and energy-transfer devices, and many such molecules have been reported.[5-11]

An extension of the porphyrin core aromaticity generally leads to a decrease in the electrochemical HOMO-LUMO gap,[12-16] and strong red shifts of absorption bands in the optical spectrum of the neutral compounds.[4,17,18] As a result of these changes there are also changes in the linear and non-linear optical properties of the compounds. Understanding the most important factors that affect the site of electron transfer in bis-porphyrins as well as the magnitude of interaction between equivalent redox active centers in these compounds is of vital interest to tune and direct the chemical reactivity of expanded porphyrins and larger arrays.[7]

A number of previously characterized bis-porphyrins have contained fused linking groups at the *meso* or *β*-pyrrole positions of the macrocycle.[4,13,15,19] In the case of transition metal derivatives with redox active central metal ions, the porphyrin metal oxidation state could sometimes be stepwise cycled between its M^{I}, M^{II}, M^{III}, M^{IV} or even M^{V} forms, as a function of the applied potential and variations in the type and number of bound axial ligands.[16] It is well-documented in the literature that the site of electron transfer in metalloporphyrins can be tuned by appropriate selection of solvent, axial ligand binding, and/or porphyrin ring substituents.[16] and this is also the case for bis-porphyrins.

Electrochemical characterization of covalently linked symmetrical and unsymmetrical bis-metalloporphyrin dyads such as M(TPP-TriPP)M and M(TPP-DEHMP)M have been reported,[20] where TPP-TriPP and TPP-DEHMP are the tetraanions of 1,4-bis-[5'-(10',15',20'-triphenyl porphyrinyl)]benzene and 1-[5-(10,15,20-triphenylporphyrinyl)]-4-[10-(2,18-diethyl-3,7,8,12,13,17-hexamethylporphyrinyl)] benzene, respectively. In each dyad, the two porphyrin macrocycles are linked by a single bond and, in the case of M(TPP-TriPP)M, might be considered as two triphenylporphyrins bridged by a single linking phenyl group. The UV-vis spectra of the neutral bisporphyrin dyads linked by a single phenyl group are almost identical to the supermoposed spectra of the two corresponding monomeric units[20] and this indicates that little or no interaction occurs between the two macrocycles in their neutral form. Evidence of non-interacting macrocycles is also given by the electrochemical data where redox potentials of the bis-porphyrins are almost identical to $E_{1/2}$ values for oxidation or reduction of the combined individual monoporphyrin units and no "splitting" of the redox processes are observed which would occur for equivalent interacting redox centers.[20]

There are numerous examples in the literature where oxidation or reduction of bis- porphyrins and bis-corroles exhibit split redox processes in oxidation or reduction.[21-27] The separation between the values of $E_{1/2}$ in the split processes will reflect the degree of interaction between the two macrocycles in the dyad, with the measured $\Delta E_{1/2}$ values ranging from as small as several millivolts for small interactions to almost 500 mV for large interactions, one example of the latter being given for tetraazaanthracene (TA) linked porphyrins such as M(P)-TA-(P)M, where M = H_2, Cu(II), Zn(II) or Pd(II).[13]

Another series of bisporphyrins which are structurally related to the TA-linked derivatives are the pyrazine linked bis-porphyrins, whose synthesis and brief electrochemistry was described in a recent publication.[19] A split redox process was reported for oxidation of the Zn(II) bisporphyrin, but the overall redox behavior was complicated by the presence of side reactions that occurred in CH_2Cl_2 and none of the other bisporphyrins were electrochemically characterized in the manuscript. Furthermore, the spectra of the oxidized or reduced Zn(II) bisporphyrin were not measured and thus a more detailed analysis of this compound's redox behavior and spectroscopic properties after oxidation or reduction is needed. This is addressed in the current paper, where we present the electrochemistry and spectroelectrochemistry of Zn(II), Cu(II) and Ag(II) *β*,*β*-pyrazino fused bis-porphyrins in benzonitrile (PhCN) containing 0.1 M tetrabutylammonium perchlorate (TBAP). The first two compounds undergo only ring-centered electron transfer reactions, while the Ag(II) bisporphyrin exhibits both a metal-centered oxidation and a metal-centered reduction prior to oxidation or reduction at the conjugated bisporphyrin macrocycle. The examined porphyrins are represented as M(TPP)-Pz-(TPP)M and shown in Chart 3-1 along with several reference compounds containing linked pyrazine and tetraazaanthracene groups. The electrochemical behavior of the currently investigated dyads are examined as a function of the type and oxidation state of the central metal ion and the type of linking group.

(a) Investigated bis-porphyrins

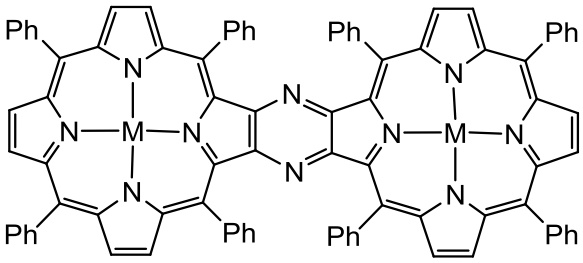

M(TPP)-Pz-(TPP)M

(b) Reference porphyrins

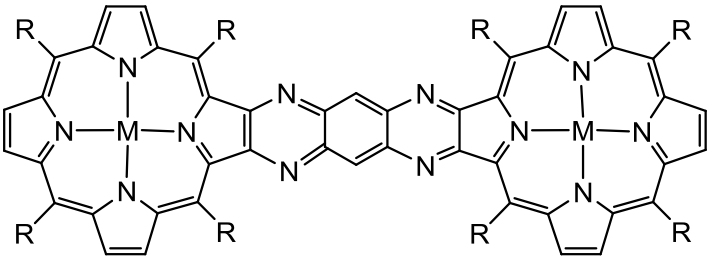

M(P)-TA-(P)M

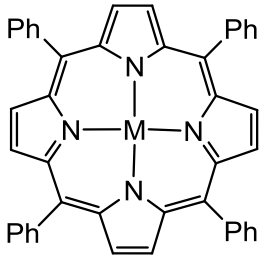

M(TPP)

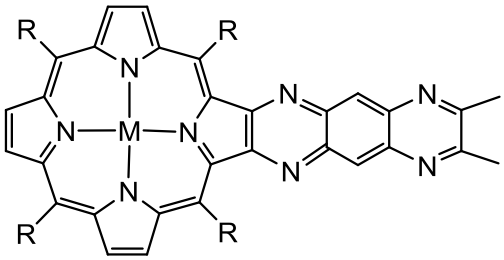

M(P-TA)

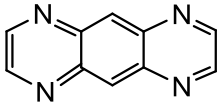

TA

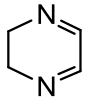

Pz

Chart 3-1. Structures of (a) investigated bis-porphyrins with Zn(II), Cu(II) and Ag(II) central metal ions and (b) related reference compounds where R is a tri-*t*-butylphenyl group.

3.2 Results and Discussion

3.2.1 UV-vis Absorption Spectra of Neutral Compounds

UV-vis spectra of M(TPP)-Pz-(TPP)M in PhCN are shown in Figure 3-1 for the Zn(II) and Cu(II) derivatives. Both bisporphyrins are characterized by a split Soret band, located at 411/500 nm for M = Zn and 425/495 nm for M = Cu. There is also a single relatively intense Q band at 600 nm (Zn) or 590 nm (Cu). A similar spectrum is seen for the Ag(TPP)-Pz-(TPP)Ag in PhCN, which is characterized by bands at 415, 489 and 578 nm. By way of comparison, the three related monometallic M(TPP) complexes in PhCN are each characterized by an unsplit Soret band at 419 to 428 nm and two weak Q bands at 537- 600 nm. The spectral data for these mono and bisporphyrins are summarized in Table 3-1, along with wavelengths and molar absorptivity for the related TA-linked porphyrins under the same solution conditions. As seen in the table and figure, the separation between the split Soret bands of the M(TPP)-Pz-(TPP)M bisporphyrins is 70 nm for M = Cu(II), 74 nm for M = Ag(II) and 89 nm for M = Zn(II). These values are much smaller than the separation in λ_{max} for the split Soret bands of the Cu and Zn TA linked porphyrins (see Table 3-1) but, as discussed below, the TA linked complexes exhibit a greater interaction between the two redox active macrocycles upon reduction as compared to the related Pz-linked derivatives.

Table 3-1. UV-visible spectra data ($\lambda_{max,}$ nm) of investigated M(TPP)-Pz-(TPP)M and related compounds in PhCN.

Macrocycle	M	Soret band (nm)		Q band (nm)	
M(TPP)	Zn	428		557	600
	Cu	419		537	579
	Ag	423		539	569
M(TPP)-Pz-(TPP)M	Zn	411	500	600	
	Cu	425	495	590	
	Ag	415	489	578	
M(P)-TA-(P)M	Zn	435	467	527	
	Cu	431	444	552	

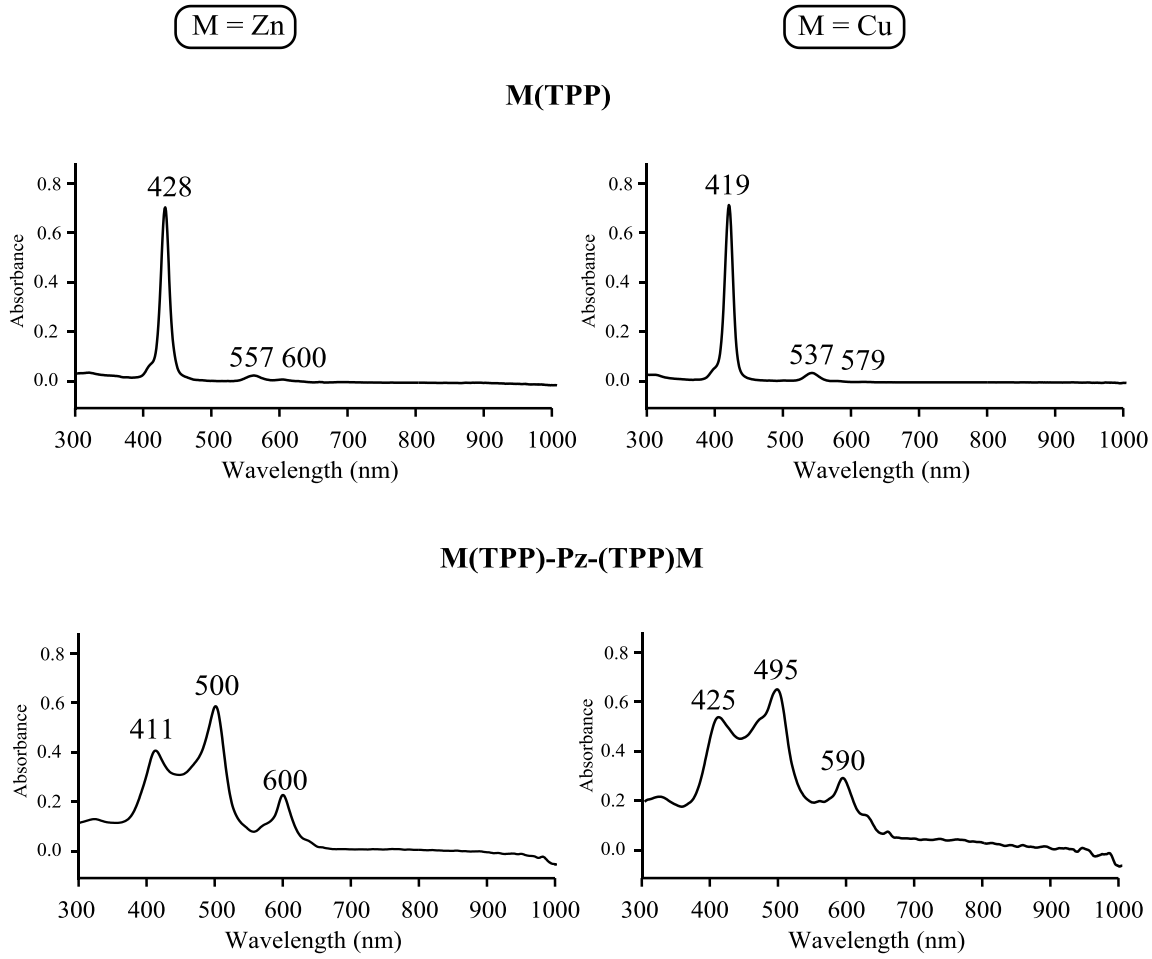

Figure 3-1. UV-vis spectra of M(TPP) and M(TPP)-Pz-(TPP)M in PhCN.

3.2.2 Electrochemistry

The electrochemistry of each M(TPP)-Pz-(TPP)M complex was characterized in PhCN containing 0.1 M TBAP. Cyclic voltammograms of the three bisporphyrins and reference M(TPP) compounds with the same central metal ions are shown in Figure 3-2, and a summary of half-wave potentials for each redox reaction is given in Table 3-2.

The M(TPP)-Pz-(TPP)M derivatives exhibit multiple reductions and oxidations in PhCN containing 0.1 M. Four reversible reductions are seen for Cu(TPP)-Pz-(TPP)Cu (Figure 3-2a) and three for Zn(TPP)-Pz-(TPP)Zn (Figure 3-2b). The first two one electron reductions are assigned as formation of a bisporphyrin monoanion radical, and bisporphyrin diradical as shown in Eqs 1a and 1b, while the next two reductions involve formation of the bisporphyrin with three and four added electrons, as written in Eqs 2a and 2b. The last two reductions of the Cu(II) bisporphyrin are well-separated ($E_{1/2}$ = -1.59 and -1.74 V) in PhCN, but the same processes (given by Eqs 2a and 2b) are overlapped in potential for the Zn(II) derivative as seen in Figure 3-2b.

$$\text{M(TPP)-Pz-(TPP)M} \overset{+\,e}{\rightleftharpoons} [\text{M(TPP)-Pz-(TPP)M}]^{-} \qquad (3\text{-}1a)$$

$$[\text{M(TPP)-Pz-(TPP)M}]^{-} \overset{+\,e}{\rightleftharpoons} [\text{M(TPP)-Pz-(TPP)M}]^{2-} \qquad (3\text{-}1b)$$

$$[\text{M(TPP)-Pz-(TPP)M}]^{2-} \overset{+\,e}{\rightleftharpoons} [\text{M(TPP)-Pz-(TPP)M}]^{3-} \qquad (3\text{-}2a)$$

$$[\text{M(TPP)-Pz-(TPP)M}]^{3-} \overset{+\,e}{\rightleftharpoons} [\text{M(TPP)-Pz-(TPP)M}]^{4-} \qquad (3\text{-}2b)$$

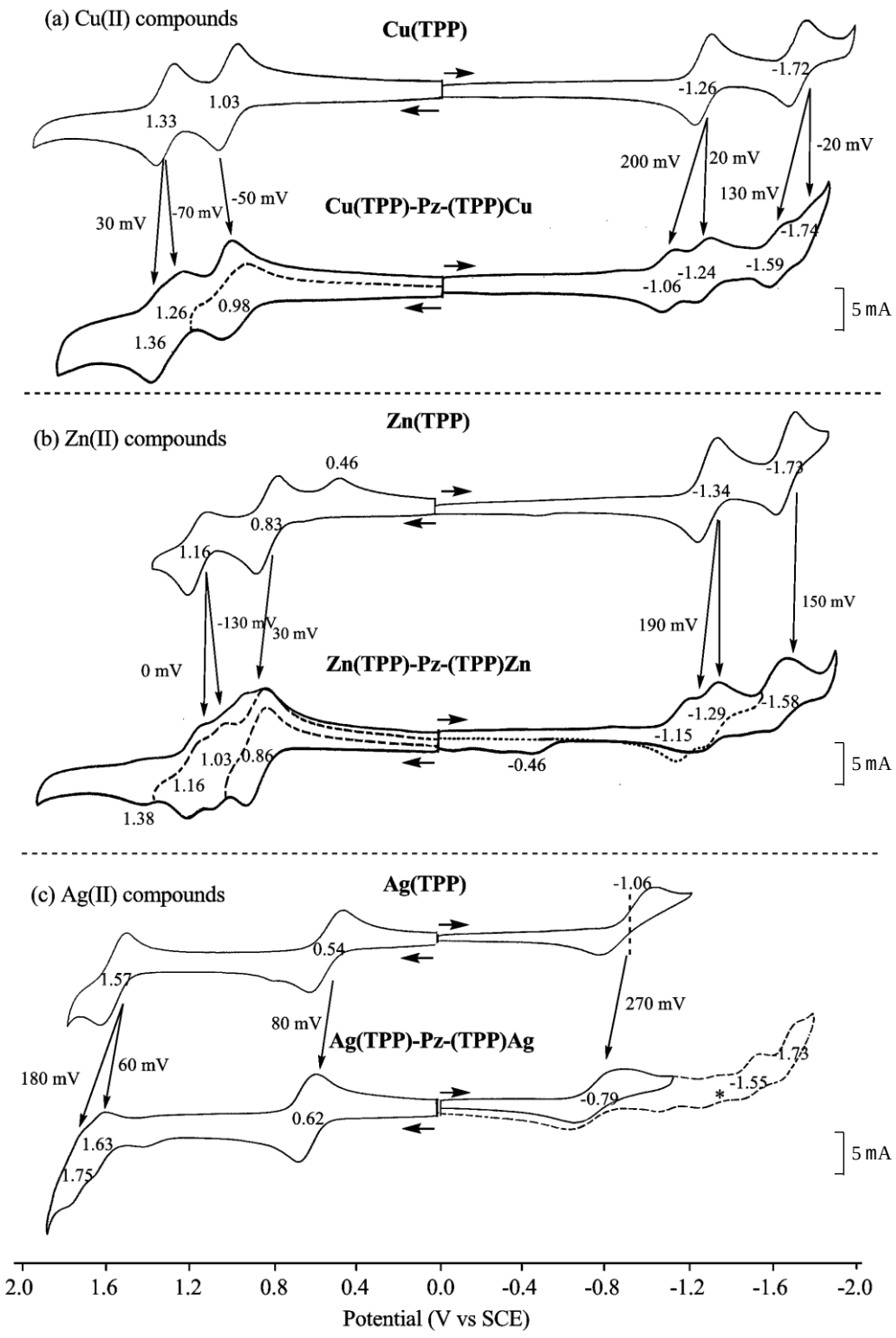

Figure 3-2. Cyclic voltammograms of M(TPP) and M(TPP)-Pz-(TPP)M in PhCN containing 0.1 M TBAP where M equals (a) Cu(II), (b) Zn(II) and (c) Ag(II).

Table 3-2. Half-wave potentials (V vs SCE) of porphyrins M(TPP)-Pz-(TPP)M, M(P)-TA-(P)M, M(P-TA) and M(TPP), where M = Zn, Cu, Ag and Co in different solvents containing 0.1 M TBAP.

Compound	Ring Oxidation			Ring Reduction				H-L Gap	ref
	2nd		1st	1st		2nd			
Cu(TPP)-Pz-(TPP)Cu	1.36	1.26	0.98	-1.06	-1.24	-1.59	-1.74	2.04	*tw*
Zn(TPP)-Pz-(TPP)Zn	1.16	1.03	0.86	-1.15	-1.29	-1.58	-1.58	2.01	*tw*
Ag(TPP)-Pz-(TPP)Ag	1.73	1.63	0.62[b]	-0.79[b]		-1.55	-1.73		*tw*
Cu(P)-TA-(P)Cu	1.20		1.00	-0.70	-1.18	-1.47	-1.92[a]	1.70	13
Zn(P)-TA-(P)Zn	1.04		0.84	-0.83	-1.33[a]	-1.48	-1.83[a]	1.67	13
Cu(P-TA)	1.19		1.01	-0.92		-1.37		1.93	13
Zn(P-TA)	1.04		0.84	-1.00		-1.40		1.84	13
Cu(TPP)	1.35		1.04	-1.27		-1.72		2.31	13
Zn(TPP)	1.18		0.83	-1.34		-1.78[a]		2.17	13
Ag(TPP)	1.57		0.54[b]	-1.06[b]		-1.67[c]			29
Pz				-2.07[d]					28
TA				-0.96[d,e]		-1.54[d,e]			28

[a]Irreversible peak potential at scan rate of 0.1 V/s; [b]Metal-centered reaction; [c]Data taken in pyridine; [d]Potentials reported in CH_3CN, 0.1 M TBAP vs an Ag/AgCl reference electrode; [e]Two overlapped one-electron transfers in single step.

The above four one-electron reductions of the Cu(II) and Zn(II) bisporphyrins can be compared with the two one-electron reductions of monometallic Cu(TPP) and Zn(TPP) to give porphyrin π anion radicals and dianions. The first reduction of the M(TPP) compounds is located at $E_{1/2}$ = -1.26 V (Cu) or -1.34 V (Zn) and the second at -1.72 or -1.73 V, respectively. Each ring-centered reduction of the monoporphyrin is split into two separate processes in the dyad, as shown in Figure 3-2 where, for example, the Cu(II) Pz complex is reversibly reduced at -1.06, -1.24, -1.59 and -1.74 V. The difference in $E_{1/2}$ between the first two sets of Cu(TPP)-Pz-(TPP)Cu reductions amounts to 180 and 150 mV, respectively, and a similar 140 mV separation in $\Delta E_{1/2}$ is seen between the first two reductions of the Zn pyrazine-linked dyad ($E_{1/2}$ = -1.15 and -1.29 V).

The 140-180 mV separation between $E_{1/2}$ values for Equations 1a and 1b is consistent with a moderate interaction between the two redox active macrocycles, but it is much less than the 480-500 separation between the first two reductions of Cu(P)-TA-(P)Cu and Zn(P)-TA-(P)Zn (see Table 3-2) where a strong interaction is observed.

Tetraazaanthracene (TA) has a larger π system than pyrazine (Pz) and it is also easier to reduce than Pz.[28] Thus one might expect to have a greater electron density on the linking TA group than on the linking Pz group of the singly reduced dyads. The TA-linked dyads should also be easier to reduce by a single electron than the Pz-linked dyads. In addition, the porphyrin dyads in both series should be easier to reduce than the unlinked M(TPP) derivatives in the same solvent. This is indeed the case, as seen in Table 3-2 where the $E_{1/2}$ values of the Cu(II) porphyrins follows the trend: -0.70 V (TA dyad) > -1.06 V (Pz dyad) > -1.27 V (Cu(TPP)). The same trend in $E_{1/2}$ for the first reduction is seen for the Zn(II) compounds, where $E_{1/2}$ follows the order: -0.83 V(TA

dyad) > -1.15 V (Pz dyad) > -1.37 V [Zn(TPP)]. Both sets of data suggested that the difference in electrochemical behavior between the two series of TA and Pz dyads is related to the electron density on the singly reduced compounds, which in the case of the TA-linked porphyrins is partially on the fused TA group, as described in an earlier publication.[13]

In contrast to what occurs for the fused TA and Pz dyads of Cu(II) and Zn(II), there is no splitting in $E_{1/2}$ values for the first reduction of Ag(TPP)-Pz-(TPP)Ag. This can be accounted for by the fact that the initial reduction of this porphyrin occurs not at the macrocycle or at the linked Pz group, but rather at the two Ag(II) metal ions, both of which accept one electron at the same half-wave potential of -0.79 V, thus indicating equivalent, but noninteracting redox centers. In this regard it should be noted that Ag(TPP)-Pz-(TPP)Ag is easier to reduce than Ag(TPP) by 270 mV and this positive shift of reduction potential can be accounted for by the extended π conjugation of the dyad formed upon fusion of the Pz group to the two TPP macrocycles.

The second reduction of Ag(TPP) could not be measured in PhCN due to demetalation but $E_{1/2}$ for the ring-centered reduction of $[Ag^{I}(TPP)]^{-}$ has been reported as -1.67 V in pyridine.[29] This potential is close to the average $E_{1/2}$ for the two, presumably ring-centered, one-electron reductions of Ag(TPP)-Pz-(TPP)Ag at -1.55 and -1.73 V in PhCN (see Figure 3-2). The peak current for each of the two ring-centered reductions is approximately half that of the Ag(II)/Ag(I) process of the dyad, consistent with two one-electron transfers, separated by 180 mV. A similar potential separation is seen between the first split ring centered reduction of the dyads with Cu(II) (180 mV) or Zn(II) (140 mV) metal ions. Also, as would be expected for the case of two equivalent interacting

redox centers, the first ring-centered reduction of $[Ag^{I}(TPP)\text{-}Pz\text{-}(TPP)Ag^{I}]^{2-}$ to give the "half reduced" dyad is easier than the potential for the ring-centered reduction of monomeric $[Ag^{I}(TPP)]^{-}$ under the same solution conditions.

Focusing further on the redox behavior of the Ag(II) dyad, it should be noted that the first oxidation of Ag(TPP)-Pz-(TPP)Ag at $E_{1/2}$ = 0.62 V is shifted positively from the $E_{1/2}$ of 0.54 V for oxidation of Ag(TPP) and this process is unsplit like the reduction. This lack of splitting is attributed to the site of electron transfer, which involves the two Ag(II) metal ion to give a bis-Ag(III) bisporphyrin. The peak current for the metal-centered oxidation of Ag(TPP)-Pz-(TPP)Ag in PhCN is equal to the peak current for the metal-centered reduction (see CV in Figure 3-2), thus indicating a transfer of two electrons in each process as shown by Equations 3-3 and 3-4.

$$Ag^{II}(TPP)\text{-}Pz\text{-}(TPP)Ag^{II} \overset{+\,2e}{\rightleftharpoons} [Ag^{I}(TPP)\text{-}Pz\text{-}(TPP)Ag^{I}]^{2-} \qquad (3\text{-}3)$$

$$Ag^{II}(TPP)\text{-}Pz\text{-}(TPP)Ag^{II} \overset{-\,2e}{\rightleftharpoons} [Ag^{III}(TPP)\text{-}Pz\text{-}(TPP)Ag^{III}]^{2+} \qquad (3\text{-}4)$$

Finally, it should be pointed out that the first ring-centered oxidation of Ag(TPP)-Pz-(TPP)Ag occurs in two steps (at $E_{1/2}$ = 1.63 and 1.75 V), which are separated by 120 mV. Similar separations are observed for the second ring-centered oxidation of Cu(TPP)-Pz-(TPP)Cu (100 mV) and Zn(TPP)-Pz-(TPP)Zn (130 mV). Thus, the +2 charge on the porphyrin may to be related to the splitting and the redox processes for oxidation of the three dyads can be written as shown in Equations 3-5, 3-6a and 3-6b, where the overall charges on the porphyrin are +2, +3 and +4, respectively.

$$M(TPP)\text{-}Pz\text{-}(TPP)M \overset{-2e}{\rightleftharpoons} [M(TPP)\text{-}Pz\text{-}(TPP)M]^{2+} \quad (3\text{-}5)$$

$$[M(TPP)\text{-}Pz\text{-}(TPP)M]^{2+} \overset{-e}{\rightleftharpoons} [M(TPP)\text{-}Pz\text{-}(TPP)M]^{3+} \quad (3\text{-}6a)$$

$$[M(TPP)\text{-}Pz\text{-}(TPP)M]^{3+} \overset{-e}{\rightleftharpoons} [M(TPP)\text{-}Pz\text{-}(TPP)M]^{4+} \quad (3\text{-}6b)$$

3.2.3 Spectroelectrochemical Monitoring of Reduction and Oxidation Products

M(TPP)-Pz-(TPP)M, M = Zn or Cu. UV-visible spectra obtained during controlled potential reduction of Zn(TPP)-Pz-(TPP)Zn in PhCN containing 0.1 M TBAP are shown in Figure 3-3. The neutral Zn(II) bisporphyrin has a split Soret band at 411 and 500 nm and single strong Q band at 600 nm. All three peaks decrease in intensity during the first reduction by one electron (Eq 1a) as a new peak grows in at 446 nm, along with a broad band at 720 nm (Figure 3-3a). Further reduction of the "half reduced" $[Zn(TPP)\text{-}Pz\text{-}(TPP)Zn]^{-}$ dyad at a controlled potential at -1.50 V leads to the bisporphyrin $[Zn(TPP)\text{-}Pz\text{-}(TPP)Zn]^{2-}$, which is assigned as a bis-anion radical (Eq 1b). This spectrum is seen in the lower half of Figure 3-3 and is characterized by bands at 438, 508, 720 and 885 nm. A very similar UV-visible spectrum is seen after reduction of Zn(TPP) to its π anion radical form at a controlled potential of -1.50 V. This spectrum has bands at 439, 638 and 887 nm (Figure 3-3), but lacks the 508 nm band, which is present in the reduced Zn(II) dyad, but not in the reduced Zn(II) monoporphyrin π anion radical.

Similar UV-visible bands are also seen in the spectra of electrogenerated $[Zn(TPP)\text{-}Pz\text{-}(TPP)Zn]^{2+}$ and $[Zn(TPP)]^{+}$. These spectra are shown in Figure 3-4. The oxidized dyad, which has lost two electrons, has bands at 413 and 500 nm and a broad band between 600 and 900 nm (Figure 3-4a). The monoporphyrin π-cation radical has bands at 415 and 458 nm and a broad band between 550 and 750 nm. The major

difference between the two spectra is the intensity of the band at 500 nm for the oxidized dyad.

Ag(TPP)-Pz-(TPP)Ag The first reduction and first oxidation of Ag(TPP)-Pz-(TPP)Ag were monitored by thin-layer spectroelectrochemistry in PhCN. The spectral changes observed during reduction are shown in Figure 3-5a and those during oxidation in Figure 3-5b. The spectrum of the neutral Ag(II) bisporphyrin is characterized by a split Soret band at 415/489 nm and a strong Q band at 578 nm. This spectrum is similar to that of the Cu(II) and Zn(II) bisporphyrins as seen in Table 3-1.

All three absorption bands of Ag(TPP)-Pz-(TPP)Ag decrease in intensity during the first controlled potential reduction at -1.05 V as a new peak for the reduced dyad grows in at 446 nm (Figure 3-5a). No major absorbances are seen between 700 and 1000 nm, consistent with the site of electron addition being located at the two metal ions and not at the conjugated macrocycles. The spectral changes in Figure 3-5a are different than those reported for reduction of Ag(TPP),[29] consistent with a strong interaction between the two Ag(I) metallomacrocycles.

The spectral changes associated with conversion of Ag(TPP)-Pz-(TPP)Ag to $[Ag(TPP)-Pz-(TPP)Ag]^{2+}$ are illustrated in Figure 3-5b. The bis-Ag(II) bisporphyrin is characterized by bands at 415, 489 and 578 nm. The 415 nm band remains unchanged upon the abstraction of two electrons and conversion of Ag(II) to Ag(III) and while the 489 nm band shifts to 461 nm and the 578 nm band shifts to 637 nm. There are no absorptions from 700-1000 nm consistent with a metal-centered electron transfer.

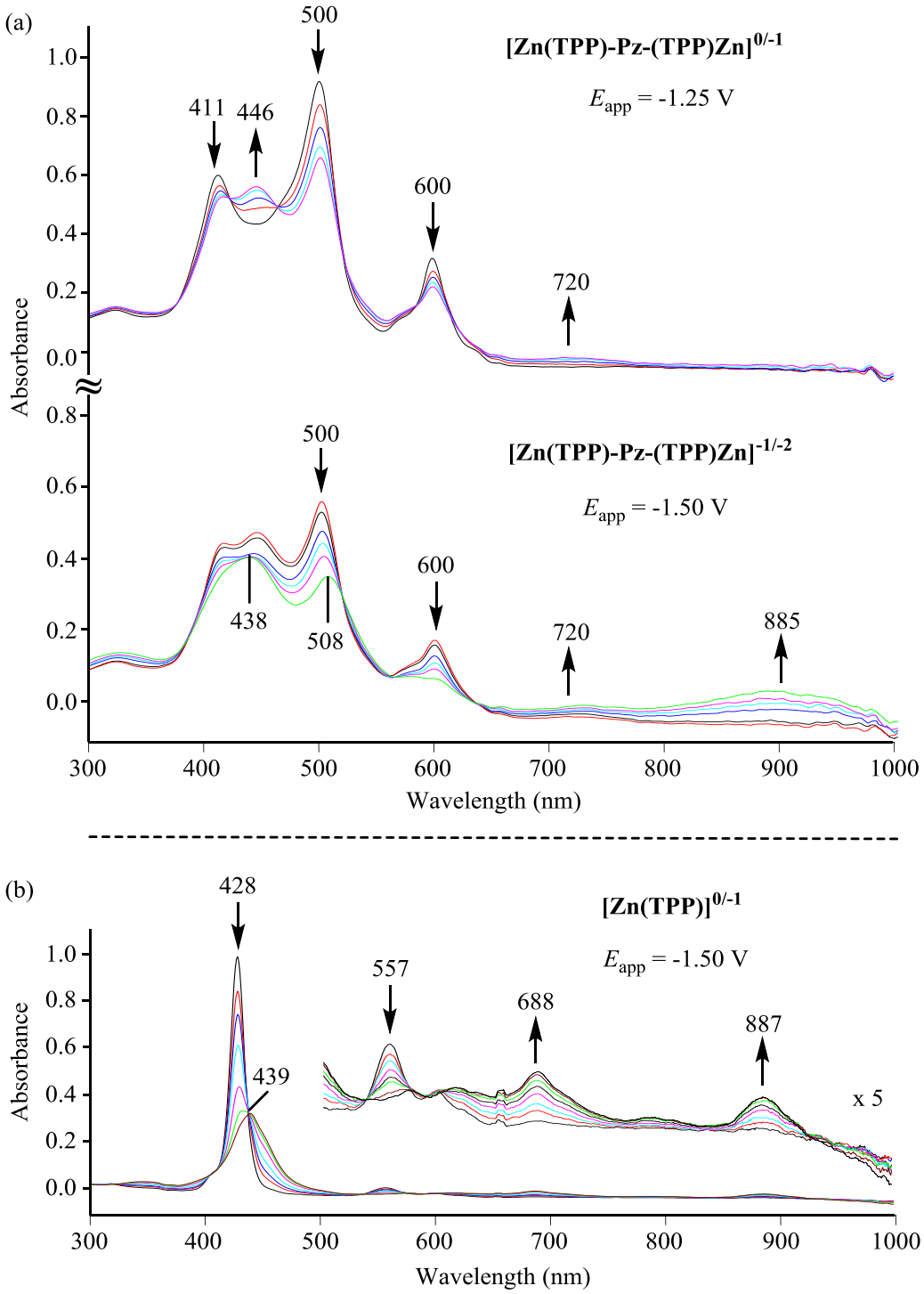

Figure 3-3. UV-visible spectral changes during the controlled potential reduction of (a) Zn(TPP)-Pz-(TPP)Zn and (b) Zn(TPP) in PhCN, 0.1 M TBAP.

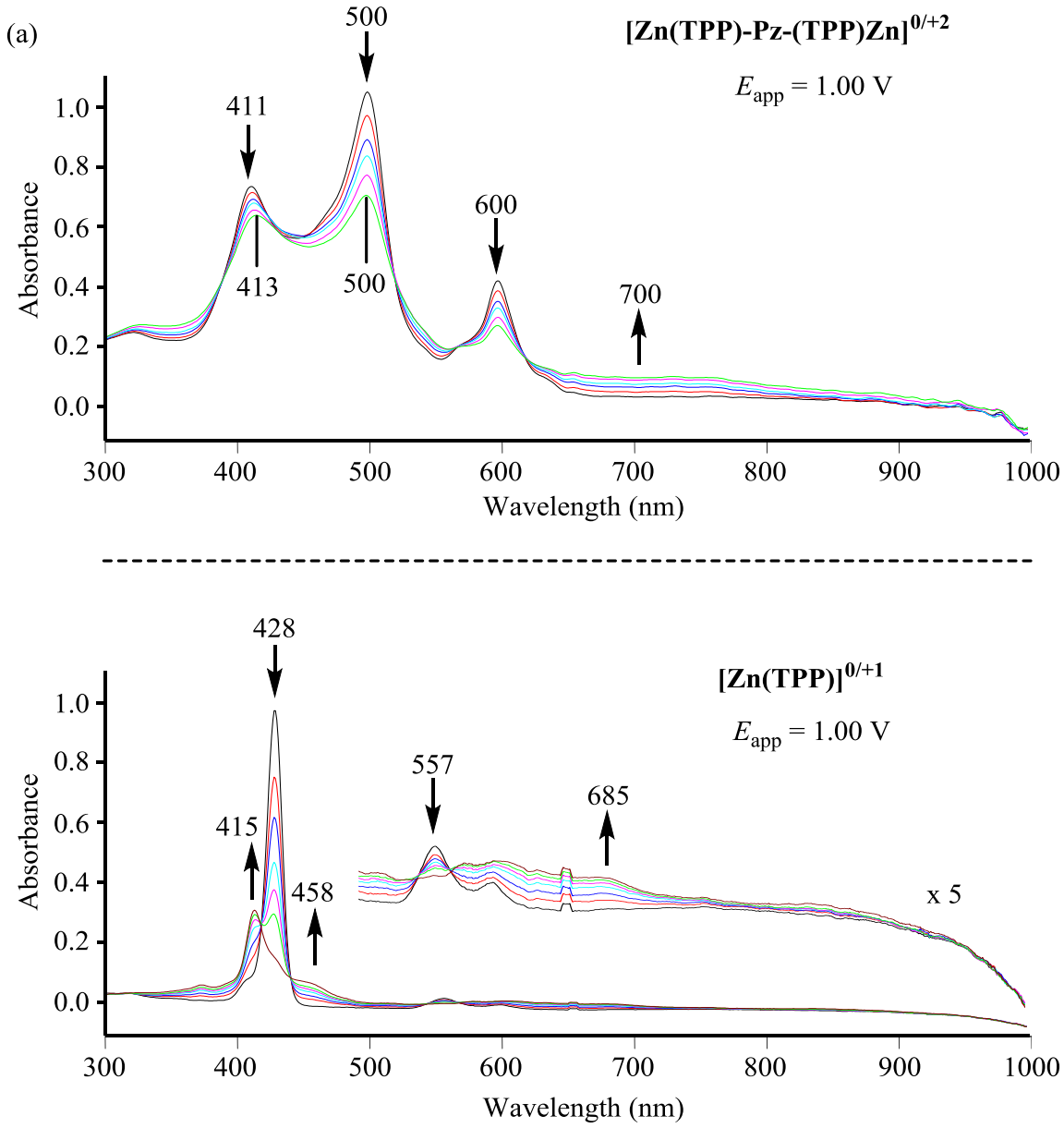

Figure 3-4. UV-visible spectral changes during the controlled potential oxidation of (a) Zn(TPP)-Pz-(TPP)Zn and (b) Zn(TPP) in PhCN, 0.1 M TBAP.

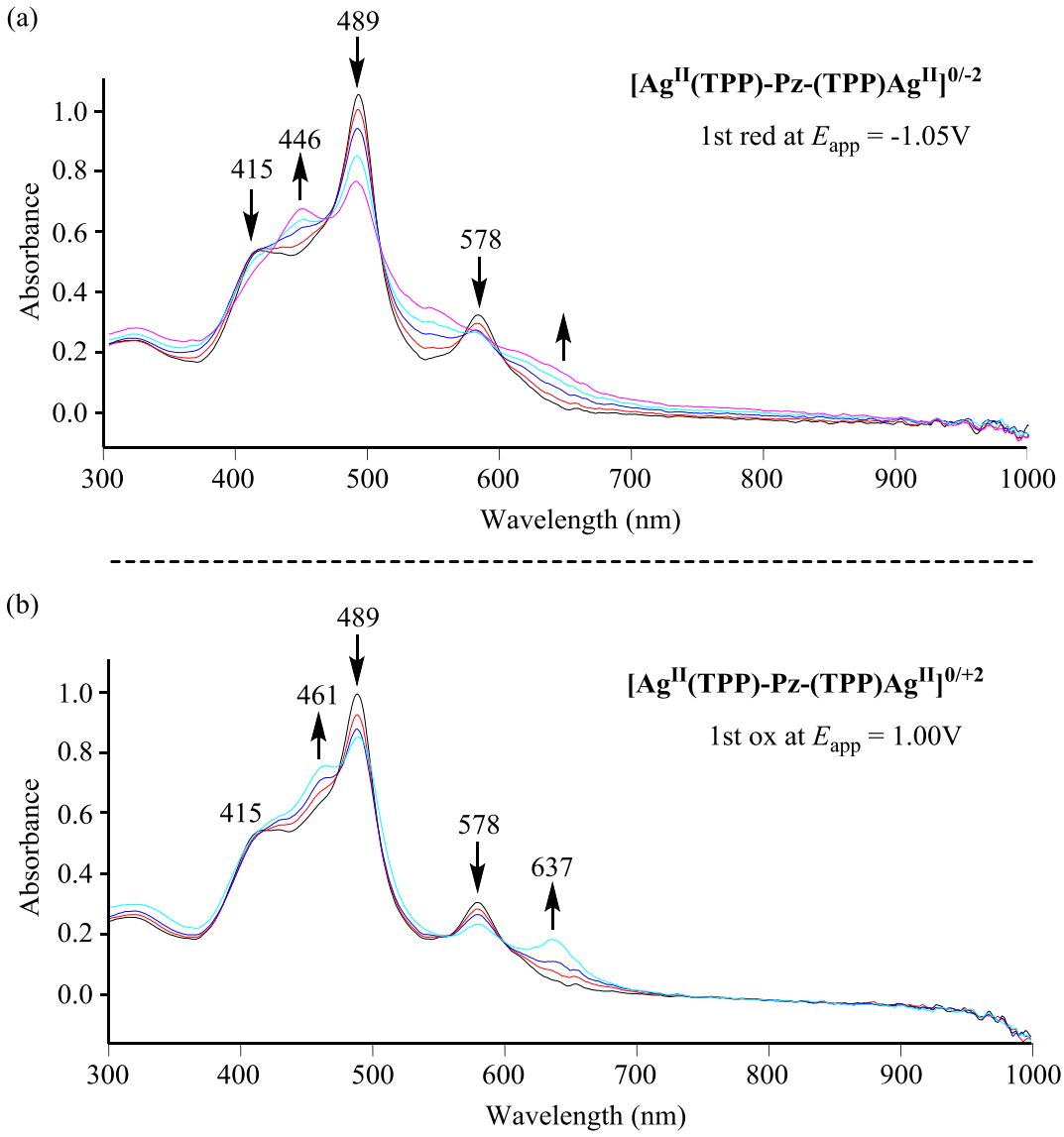

Figure 3-5. UV-visible spectral changes for Ag(TPP)-Pz-(TPP)Ag during controlled potential (a) reduction and (b) oxidation in PhCN, 0.1 M TBAP.

3.3 Conclusions

In summary, the linking of two porphyrins by a fused pyrazine group leads to a splitting of reduction potentials for ring centered reactions, but not for reduction at the central metal ion that occurs in the case of the Ag(II) bisporphyrin. The difference between the two $E_{1/2}$ values for formation of the half reduced and fully reduced macrocycle of the dyad ranges from 140-180 mV, consistent with a moderate interaction between the two redox active π ring systems of the bisporphyrins. There is no significant difference in $\Delta E_{1/2}$ with changes in the metal ion (Cu^{II}, Zn^{II} or Ag^{II}), and also seems to be the case for the TA-linked dyads of Cu^{II} and Zn^{II}, which show a very large interaction between the two equivalent redox active macrocycles, as indicated by a $\Delta E_{1/2}$ between the split redox processes of close to 500 mV (see Table 3-2).

The fused Pz and TA linking groups are both electroactive in the absence of a fused porphyrin, with $E_{1/2}$ values being reported as -2.07 and -0.96 V vs Ag/AgCl,[28] respectively. Because TA itself is easier to reduce than any of the three investigated monoporphyrins (Table 3-2), the location of the first added electron in the TA-linked bisporphyrins should be located on the linker far more than in the case of the Pz group of the M(TPP)-Pz-(TPP)M derivatives. No separation in half wave potentials is observed for the reduction at the two metal centers of Ag(TPP)-Pz-(TPP)Ag and this is consistent with the added electron being on the metal center and not on the fused linking Pz group.

As earlier indicated, the ease of the first reduction for the metalloporphyrins in Table 2 follows the order: M(P)-TA-(P)M > M(P-TA) > M(TPP)-Pz-(TPP)M > M(TPP). As also seen in this table, the easier the ring-centered reduction of the metalloporphyrin, the smaller the HOMO-LUMO gap, which ranges from 1.67 to 2.31 V as shown in Figure

3-6. No splitting of the redox processes are seen for the first oxidation of the three examined M(TPP)-Pz-(TPP)M compounds. However, the second oxidation of each bisporphyrin is split into two processes, with $\Delta E_{1/2}$ values ranging from 100 to 130 mV for the reactions given by Equations 3-5 and 3-6. Finally, it should be noted that a plot of $E_{1/2}$ for the first reduction of M(TPP)-Pz-(TPP)M vs $E_{1/2}$ for the first reduction of M(TPP) in PhCN is linear with a slope of 1.23 and a correlation coefficient of 0.99 (see Figure 3-7). The larger than unity slope of 1.23 indicates that the degree of interaction between the macrocycles of M(TPP)-Pz-(TPP)M upon reduction depends upon the type of central metal ion.

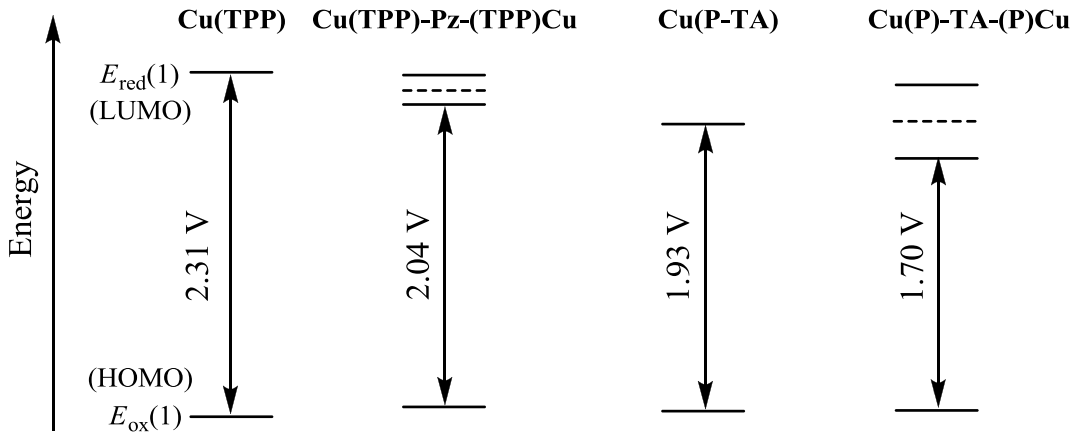

Figure 3-6. Measured HOMO-LUMO gap for related Cu(II) porphyrins in PhCN, containing 0.1 M TBAP.

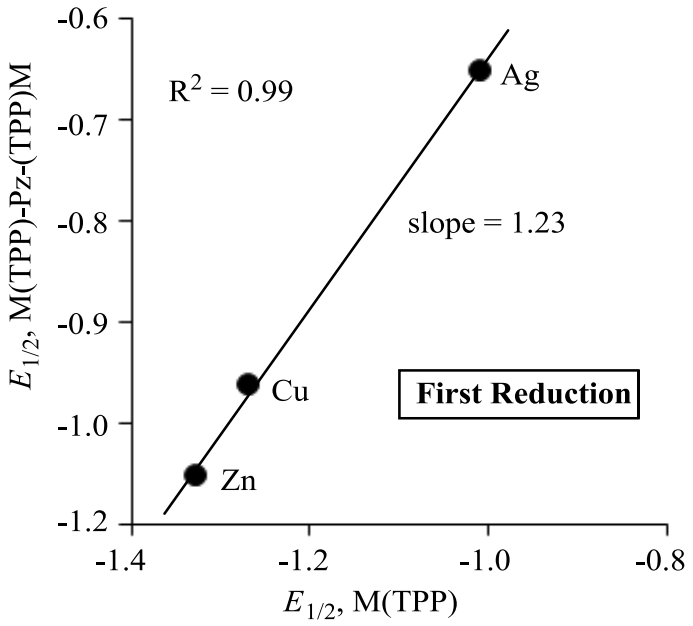

Figure 3-7 Correlation of reduction potential between M(TPP) and M(TPP)-Pz-(TPP)M.

3.4 References

(1) Martinez-Diaz, V. M.; Torres, T. In *Handbook of Porphyrin Science*; Kadish, K. M., Smith, K. M., Guilard, R., Eds.; World Scientific: Signapore, 2010; Vol. 10, p 141-181.

(2) Duclairoir, F.; Marchon, J.-C. In *Handbook of Porphyrin Science*; Kadish, K. M., Smith, K. M., Guilard, R., Eds.; World Scientific: Signapore, 2010; Vol. 10, p 245-311.

(3) Ethirajan, M.; Patel, N. J.; Pandey, R. K. In *Handbook of Porphyrin Science*; Kadish, K. M., Smith, K. M., Guilard, R., Eds.; World Scientific: Signapore, 2010; Vol. 4, p 249-323.

(4) Lewtak, J. P.; Gryko, D. T. *Chem. Commun. (Cambridge, U. K.)* **2012**, *48*, 10069-10086.

(5) Sintic, P. J.; E, W.; Ou, Z.; Shao, J.; McDonald, J. A.; Cai, Z.-L.; Kadish, K. M.; Crossley, M. J.; Reimers, J. R. *Phys. Chem. Chem. Phys.* **2008**, *10*, 268-280.

(6) Armstrong, R. S.; Foran, G. J.; Hough, W. A.; D'Alessandro, D. M.; Lay, P. A.; Crossley, M. J. *Dalton Trans.* **2006**, 4805-4813.

(7) Crossley, M. J.; Sintic, P. J.; Walton, R.; Reimers, J. R. *Org. Biomol. Chem.* **2003**, *1*, 2777-2787.

(8) Sendt, K.; Johnston, L. A.; Hough, W. A.; Crossley, M. J.; Hush, N. S.; Reimers, J. R. *J. Am. Chem. Soc.* **2002**, *124*, 9299-9309.

(9) Reimers, J. R.; Hall, L. E.; Crossley, M. J.; Hush, N. S. *J. Phys. Chem. A* **1999**, *103*, 4385-4397.

(10) Chou, J.-H.; Nalwa, H. S.; Kosal, M. E.; Rakow, N. A.; Suslick, K. S. In *The Porphyrin Handbook*; Kadish, K. M., Smith, K. M., Guilard, R., Eds.; Academic Press: San Diego, 2000; Vol. 6, p 45-118.

(11) Malinski, T. In *The Porphyrin Handbook*; Kadish, K. M., Smith, K. M., Guilard, R., Eds.; Academic Press: San Diego, 2000; Vol. 6, p 231-256.

(12) Kadish, K. M.; Ou, Z.; Zhan, R.; Khoury, T.; E, W.; Crossley, M. J. *J. Porphyrins Phthalocyanines* **2010**, *14*, 866-876.

(13) Ou, Z.; Zhu, W.; Sintic, P. J.; Fang, Y.; Crossley, M. J.; Kadish, K. M. *J. Porphyrins Phthalocyanines* **2012**, *16*, 674-684.

(14) Fukuzumi, S.; Ohkubo, K.; Zhu, W.; Sintic, M.; Khoury, T.; Sintic, P. J.; E, W.; Ou, Z.; Crossley, M. J.; Kadish, K. M. *J. Am. Chem. Soc.* **2008**, *130*, 9451-9458.

(15) Zhu, W.; Sintic, M.; Ou, Z.; Sintic, P. J.; McDonald, J. A.; Brotherhood, P. R.; Crossley, M. J.; Kadish, K. M. *Inorg. Chem.* **2010**, *49*, 1027-1038.

(16) Kadish, K. M.; Van Caemelbecke, E.; Royal, G. In *The Porphyrin Handbook*; Kadish, K. M., Smith, K. M., Guilard, R., Eds.; Academic Press: New York, 2000; Vol. 8, p 1-114.

(17) Davis, N. K. S.; Pawlicki, M.; Anderson, H. L. *Org. Lett.* **2008**, *10*, 3945-3947.

(18) Davis, N. K. S.; Thompson, A. L.; Anderson, H. L. *Org. Lett.* **2010**, *12*, 2124-2127.

(19) Mandoj, F.; Nardis, S.; Pudi, R.; Lvova, L.; Fronczek, F. R.; Smith, K. M.; Prodi, L.; Genovese, D.; Paolesse, R. *Dyes Pigm.* **2013**, *99*, 136-143.

(20) Kadish, K. M.; Guo, N.; Van Caemelbecke, E.; Paolesse, R.; Monti, D.; Tagliatesta, P. *J. Porphyrins Phthalocyanines* **1998**, *2*, 439-450.

(21) Guilard, R.; Jerome, F.; Barbe, J.-M.; Gros, C. P.; Ou, Z.; Shao, J.; Fischer, J.; Weiss, R.; Kadish, K. M. *Inorg. Chem.* **2001**, *40*, 4856-4865.

(22) Chen, P.; Lau, H.; Habermeyer, B.; Gros, C. P.; Barbe, J.-M.; Kadish, K. M. *J. Porphyrins Phthalocyanines* **2011**, *15*, 467-479.

(23) Barbe, J.-M.; Habermeyer, B.; Khoury, T.; Gros, C. P.; Richard, P.; Chen, P.; Kadish, K. M. *Inorg. Chem.* **2010**, *49*, 8929-8940.

(24) Guilard, R.; Gros, C. P.; Barbe, J.-M.; Espinosa, E.; Jerome, F.; Tabard, A.; Latour, J.-M.; Shao, J.; Ou, Z.; Kadish, K. M. *Inorg. Chem.* **2004**, *43*, 7441-7455.

(25) Kadish, K. M.; Ou, Z.; Shao, J.; Gros, C. P.; Barbe, J.-M.; Jerome, F.; Bolze, F.; Burdet, F.; Guilard, R. *Inorg. Chem.* **2002**, *41*, 3990-4005.

(26) Ngameni, E.; Laouenan, A.; L'Her, M.; Hinnen, C.; Hendricks, N. H.; Collman, J. P. *J. Electroanal. Chem. Interfacial Electrochem.* **1991**, *301*, 207-226.

(27) Guilard, R.; Brandes, S.; Tardieux, C.; Tabard, A.; L'Her, M.; Miry, C.; Gouerec, P.; Knop, Y.; Collman, J. P. *J. Am. Chem. Soc.* **1995**, *117*, 11721-11729.

(28) Fogel, Y.; Kastler, M.; Wang, Z.; Andrienko, D.; Bodwell, G. J.; Muellen, K. *J. Am. Chem. Soc.* **2007**, *129*, 11743-11749.

(29) Kadish, K. M.; Lin, X. Q.; Ding, J. Q.; Wu, Y. T.; Araullo, C. *Inorg. Chem.* **1986**, *25*, 3236-3242.

Chapter Four

A Rare Class of Uncharged Highly Water-Soluble Homo/Heteropentametallic Porphyrazine Macrocycles: Electrochemistry and Spectroelectrochemistry

4.1 Introduction

Phthalocyanines (tetrabenzoporphyrazines) are porphyrin-like macrocycles used in a variety of technological and biomedical applications.[1] Characterized by strong thermal resistance to skeletal degradation, the phthalocyanines offer an advantage over the structurally related porphyrins in that they possess highly intense extinction coefficients in a region of the spectrum (600-800 nm) which is of utmost importance in the area of photodynamic therapy (PDT), a well known anticancer curative modality.[2-6] In addition to phthalocyanines, alternative families of porphyrazines have attracted increasing attention in recent years.[7,8] Phthalocyanines and porphyrazines are normally only slightly soluble in nonaqueous solvents and they are virtually insoluble in water. This lack of solubility has presented a serious drawback to characterizing the compounds in solution and has also limited their use for applications in the fields of biochemistry and medicine. Thus, in order to solve the problem of insolubility, extensive efforts have been directed towards the syntheses of multiply charged cationic and anionic phthalocyanines, which are water soluble.[9] Some of these charged macrocycles have led to important advances in PDT, although aggregation was often still a problem, which severely hindered the use of these macrocycles in many applications. Interestingly, neutral water soluble phthalocyanines bearing external chains of polyethylene glycol residues, carbohydrate groups or polyhydroxylated substituents are also known,[9] but for most of these compounds, their solubility in water and aspects of their possible applications still remains a point to be further examined.

Unlike phthalocyanines, the synthesis of water-soluble porphyrazines in the past was initially limited to cationic pyridino- or pyrazinoporphyrazines,[10] and this was

followed by preparation of octacationic porphyrazines bearing external N-methylated 4-pyridyl groups which are soluble in water over a wide range of pH.[11] Despite the presence of aggregation, the pyrazinoporphyrazine Zn^{II} octacation $[(CH_3)_8LZn]^{8+}$ (Chart 4-1a) and the Zn^{II}/Pt^{II} hexacation $[(PtCl_2)(CH_3)_6LZn]^{6+}$ (Chart 4-1b) were reported to interact in their monomeric form in water solution with a telomeric G-quadruplex structure[12,13] and with B-DNA,[14] thus providing multimodal anticancer potentialities.

Prior to the work described in this thesis, the electrochemistry of porphyrazine had been limited to studies in non-aqueous media due to insolubility and known aggregation of the compounds in water. However, the problem of porphyrazine insolubility in water has been addressed by the synthesis of a new series of pentanuclear "pyrazinoporphyrazine" macrocycles represented as $[\{Pd(OAc)_2\}_4LM]$, where M = $Mg^{II}(H_2O)$, Zn^{II}, Cu^{II}, Co^{II}, Pd^{II}, Pt^{II} and L = tetrakis-2,3-[5,6-di(2-pyridyl)pyrazino]porphyrazinato dianion. These compounds provided by our collaborator Dr. Maria Pia Donzello and Dr. Claudio Ercolani in Rome, Italy were obtained from the mononuclear species [LM] by exocyclic coordination of four $Pd(OAc)_2$ units (Chart 4-2). Preparative procedures for synthesizing the different metal derivatives and their general physicochemical and redox behavior are described in this chapter. Their potential for applications, with attention centered on their photoactive properties is also considered. It should be emphasized that these new species represent a rare example of neutral porphyrazine macrocycles which exhibit higher water solubility (ca. 10^{-3}-10^{-4} M) than what is found for the above mentioned octacationic and hexacationic species (ca. 10^{-4}-10^{-5} M). In addition, the $[\{Pd(OAc)_2\}_4LM]$ complexes are present in aqueous solution

almost exclusively in their monomeric form, which is quite a remarkable feature for uncharged porphyrazine compounds.

4.2 Results and Discussion

4.2.1 Synthetic Aspects and Properties

The pentanuclear species [{$Pd(OAc)_2$}$_4$LM] (M = $Mg^{II}(H_2O)$, Zn^{II}, Cu^{II}, Co^{II}, Pd^{II}, Pt^{II}) were synthesized by reaction of the respective mononuclear complex [LM] with $Pd(OAc)_2$ in DMSO at 50 ℃ for 3 h (see Experimental Section), a longer reaction time (24 h) being required exclusively for the complete formation of the product with a central Pt^{II} ion. All the species were obtained as air stable, hydrated dark-green/blue solid species in fairly good yield (80-90%), although the yield was lower (50%) for Pt^{II} derivative.

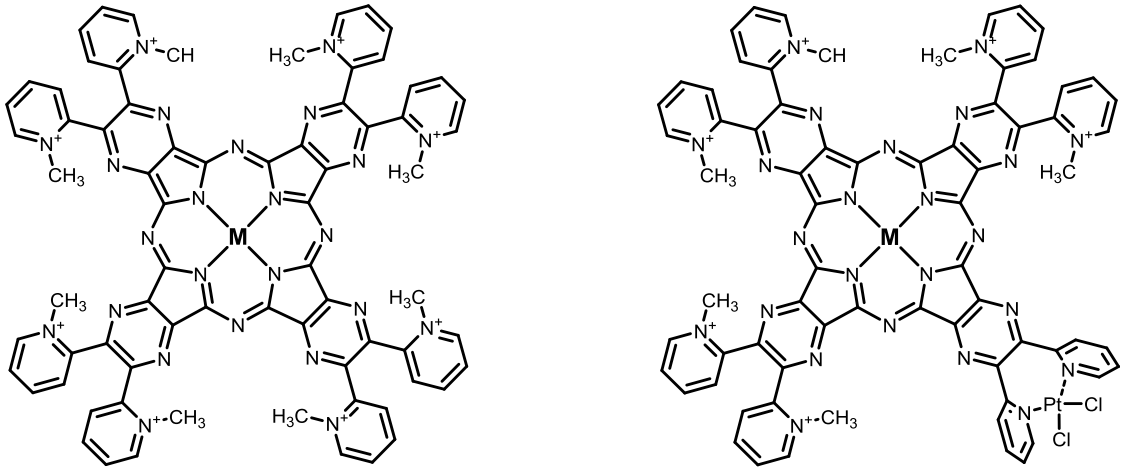

(a) **(b)**

Chart 4-1. Schematic formulations of the Zn^{II} octacation $[(CH_3)_8LZn]^{8+}$ and the Zn^{II}/Pt^{II} hexacation $[(PtCl_2)(CH_3)_6LZn]^{6+}$ (both neutralized by I^- ions).

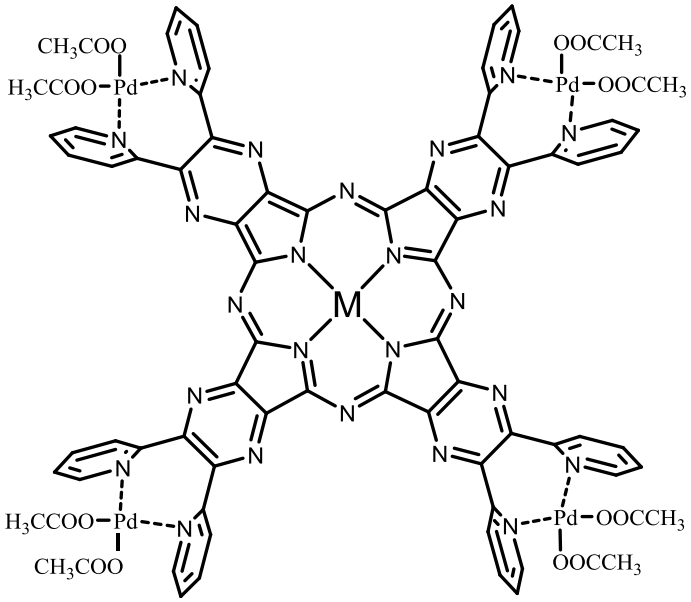

Chart 4-2. Structures of [{Pd(OAc)$_2$}$_4$LM] (M = Mg^{II}(H$_2$O), Zn^{II}, Cu^{II}, Co^{II}, Pd^{II}, Pt^{II}).

The Mg^{II} complex is formulated with one water molecule directly ligated to the central metal ion, in line with a similar formulation for the precursor complex [$LMg(H_2O)$].[15] The presence of such a water molecule in both species is difficult to be proved directly since unsuccessful were attempts to obtain single crystals suitable for X-ray elucidation. Nevertheless, its presence is implied by the fact that the $Mg^{II}(H_2O)$ moiety is commonly observed in Mg^{II} porphyrazine macrocycles. Examples are given by the structures of (aquo)(octakis(methylthio)porphyrazinato)-magnesium(II), [(omtp)$Mg(H_2O)$][16] and [$PcMg(H_2O)]_2Py$[17] (Pc = phthalocyaninato dianion, $C_{32}H_{16}N_8^{2-}$). Additional support for the mono-aquo moiety $Mg(H_2O)$ is given by its presence in the Mg^{II} complexes of the tetrakis(thia/selenodiazole)porphyrazines[18] and tetrakis-2,3-(5,7-diphenyl-6*H*-diazepino)porphyrazine.[19] Interestingly, a Mg^{II} bis-hydrate, [$PcMg(H_2O)_2$], has also been reported[20] and a dimerized monohydrate of a low-symmetry porphyrazine macrocycle has been structurally elucidated,[21] both examples again proving the tendency of Mg^{II}, present in the cavity of a porphyrazine macrocycle, to coordinate water molecules.

The IR spectrum of the Zn^{II} complex [$\{Pd(OAc)_2\}_4LZn$] in the range 1800-600 cm^{-1} is illustrated in Figure 4-1a, together with the spectrum of the corresponding tetrapalladated species [$(PdCl_2)_4LZn$] and the monometallic complex [LZn] (Figure 4-1b and 4-1c, respectively). The spectrum of [$\{Pd(OAc)_2\}_4LZn$] shows a medium-to-low intensity absorption at 957 cm^{-1}, also present, with higher intensity, in the spectra of the parent species [$(PdCl_2)_4LZn$] and [LZn] (954 cm^{-1}). The conversion of the monometallic species [LM] to the complexes carrying external $Pd(OAc)_2$ or $PdCl_2$ units results in a disappearance of the absorption at 994 cm^{-1}, which is present in all of the monometalated

analogs. This absorption can be used as a reference peak to monitor the formation of the pentanuclear species. The spectrum of [{$Pd(OAc)_2$}$_4$LZn] (Figure 4-1a) also shows a strong broad peak centred at ca. 1590 cm^{-1} and a peak of lower intensity is observed at ca. 1400 cm^{-1}. Both absorptions are due to the presence of the acetate groups, and assigned as $\nu_{C=O}$ and ν_{C-O}, respectively.

Similarly informative were found the IR spectral data for the parallel triads of macrocycles [{$Pd(OAc)_2$}$_4$LM], [$(PdCl_2)_4$LM] and [LM] (M = $Mg^{II}(H_2O)$, Cu^{II}, Co^{II}, Pd^{II}, Pt^{II}).

4.2.2 UV-visible Spectra

The [{$Pd(OAc)_2$}$_4$LM] complexes (M = $Mg^{II}(H_2O)$, Zn^{II}, Cu^{II}, Co^{II}, Pd^{II}, Pt^{II}), are insoluble in organic non donor solvents (CH_2Cl_2, $CHCl_3$) and scarcely soluble in the polar solvents pyridine, DMSO and DMF (c = 10^{-4} ~ 10^{-5} M). In each of these latter solvents, the macrocycles generally appear to be stable in solution, as indicated by a constant UV-visible spectrum over time (24~48 h). Interestingly, all of the compounds exhibit good solubility in water, with relatively high concentrations obtained for the saturated solution (c = 10^{-3} ~ 10^{-4} M), something rarely encountered for other neutral porphyrazine macrocycles.

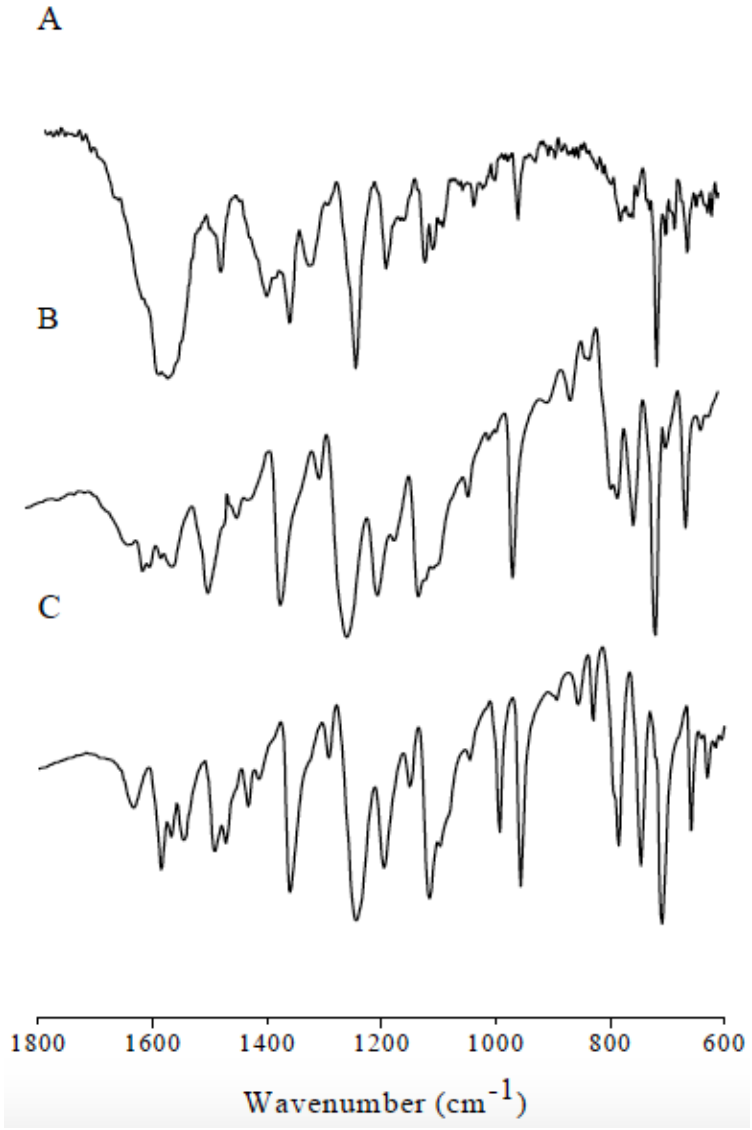

Figure 4-1. IR spectra in KBr of A) [{$Pd(OAc)_2$}$_4$LZn], B) [($PdCl_2$)$_4$LZn], C) [LZn].

The UV-visible spectra of the [{$Pd(OAc)_2$}$_4$LM] complexes in pyridine, DMSO, and DMF all show similar clean profiles, with absorptions in the Soret region (340-450 nm) and sharp narrow Q bands in the region of 620-670 nm, these latter bands being accompanied by vibrational peaks at higher energies. These spectra clearly indicate that the compounds are in their monomeric form (see spectrum for the Zn^{II} complex in DMSO in Figure 4-2a, red line), approaching closely spectra of related monomeric phthalocyanine or porphyrazine macrocycles, with the main peaks attributable to ligand-centered π - π^* transitions. Worthy of notice, the currently investigated compounds remain stable in pyridine solutions for 2-4 days. This behavior is different from what occurs in the same solvent for the parent complexes carrying externally bound $PdCl_2$ groups, i.e., [$(PdCl_2)_4$LM], where detachment of the external $PdCl_2$ units occurs immediately after dissolution, with consequent formation of the corresponding [LM] species.[22,23] Moreover, it has been observed that among the present species, those carrying the central Zn^{II}, Pd^{II} and Pt^{II} ions, when dissolved in DMF at c $\approx 10^{-5}$ M or lower, tend to undergo a one-electron reduction to their corresponding -1 charged species. This behavior parallels what was previously reported for the related [$(PdCl_2)_4$LM] species (M = Pd^{II}, Co^{II}, Cu^{II}).[24,25] It was verified that a reducing agent, present in trace amounts in DMF (ca. 10^{-5} M) is able to bring the species to their one-electron reduced state. Reoxidation of the generated monoanions to the corresponding neutral species could be accomplished in DMF upon addition of a slight excess of HCl to solution (c = 1 x 10^{-4} M, approximately ten times the concentration of the macrocycle) to the solutions. Noteworthy, dissolution of the compounds [{$Pd(OAc)_2$}$_4$LM] carrying central M = Zn^{II}, Pd^{II}, Pt^{II} in preacidified DMF ([HCl] = 1 x 10^{-4} M,) prevents reduction in all cases, and

well defined spectra for the neutral monomeric species are obtained. Quantitative spectral data of the present series [{$Pd(OAc)_2$}$_4$LM] are summarized in Table 4-1, together with those of the corresponding [($PdCl_2$)$_4$LM] and [LM] species.

The spectral data of the compounds [{$Pd(OAc)_2$}$_4$LM] in nonaqueous solvents (Table 4-1) deserve special attention. In general, only a small solvent effect is observed for each species as to the position of the Soret and Q bands. Instead, there is a more marked change in the spectra with change of the central metal ion. In fact, the Q-band maximum is located in the range of 620-630 nm for the Pt^{II} complex, but the band shifts to 630-640 nm for the related Pd^{II} and Co^{II} species, to 650-655 nm for the Cu^{II} complex, and to 655-660 nm for the complexes with Mg^{II} and Zn^{II} central metal ions; a comparable dependence on the central metal ion is also exhibited by the parent monometallic [LM][15,22,26] derivatives and the analogous tetrapalladated complexes [($PdCl_2$)$_4$LM].[22,23] Noteworthy, the Q-band position is slightly red-shifted (Table 4-1) in going from the [LM] species to the corresponding [{$Pd(OAc)_2$}$_4$LM], similarly to what was observed for the change of [LM] to the related [($PdCl_2$)$_4$LM] compounds.[15,23] This evidently occurs as a result of the electron withdrawing effect caused by the external coordination of $Pd(OAc)_2$ or $PdCl_2$ units on the π-conjugated central macrocyclic framework. This effect is remarkable, if account is taken that coordination of Pd^{II} occurs at the extreme periphery of the macrocycle and the formed coordination sites, $N_{2(py)}Pd(OAc)_2$ or $N_{2(py)}PdCl_2$, are oriented almost perpendicular to the plane of the central tetrapyrazinoporphyrazine core, as was proved by NMR spectral and theoretical data for the [($PdCl_2$)$_4$LPd] species[22] and proposed for the entire series [($PdCl_2$)$_4$LM].[23] The electrochemical data reported below

provide additional evidence for the strong influence of the $Pd(OAc)_2$ units on the electronic properties of the macrocycles $[\{Pd(OAc)_2\}_4LM]$.

As anticipated above, this new class of neutral pentanuclear porphyrazine macrocycles, $[\{Pd(OAc)_2\}_4LM]$, due to the presence of externally coordinated Pd^{II}-acetate groups, exhibits good solubility in water, often higher than that observed in the nonaqueous solvents (pyridine, DMSO, DMF). Practically no changes of spectral band positions are observed for these compounds in water solution with respect to the absorptions seen in the nonaqueous solvents. As already observed in other solvents, there is an effect of the central metal ion also in the water solution. The Pd^{II} and Pt^{II} complexes show Q-band maxima at 638 and 622 nm, respectively, while the Co^{II} species shows an unsplit Q band at 636 nm. with a vibrational component on the blue side, a symmetrical B band at 356 nm, and a low intensity absorption at 453 nm. The Mg^{II}, Zn^{II}, and Cu^{II} complexes show similar spectra with a narrow intense unsplit Q band with maximum in the range 652-658 nm, and a B band at 364-367 nm. The spectra are stable and do not change significantly as a function of time (hours).

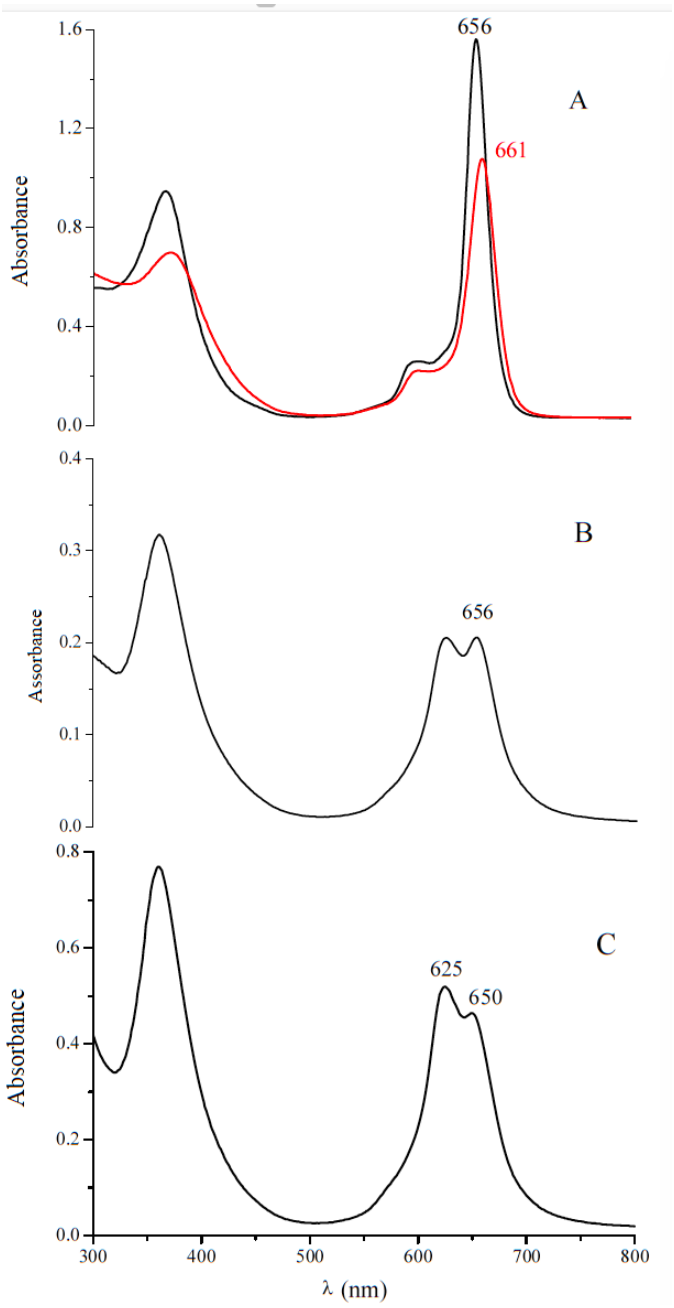

Figure 4-2. UV-visible spectra of A) $[\{Pd(OAc)_2\}_4LZn]$ in DMSO (red line, c = 9.55 x 10^{-6} M) and in H_2O (black line, c = 1.06 x 10^{-5} M); B) $[(CH)_8LZn]^{8+}$ in H_2O (c = 4.09 x 10^{-6} M); C) $[(PtCl_2)(CH_3)_6LZn]^{6+}$ in H_2O (c = 1.18 x 10^{-5} M).

Table 4-1. UV-visible spectral data of the species [{$Pd(OAc)_2$}$_4$LM] and the related compounds [LM] and [$(PdCl_2)_4$LM], (M = $Mg^{II}(H_2O)$, Zn^{II}, Cu^{II}, Co^{II}, Pd^{II}, Pt^{II}) in different solvents.

Complex	Solvent	lmax/nm (e)						ref
		Soret Band			Q Band			
[$LMg(H_2O)$]	Py	375 (5.23)		566sh (3.96)	596 (4.65)	631sh (4.64)	658 (5.54)	15
	DMSO	374 (5.08)			594 (4.36)	629sh (4.55)	653 (5.34)	28
	DMF	370 (4.94)			597 (4.39)	628sh (4.43)	658 (5.20)	25
	DMF/HCl	372 (4.74)			597 (4.20)		654 (4.94)	25
[$(PdCl_2)_4LMg(H_2O)$]	DMSO	342	368sh		597		656	25
	DMF	342			600		662	25
	DMF/HCl	344			600		664	25
[{$Pd(OAc)_2$}$_4$LMg(H_2O)]	Py	372 (5.02)			599 (4.40)		660 (5.13)	tw
	DMSO	372 (4.91)			599 (4.46)	632sh (4.51)	661 (5.31)	tw
	DMF	369 (4.87)			598 (4.33)		660 (5.05)	tw
	H_2O	367 (4.91)			603 (4.43)		658 (5.11)	tw
[LZn]	Py	378 (4.90)			598 (4.31)	626sh (4.50)	658 (5.18)	15
	DMSO	372 (5.10)		565sh (4.02)	592 (4.54)	626sh (4.84)	655 (5.36)	28
	DMF	375 (4.90)			600 (4.38)	626sh (4.61)	657 (5.15)	25
	DMF/HCl	376 (4.98)			596 (4.45)	626sh (4.35)	657 (5.27)	25
[$(PdCl_2)_4$LZn]	DMSO	370 (5.03)			598 (4.47)		657 (5.23)	25
	DMF	377 (4.86)	423sh (4.57)		600 (4.38)		662 (5.26)	25
	DMF/HCl	377 (4.86)	420sh (4.57)		600 (4.40)	633sh (4.43)	662 (5.28)	25
[{$Pd(OAc)_2$}$_4$LZn]	Py	375 (4.93)			596 (4.35)	628sh (4.36)	658 (5.20)	tw
	DMSO	371 (4.85)			599 (4.34)		661 (5.03)	tw

Table 4-1 (continued). UV-visible spectral data of the species [{$Pd(OAc)_2$}$_4$LM] and the related compounds [LM] and [$(PdCl_2)_4$LM], (M = $Mg^{II}(H_2O)$, Zn^{II}, Cu^{II}, Co^{II}, Pd^{II}, Pt^{II}) in different solvents.

Complex	Solvent	lmax/nm (e)					ref
		Soret Band		Q Band			
[{$Pd(OAc)_2$}$_4$LZn]	DMF/HCl	309 (4.83)	377 (4.87)	600 (4.38)	631sh (4.41)	662 (5.26)	tw
	H_2O	367 (4.95)		597 (4.38)		656 (5.17)	tw
[LCu]	Py	379 (4.64)		591 (4.18)		650	15
	DMSO	365 (4.91)		590 (4.44)		648 (5.18)	28
	DMF/HCl	370		595		653 (4.93)	25
[$(PdCl_2)_4$LCu]	DMSO	358 (4.79)		593 (4.33)		651 (4.95)	25
	DMF/HCl	370 (4.84)		598 (4.37)		654 (5.05)	25
[{$Pd(OAc)_2$}$_4$LCu]	Py	377 (4.93)		591 (4.46)		653 (5.25)	tw
	DMSO	353 (4.71)		593 (4.26)		650 (5.02)	tw
	DMF	366 (4.85)		588 (4.35)		651 (4.90)	tw
	H_2O	364 (4.83)		601 (4.38)		652 (4.97)	tw
[LCo]	Py	364 (5.01)	442	575sh (4.38)			15
	DMSO	355 (5.23)	450sh (4.65)	586sh (4.71)			28
	DMF/HCl	353	441	579			25
[$(PdCl_2)_4$LCo]	DMSO	357 (5.00)	448 (4.43)	587 (4.47)			25
	DMF/HCl	353 (5.00)	4.29	587 (4.43)			25
[{$Pd(OAc)_2$}$_4$LCo]	Py	364 (4.97)	452 (4.35)	578sh (4.32)			tw
	DMSO	375 (4.88)	442 (4.38)	580sh (4.99)			tw
	DMF	364 (4.96)	442 (4.30)	583sh (4.36)			tw
	H_2O	356 (5.02)	453 (4.29)	584sh (4.41)			tw

The solubility corresponding to saturation for the species [{$Pd(OAc)_2$}$_4$LM] was measured and the respective values are given in Table 4-2. The highest solubility is observed for Mg^{II}, Zn^{II} and Pd^{II} complexes (ca. 10^{-3} M), followed by the Co^{II} and Cu^{II} derivatives (ca. 10^{-4} M); the lowest is observed for the Pt^{II} complex (ca. 10^{-5} M). This level of water solubility is definitely rare when considering that the compounds in Table 4-2 are neutral species, exhibiting a more compact structure with respect to that of derivatives with peripherally branched porphyrazines.[9] It should again be pointed out that all of the compounds examined in the present study exhibit solution UV-visible spectra in water which are typical of the monomeric species (see spectrum of the Zn^{II} complex in Figure 4-2a; black line). Moreover, the monomeric form of the macrocycle persists at all concentrations, even at the highest concentrations listed in Table 4-3. In this context, it must be noted that the already cited Zn^{II} octacationic[15,22] (Chart 4-1a) and the hexacationic[27] species (Chart 4-1b) sharing the same central pyrazinoporphyrazine macrocycle exhibit spectra in water which are characterized by the presence of aggregation, proven by the appearance of two peaks of comparable intensity in the spectral Q-band region (Figure 4-1b and 1c), the peak at lower wavelength belonging to the aggregated form.[12,13]

Table 4-2. Molar concentration of saturated solutions in water of [{Pd(OAc)$_2$}$_4$LM] complexes (M = Mg^{II}(H$_2$O), Zn^{II}, Cu^{II}, Co^{II}, Pd^{II}, Pt^{II}).

Complex	Concentration (M)
[{Pd(OAc)$_2$}$_4$LMg(H$_2$O)]	1×10^{-3}
[{Pd(OAc)$_2$}$_4$LZn]	0.8×10^{-3}
[{Pd(OAc)$_2$}$_4$LCu]	1.2×10^{-4}
[{Pd(OAc)$_2$}$_4$LCo]	1.6×10^{-4}
[{Pd(OAc)$_2$}$_4$LPd]	2×10^{-3}
[{Pd(OAc)$_2$}$_4$LPt]	2×10^{-5}

4.2.3 Electrochemical and Spectroelectrochemical Measurements.

Cyclic voltammetry and thin layer spectroelectrochemistry measurements on the presently investigated compounds [{Pd(OAc)$_2$}$_4$LM] were carried out in both DMSO containing 0.1 M TBAP and in H_2O containing 0.1 M KCl or 0.1 M NaOAc. The half wave potentials ($E_{1/2}$ V vs SCE) for reduction in DMSO and H_2O are listed in Table 4-3 which also includes data on the related [LM] and [(PdCl$_2$)$_4$LM] derivatives. No oxidations were observed for any of the [{Pd(OAc)$_2$}$_4$LM] compounds within the solvent potential window, as was also previously noted for the corresponding [LM][28] series, with the only exception of the Co^{II} compound [LCo], able to form electrochemically the one-electron oxidized Co^{III} species $[LCo^{III}]^{1+}$ (DMSO, +0.67 V vs SCE),[28] which was isolated as salt-like species, [LCo](SbCl$_6$),[29] and observed also for the [(PdCl$_2$)$_4$LM] derivatives.[22,23]

As earlier mentioned, the currently investigated compounds are soluble in both DMSO and H_2O where they exist exclusively in their monomeric form at the concentrations required for electrochemical experiments to be carried out (ca. 10^{-4} M or higher). The absence of molecular aggregation is probably due to steric hindrance of the four bulky external $N_2Pd(OAc)_2$ moieties, which are all proposed to be oriented on the same side of the central pyrazinoporphyrazine core, as was reported for [(PdCl$_2$)$_4$LM] compounds.[22,23] and the [(PtCl$_2$)$_4$LM] analogs.[25,26] Results on the electrochemical behavior of the examined [{Pd(OAc)$_2$}$_4$LM] are presented below, first in DMSO, followed by results in aqueous media.

Cyclic voltammograms in DMSO showing the first two reductions of the [{Pd(OAc)$_2$}$_4$LM] compounds, where M = Mg^{II}, Zn^{II}, Cu^{II} and Pd^{II} are illustrated in Figure 4-3 which also shows the first three reductions of the Pt^{II} derivative. These reductions are all reversible and involve electron addition to the conjugated

macrocycle to give π-anion radicals and dianions. The investigated compounds containing four externally bound $Pd(OAc)_2$ units are in each case easier to be reduced than the monometallic derivatives with the same central metal ion (see Table 4-3). The $E_{1/2}$ values for the first two reductions in DMSO are shifted positively by 30-100 mV for the $Mg^{II}(H_2O)$, Zn^{II} and Cu^{II} complexes and by 240-260 mV for the M = Pd^{II} and Pt^{II} compounds as compared to potentials for reduction of the parent [LM] compounds with the same central metal ion. These positive shifts are smaller, in any case, than what was observed upon going from [LM] to $[(PdCl_2)_4LM]$ (data in Table 4-3), where the ease of reduction for the three series of compounds in DMSO increases in the order [LM] < $[\{Pd(OAc)_2\}_4LM]$ < $[(PdCl_2)_4LM]$. The present electrochemical data demonstrate that external coordination of the four $Pd(OAc)_2$ units results in an easier acceptance of excess negative charge within the macrocyclic framework, independent of the nature of the central metal ion. This is in accordance with the enhanced electron-withdrawing properties of the external dipyridinopyrazine fragments once they are metalated. This behavior parallels what has been observed upon exocyclic coordination of $PdCl_2$ units.[22,23]

As seen in Table 4-3, the potential variation in $E_{1/2}$ for the first reductions of $[\{Pd(OAc)_2\}_4LM]$ amounts to 280 mV in DMSO, with a systematic shift of the $E_{1/2}$ values toward less negative potentials in the following sequence: Mg^{II} (-0.27 V) → Zn^{II} (-0.23 V) → Cu^{II} (-0.12 V) → Pd^{II} (-0.03 V) Pt^{II}→ (0.01 V). A plausible explanation for this trend is that there is a high combination of the σ and M(dπ)-N(pπ) interaction in the central M-N_4 (M = Pd^{II}, Pt^{II}) bond system, whereas in the Mg-N_4 bonded systems there is a significant presence of ionic character. From this it can be concluded that more negative charge resides on the macrocycle of the Mg^{II}

derivative, which would make it less easy to be reduced. Noticeably, the same trend in $E_{1/2}$ values is observed in half wave potentials for the first and second reductions of the mononuclear [LM] and pentanuclear [$(PdCl_2)_4$LM] compounds (Table 4-3).

The first two one-electron additions to [$\{Pd(OAc)_2\}_4$LM] are followed by reduction of Pd^{II} from the four bound $Pd^{II}(Oac)_2$ groups. This reaction occurs at E_p = -1.08 V (see Figure 4-4 for Cu^{II} complex), leading to formation of Pd^{I} or Pd^{0} and free OAc^- in solution, and is followed by two reversible one-electron reductions at $E_{1/2}$ values which are identical within experimental error to the half wave potentials for the third and fourth reductions of [LM] in DMSO (see Table 4-3). This gives further evidence for a reductive loss of the bound $Pd(OAc)_2$ units with formation of [LM] at the electrode surface, as previously described for [$(PdCl_2)_4$LM].[22,23]

The good solubility of the [$\{Pd(OAc)_2\}_4$LM] complexes in water, combined with the absence of molecular aggregation, enabled electrochemical measurements to be carried out in water for the five tetraacetate derivatives with redox inactive central metal ions. These measurements were made with 0.1 M KCl or 0.1 M NaOAc as supporting electrolyte (Table 4-3). Examples of cyclic voltammograms for the Mg^{II} and Zn^{II} complexes in water containing 0.1 M KCl are illustrated in Figure 4-5a, where only the initial reductions of the tetraacetate complex are illustrated.

Table 4-3. Half-wave potentials of reductions ($E_{1/2}$, V vs. SCE) of [{$Pd(OAc)_2$}$_4$LM], [LM] and [($PdCl_2$)LM] in DMSO and H_2O (0.1M KCl or 0.1M NaOAc).

solvent	compound	macrocycle				ref
		first	second	third	fourth	
H_2O (0.1 M NaOAc)	[{$Pd(OAc)_2$}$_4$LMg(H_2O)]	-0.17	-0.35	-0.50		tw
	[{$Pd(OAc)_2$}$_4$LZn]	-0.11	-0.37	-0.53		tw
	[{$Pd(OAc)_2$}$_4$LCu]	-0.05	-0.60[a]			tw
	[{$Pd(OAc)_2$}$_4$LPd]	-0.06	-0.56[a]			tw
H_2O (0.1 M KCl)	[{$Pd(OAc)_2$}$_4$LMg(H_2O)]	-0.23	0.42	-0.60		tw
	[{$Pd(OAc)_2$}$_4$LZn]	-0.20	-0.39	-0.59		tw
	[{$Pd(OAc)_2$}$_4$LCu]	-0.07	0.45			tw
	[{$Pd(OAc)_2$}$_4$LPd]	-0.08				tw
	[{$Pd(OAc)_2$}$_4$LPt]	-0.11				tw
DMSO	[{$Pd(OAc)_2$}$_4$LMg(H_2O)]	-0.31	-0.55	-1.47	-1.68	tw
	[{$Pd(OAc)_2$}$_4$LZn]	-0.22	-0.52	-1.35	-1.57	tw
	[{$Pd(OAc)_2$}$_4$LCu]	-0.12	-0.48	-1.20	-1.58	tw
	[{$Pd(OAc)_2$}$_4$LPd]	-0.03	-0.42	-1.24	-1.60	tw
	[{$Pd(OAc)_2$}$_4$LCo]	-0.07	-0.66[a]	-1.39	-1.77	tw
	[{$Pd(OAc)_2$}$_4$LPt]	0.01	-0.17	-0.42		tw
	[($PdCl_2$)$_4$LMg(H_2O)]	-0.15				9
	[($PdCl_2$)$_4$LZn]	-0.13	-0.54	-1.39	-1.63	9
	[($PdCl)_2$)$_4$LCu]	-0.03	-0.41	-1.24	-1.60	9
	[($PdCl)_2$)$_4$LPd]	0.00	-0.37	-1.24	-1.59	1
	[LMg(H_2O)]	-0.33	-0.70	-1.39	-1.70	7
	[LZn]	-0.26	-0.67	-1.38	-1.64	7
	[LCu]	-0.22	-0.58	-1.22	-1.58	7
	[LPd]	-0.26	-0.60	-1.26	-1.61	1
	[LPt]	-0.25	-0.61			2

[a]Peak potential E_{pc} at scan rate = 0.1 V/s.

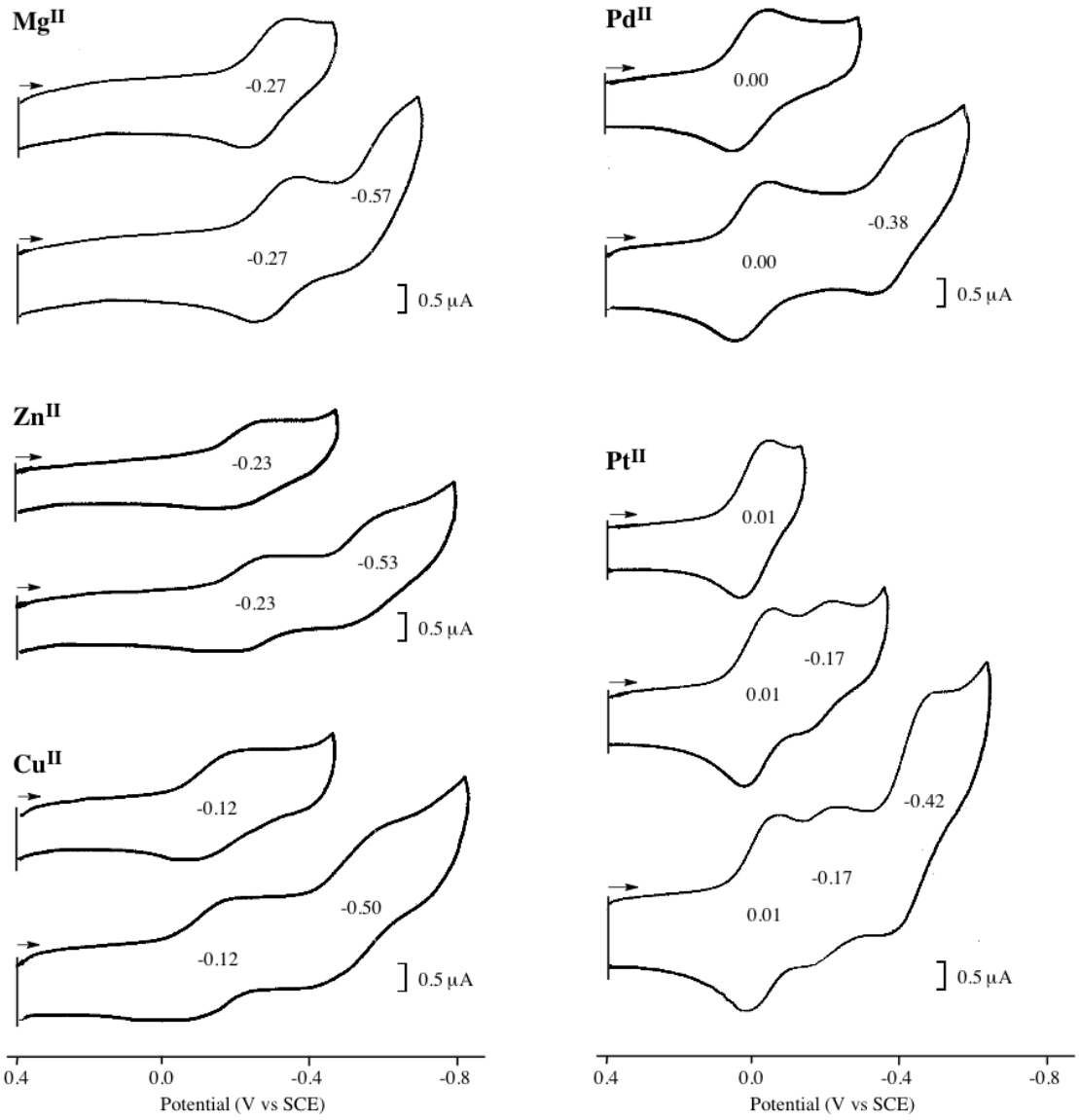

Figure 4-3. Cyclic voltammograms of [{$Pd(OAc)_2$}$_4$LM] in DMSO, 0.1 M TBAP.

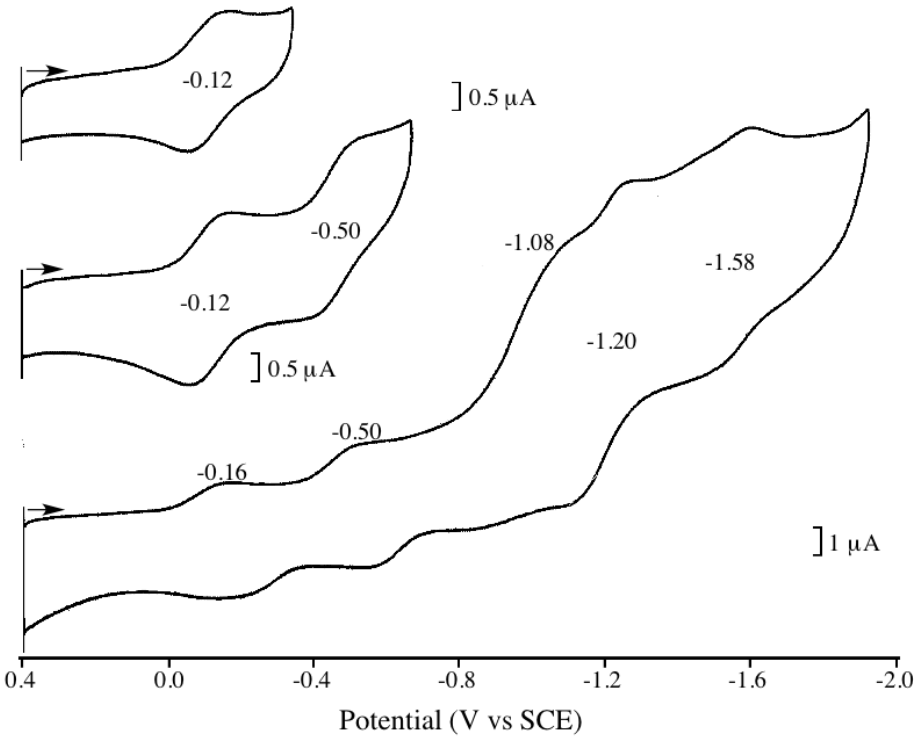

Figure 4-4. Cyclic voltammograms of [{$Pd(OAc)_2$}$_4$LCu] in DMSO containing 0.1 M TBAP.

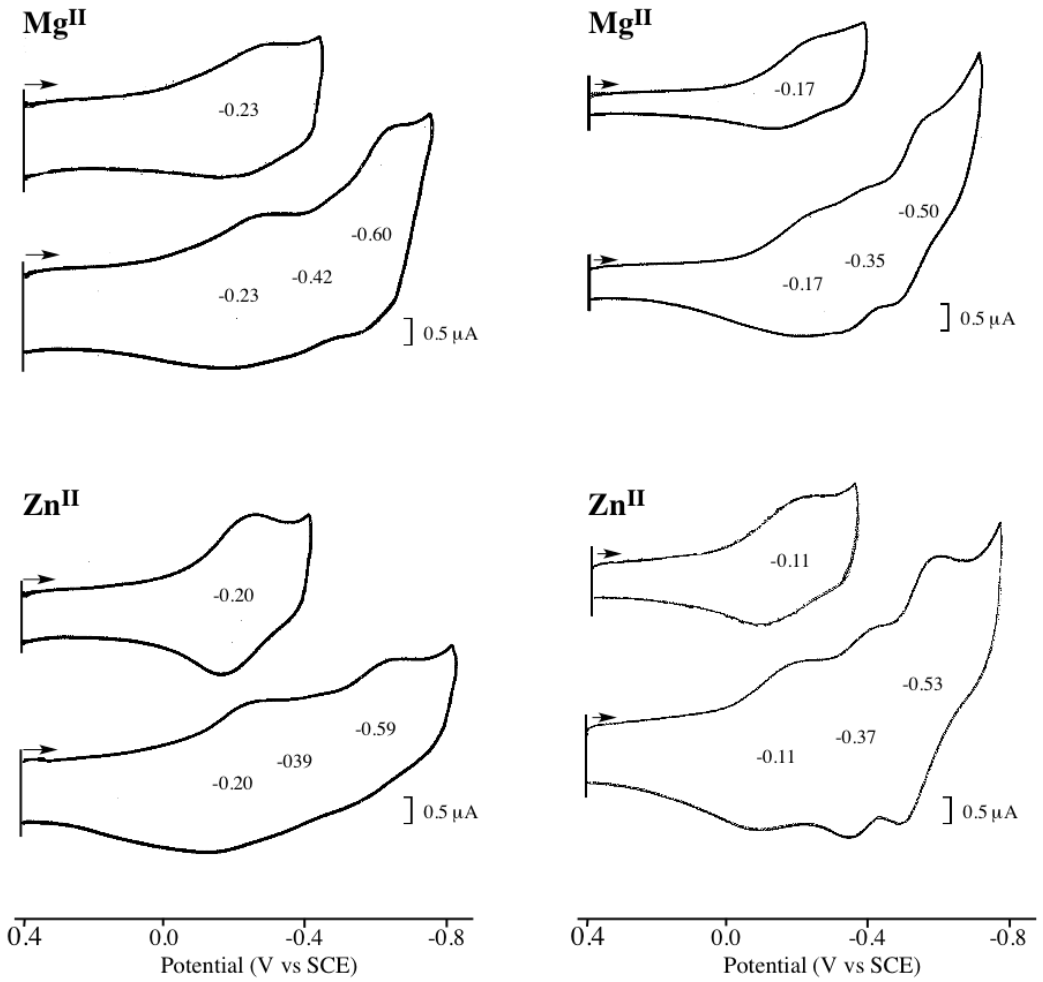

Figure 4-5. Cyclic voltammograms of [{$Pd(OAc)_2$}$_4$LM] (M = Mg^{II}, Zn^{II}) in H_2O with 0.1 M a) KCl and b) NaOAc.

In the presence of KCl, a gradual insolubilization of the compounds was observed, very likely due to a substitution of the OAc^- ligands by Cl^- ions, resulting in formation of the $[(PdCl_2)_4LM]$ species which are insoluble in water. Nevertheless, replacement of the acetate groups and formation of the corresponding $PdCl_2$ derivatives was slow enough such that cyclic voltammetry data of the original neutral compounds could be obtained (see Figure 4-5a and Table 4-3). The $E_{1/2}$ values in water are similar to the measured potentials in DMSO and the trend of half wave potentials as a function of the different central metal ions is similar to that observed in DMSO, ie Mg^{II} (-0.23 V) $\rightarrow$ Zn^{II} (-0.20 V) $\rightarrow$ Cu^{II} (-0.07 V). Slightly lower $E_{1/2}$ values were obtained by using 0.1 M NaOAc as supporting electrolyte.

The $[\{Pd(OAc)_2\}_4LM]$ complexes are more soluble in H_2O containing 0.1 M NaOAc than in aqueous solutions containing 0.1 M KCl and examples of cyclic voltammograms ìn H_2O with 0.1 M NaOAc are shown in Figure 4-5b. More positive $E_{1/2}$ values for the first reduction are obtained for different metal centers (see Table 4-3) and increase in the same sequence as in DMSO, i.e., Mg^{II} (-0.17 V) $\rightarrow$ Zn^{II} (-0.11 V) $\rightarrow$ Cu^{II} (-0.05 V) $\rightarrow$ Pd^{II} (-0.03 V).

Figure 4-6a shows the UV-visible spectral changes obtained during the first one-electron reduction of $[\{Pd(OAc)_2\}_4LPd]$ in DMSO containing 0.2 M TBAP. The spectral changes which occur as the reduction proceeds are similar to what was earlier reported for the $[(PdCl_2)_4LPd]$ analog (Figure 4-6b).[22] Several isosbestic points are observed in the spectra of Figure 4-6, indicating the lack of detectable intermediates upon going from the neutral form of the complex to the corresponding -1 charged species. There is also a similar evolution of the spectra during the first reduction of $[\{Pd(OAc)_2\}_4LPd]$ and $[(PdCl_2)_4LPd]$, expressed by the disappearance of the intense Q band at 638 nm and the appearance of new bands at 551-553 and 686 nm, in

addition to a broad absorption in the region of 800-900 nm. These spectral features are similar to those seen during reductions of the corresponding mononuclear species [LPd] in the same solvent.[22] Finally, similar types of spectral changes are also seen during reductions in DMSO of the related tetrapalladated [$(PdCl_2)_4$LM] (M = Zn^{II}, Cu^{II}, $Mg^{II}(H_2O)$, Cd^{II})[23] species in keeping with the assumption of ligand-centered reductions.

4.2.4 Singlet Oxygen Quantum Yield Measurements[30]

The involvement of porphyrins[2-6] and phthalocyanines[5,6,31-37] as photosensitizers for the generation of singlet oxygen, $^1O_2$, is of expanding interest in the photodynamic therapy of cancer, whereas porphyrazines in general have so far received only limited attention, pertinent work having being mostly developed on the photoactivity of seco-,[38-40] banzonaphtho-,[41] and pyrazinoporphyrazines.[24-26,42,43] The efficiency of a macrocyclic photosensitizer depends on its tendency to undergo, upon irradiation, an excitation from the ground state S_0 to the triplet state T_1 with high quantum yield, and to have a T_1 adequate energy and lifetime to allow for a proper energy transfer to dioxygen for the process $^3O_2 \rightarrow {}^1O_2$ to occur. Besides, the type of central metal ion in the macrocycle can strongly influence this process and, in this regard, it is known that closed shell metal ions like Zn^{II} and Mg^{II}, and in some cases, open shell diamagnetic d^8 metal centers, like Pd^{II} and Pt^{II}, lead to high photoactivity.

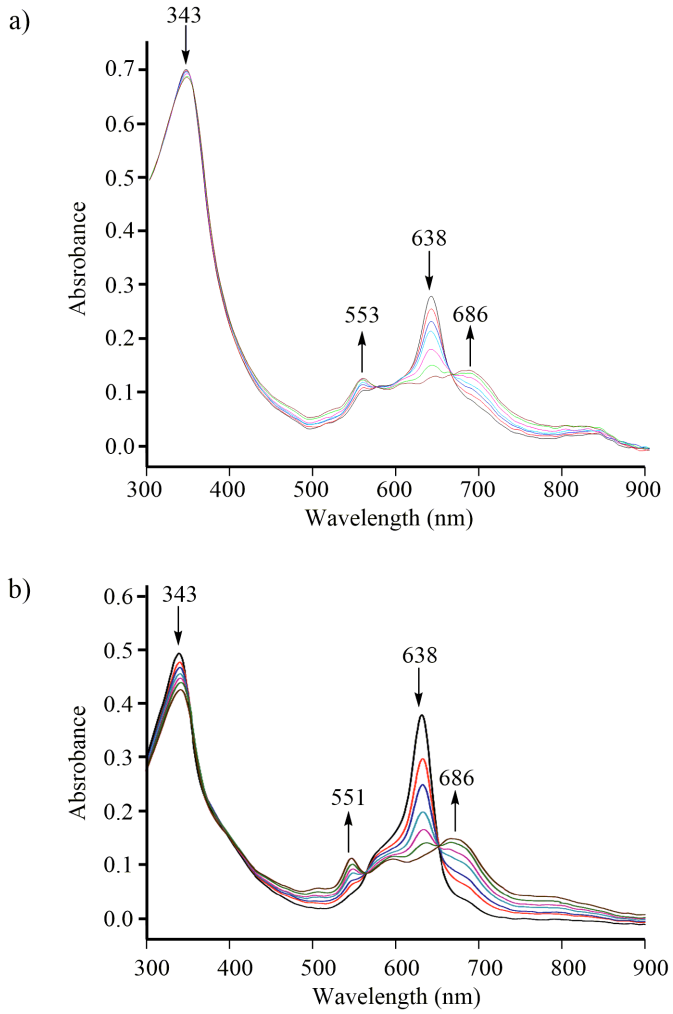

Figure 4-6. UV-visible spectral changes in DMSO containing 0.2 M TBAP during first reduction of a) [{Pd(OAc)$_2$}$_4$LPd] at E_{app} = -0.55 V and b) [(PdCl)$_2$)$_4$LPd] at E_{app} = -0.20 V.

As part of a joint study, the compounds described on the previous pages were also examined by our collaborators in Italy as to their possible use in the area of PDT. Details of these measurements are given in the literature[30] and are briefly described below. The pentanuclear species [{Pd(OAc)$_2$}$_4$LM] carrying centrally M = Zn^{II}, $Mg^{II}(H_2O)$, Pd^{II} and Pt^{II} were examined as to their photosensitizing activity for the generation of singlet oxygen, $^1O_2$.[30] Singlet oxygen quantum yields (Φ_Δ) were obtained in DMF ([complex] $\cong 10^{-5}$ M), and/or in DMF acidified with HCl (DMF/HCl; [HCl] = 10^{-4} M) by the above mentioned absolute method,[44,45] using a laser source at 660 nm for the Zn^{II} and Mg^{II} complexes, and at 635 nm for the Pd^{II} and Pt^{II} species, close to the maxima of the Q-band absorption peaks of the corresponding compounds. UV-visible spectral features and the Stern-Volmer plot of a typical experiment used to calculate the Φ_Δ values of the sensitizers, are shown in Figure 4-7 for [{Pd(OAc)$_2$}$_4$LZn].

The inset illustrates the related experimental data corresponding to the absorption decay at 414 nm for the $^1O_2$ scavenger, DPBF, recorded during the irradiation time of the solution. Table 4-4 lists the singlet oxygen quantum yields (Φ_Δ) of [{Pd(OAc)$_2$}$_4$LM]. Data for the related tetrapalladated complexes [(PdCl$_2$)$_4$LM] (M = Zn^{II}, Mg^{II}, Pd^{II})[25] and for [(PtCl$_2$)$_4$LPt][26] are also included for comparison purposes.

In order to prevent one-electron reduction in DMF solution for the complexes [{Pd(OAc)$_2$}$_4$LM] with central M = Zn^{II}, Pd^{II}, and Pt^{II}, Φ_Δ values for these compounds were measured in preacidified DMF. For the Mg^{II} complex, stable in DMF, measurements of Φ_Δ were made in both DMF and DMF/HCl. Solutions in DMF and/or DMF/HCl of all the complexes are generally stable under irradiation.

The observed Φ_Δ values for the Zn^{II} and the Mg^{II} complexes follow the order $Zn^{II} > Mg^{II}$, according to the "heavy atom effect" which enhances the triplet excited state quantum yield for Zn^{II} with respect to Mg^{II}. The Φ_Δ value of the Zn^{II} complex [{$Pd(OAc)_2$}$_4$LZn] (0.43) is in the range 0.4-0.7 observed for a number of Zn^{II} phthalocyanines,[31-37,46] and porphyrazines,[38-30,47] (including macrocycles of this latter type studied by us[25,27]) and this qualifies it as a highly active photosensitizer for the generation of singlet oxygen.

The Φ_Δ value for the complex with a central Pd^{II} ion, [{$Pd(OAc)_2$}$_4$LPd], measured exclusively in DMF/HCl is lower (0.34) than the value of the Zn^{II} complex measured under the same experimental conditions. Markedly lower (0.22) is the value measured for the Pt^{II} complex, [{$Pd(OAc)_2$}$_4$LPt]. The Φ_Δ value measured for the Mg^{II} compound shows a large increment in the presence of HCl, as already observed for the pentanuclear Mg^{II} species [$(PdCl_2)_4$LMg(H_2O)] and other analogs.[25,27] This problematic aspect necessitates further inspection.

Additional observations refer to the trend of the observed Φ_Δ values upon changing the type of ligand attached to the exocyclic Pd^{II}. On going from the pentanuclear species [$(PdCl_2)_4$LM] having four $PdCl_2$ units externally coordinated, to the new pentanuclear complexes [{$Pd(OAc)_2$}$_4$LM] having four exocyclic $Pd(OAc)_2$ units, a decrease of the singlet oxygen quantum yield production is observed, no matter which the metal center. The effect is particularly evident in the case of the Pd^{II} derivatives.

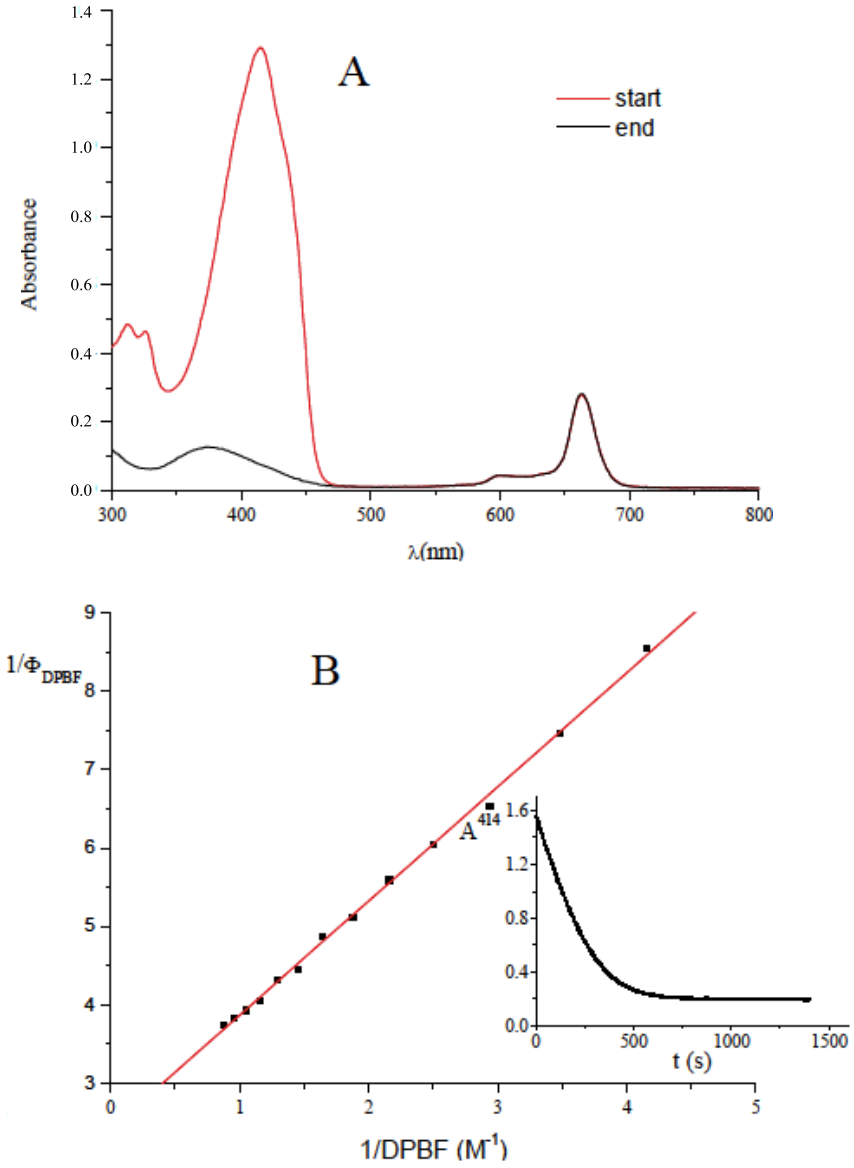

Figure 4-7. a) UV-visible spectra of a DMF/HCl solution ([HCl] = 1 x 10^{-4} M) containing [{$Pd(OAc)_2$}$_4$LZn] and DPBF before (red line) and after (black line) laser irradiation; b) Stern-Volmer data analysis of the DPBF photooxidation (shown in the inset).

Table 4-4. Singlet Oxygen Quantum Yields (Φ_Δ) in DMF and/or DMF preacidified with HCl (1÷2 x 10^{-4} M) of [{$Pd(OAc)_2$}$_4$LM] (M = Zn^{II}, $Mg^{II}(H_2O)$, Pd^{II}, Pt^{II}) and related species.[30]

Photosensitizer	HCl (M)	λ_{max} (Q band) /nm	Singlet oxygen		Ref.
			λ_{irr}[nm]	Φ_Δ [a]	
[{$Pd(OAc)_2$}$_4$LZn]	1 x 10^{-4}	662	660	0.43	tw
[($PdCl_2$)$_4$LZn]	0	662	670	0.48	25
	1x10^{-4}	662	670	0.52	
[{$Pd(OAc)_2$}$_4$LMg(H_2O)]	0	660	660	0.05	tw
	1x10^{-4}	660	660	0.29	tw
[($PdCl_2$)$_4$LMg(H_2O)]	0	662	670	0.23	25
	1x10^{-4}	660	670	0.37	
[{$Pd(OAc)_2$}$_4$LPd]	1x10^{-4}	636	635	0.34	tw
[($PdCl_2$)$_4$LPd]	1x10^{-4}	635	635	0.56	25,26
[{$Pd(OAc)_2$}$_4$LPt]	1x10^{-4}	624	635	0.22	tw
[($PtCl_2$)$_4$LPt]	2x10^{-4}	624	635	0.36	26

[a] Mean value of at least three measurements. Uncertainty is half-dispersion it is typically ± 0.03.

4.3 Conclusions

The synthesized new homo/heterometallic pentanuclear complexes of formula [{(Pd(OAc)$_2$}$_4$LM], (M = Mg^{II}(H$_2$O), Zn^{II}, Cu^{II}, Co^{II}, Pd^{II}, Pt^{II}), bearing exocyclic coordinated four Pd(OAc)$_2$ units, are stable to air materials, characterized by the presence of abundant chlatrated water molecules most probably interacting with the external OAc$^-$ groups. All the species, poorly soluble (10^{-4}-10^{-5}M) in low donor solvents (pyridine, DMSO, DMF), exhibit solubility values in water up to 10^{-3}-10^{-4} M, which is a very rare occurrence for neutral porphyrazine or phthalocyanine macrocycles. Noteworthy, even at the highest concentrations in solution of low donor solvents or water, the compounds are present in their monomeric form, thus in the absence of detectable aggregation, as clearly suggested by UV-visible solution spectra and spectroelectrochemical behaviour. Exploration of the UV-visible spectral and electrochemical response in DMSO indicates that coordination of Pd(OAc)$_2$ units makes the macrocycles more electron-deficient as shown by the red shift of the Q-band positions and by the less negative values of half-wave potentials (V vs SCE; both in DMSO and in water) compared to those of the related mononuclear [LM] compounds. Studies performed in DMF solution prove that the selected species [{(Pd(OAc)$_2$}$_4$LM] (M = Mg^{II}(H$_2$O), Zn^{II}, Pd^{II}, Pt^{II}) behave as active photosensintizers for the generation of singlet oxygen, ^{1}O$_2$, the quantum yield values (Φ_Δ), measured in DMF or in acidified DMF ([HCl] = 1÷2x10^{-4}M] moving in DMF along the series Zn^{II} > Pd^{II} > Mg^{II}(H$_2$O) > Pt^{II}, the observed sequence reproducing the findings for the parallel series of [LM] and [(PdCl$_2$)$_4$LM] parent compounds. Measurements of Φ_Δ in water solution are seen as an important target for the present water soluble neutral porphyrazine materials and studies in this direction should be carried out in the near future.

4.4 References

(1) *The Porphyrin Handbook*, Kadish K. M., Smith K. M., Guilard R., Eds.; Academic Press: New York, 2003, Vols. 15-20; b) *Phthalocyanines: Properties and Applications*, Leznoff C. C., Lever, A. B. P. Eds.; VCH Publishers, Inc.: New York, 1989-96, Vols. 1-4.

(2) Ethirajan, M.; Chen, Y.; Joshi, P.; Pandey, R. K. *Chem. Soc. Rev.*, **2011**, *40*, 340–362

(3) Celli, J. P.; Spring, B. Q.; Rizvi, I.; Evans, C. L.; Samkoe, K. S.; Verma, S.; Pogue, B. W.; Hasan T. *Chem. Rev.* **2010,** *110*, 2795–2838

(4) Moreira, L. M.; Vieira dos Santos, F.; Pereira Lyon, J.; Maftoum-Costa, M.; Pacheco-Soares, C.; Soares da Silva, N. *Aust. J. Chem.* **2008**, *61*, 741-754

(5) O'Connor, A. E.; Gallagher, W. M.; Byrne, A. T. *Photochem. Photobiol.* **2009**, *85*, 1053-1074

(6) Szacilowski, K.; Macyk, W.; Drzewiecka-Matuszek, A.; Brindell, M.; Stochel, G. *Chem. Rev.* **2005**, *105*, 2647-2694.

(7) Stuzhin P. A., Ercolani C., *The Porphyrin Handbook*, Kadish K. M., Smith K. M., Guilard R., Eds.; Academic Press: New York, 2003, Vol. 15, Chapter 101, pp. 263-364

(8) Michel S. L. J., Hoffman B. M., Baum S. M., Barrett A. G. M., *Progress in Inorganic Chemistry*, Karlin K. D., Editor, J. Wiley & Sons, 2001, Vol. 50, pp. 473-591.

(9) Dumoulin, F.; Durmus, M.; Ahsen, V.; Nyokong, T. *Coord. Chem. Rev.*, **2010**, *254*, 2792-2847.

(10) Kudrevich, S. V.; van Lier, J. E. *Coord. Chem. Rev.*, **1996**, *156*, 163-182.

(11) Anderson E. Mim, Barrett, A. G. M.; Hoffman B. M. *Inorg. Chem.*, **1999**, *38*, 6143-6151.

(12) Manet, I.; Manoli, F.; Donzello, M. P.; Viola, E.; Andreano, G.; Masi, A.; Cellai, L.; Monti, S. *Org. Biomol. Chem*. **2011**, *9*, 684-688

(13) Manet, I.; Manoli, F.; Donzello, M. P.; Ercolani, C.; Vittori, D.; Cellai, L.; Masi, A.; Monti, S. *Inorg. Chem*. **2011**, *50*, 7403-7411.

(14) Manet, I; Manoli, F.; Donzello, M. P.; Viola, E.; Masi, A.; Andreano, G.; Ricciardi, G.; Rosa, A.; Cellai, L.; Ercolani, C.; Monti, S. *Inorg. Chem.*, **2013**, *52*, 321-328.

(15) Donzello, M. P.; Ou, Z.; Dini, D.; Meneghetti, M.; Ercolani, C.; Kadish, K. M. *Inorg. Chem*. **2004**, *43*, 8637-8648.

(16) Velasquez, S. V.; Fox, G. A.; Broderick, W. E.; Anderesen, K. A.; Anderson, O. P.;

(17) Fischer, M. S.; Templeton, D. H.; Zalkin, A.; Calvin, M. *J. Am. Chem. Soc.*, **1971**, *93*, 2622-2628.

(18) Stuzhin, P.A.; Bauer, E. M.; Ercolani, C. *Inorg. Chem*., **1998**, *37*, 1533-1539; b) Bauer, E. M.; Ercolani, C.; Galli, P.; Popkova, I.A.: Stuzhin, P. A. *J. Porphyrins Phthalocyanines*, **1999**, *3*, 371-379.

(19) Donzello, M. P.; Ercolani, C.; Stuzhin, P. A.; Chiesi-Villa, A.; Rizzoli, C. *Eur. J. Inorg. Chem.* **1999**, 2075-2084.

(20) Matzumoto, S.; Endo, A.; Mizuguchi, J.Z. *Krystallogr.*, **2000**, *215*, 182-186.

(21) Baum, S. M.; Trabanco, A. A.; Montalban, A. G.; Micallef, A. S.; Zhong, C.; Meunier, H. G.; Suhling, K.; Phillips, D.; White, A. J. P.; Williams, D. J.; Barrett, A.G. M.; Hoffman, B. M. *J. Org. Chem.*, **2003**, 68, 1665-1670.

(22) Donzello M. P.; Viola, E.; Xiaohui C.; Mannina, L.; Rizzoli, C.; Ricciardi, G.; Ercolani, C.; Kadish, K. M.; Rosa, A. *Inorg. Chem*., **2008**, *47*, 3903-3919.

(23) Donzello, M. P.; Viola, E.; Cai, X.; Mannina, L.; Ercolani, C.; Kadish, K. M. *Inorg. Chem*. **2010**, *49*, 2447-2456.

(24) Donzello, M. P.; Viola, E.; Bergami, C.; Dini, D.; Ercolani, C.; Giustini, M., Kadish, K. M.; Meneghetti, M.; Monacelli, F.; Rosa, A.; Ricciardi, G. *Inorg. Chem*., **2008**, *47*, 8757-8766. 8757-

(25) Donzello, M. P.; Viola, E.; Ercolani, C.; Fu, Z.; Futur, D.; Kadish, K. M. *Inorg. Chem*. **2012**, *51*, 12548-12559.

(26) Donzello, M. P.; Viola, E.; Mannina, L.; Barteri, M.; Fu, Z.; Ercolani, C. *J. Porphyrins Phthalocyanines*, **2011**, *15*, 984-994.

(27) Donzello, M. P.; Vittori, D.; Viola, E.; Manet, I.; Mannina, L.; Cellai, L.; Monti, S.; Ercolani, C. *Inorg. Chem.* **2011**, 50, 7391-7402.

(28) Bergami, C.; Donzello M. P.; Monacelli, F.; Ercolani, C.; Kadish, K. M. *Inorg. Chem.*, **2005**, *44*, 9862-9873.

(29) Viola, E.; Donzello, M. P.; Ciattini, S.; Portalone, G..; Ercolani, C. *Eur. J. Inorg. Chem.* **2009**, 1600-1607.

(30) Donzello, M. P.; Vittori, D.; Viola, E.; Zeng, L.; Cui, Y.; Kaidhs, K. M.; Ercolani, C. *J. Porphyrins Phthalocyanines*, **2015**, In Press.

(31) Shinohara, H.; Tsaryova, O.; Schnurpfeil, G.; Wöhrle, D. J. *Photochem. Photobiol*., A **2006**, *184*, 50-57

(32) Spiller, W.; Kliesch, H.; Wöhrle., D.; Hackbarth, S.; Röder, B.; Schnurpfeil, G. *J. Porphyrins Phthalocyanines* **1998**, *2*, 145-148

(33) Schnurpfeil, G.; Sobbi, A. K.; Spiller, W.; Kliesch, H.; Wöhrle., D. *J. Porphyrins Phthalocyanines* **1997**, *1*, 159-167

(34) Fernandez, D. A.; Awruch, J.; Dicelio, L. E. *Photochem. Photobiol*. **1996**, *63*, 784-792

(35) Müller, S.; Mantareva, V.; Stoichkova, N.; Kliesch, H.; Sobbi, A.; Wöhrle., D.; Shopova, M. J. *Photochem. Photobiol., B* **1996**, 35, 167-174

(36) Maree, S. E.; Nyokong, T. *J. Porphyrins Phthalocyanines* **2001**, *5*, 782-792

(37) Lawrence, D. S.; Whitten, D. G. *Photochem. Photobiol*. **1996**, *64*, 923-935.

(38) Baum, S. M.; Trabanco, A. A.; Montalban, A. G.; Micallef, A. S.; Zhong, C.; Meunier, H. G.; Suhling, K.; Phillips, D.; White, A. J. P.; Williams, D. J.; Barrett, A. G. M.; Hoffman, B. M. *J. Org. Chem*. **2003**, *68*, 1665-1670

(39) Sakellariou, E. G.; Montalban, A. G.; Meunier, Hubert, Rumbles, G.; Philips, D.; Ostier, R. B.; Suhling, K.; Barrett, A. G. M.; Hoffman, B. M. *Inorg. Chem*. **2002**, *41*, 2182-2187

(40) Montalban, A. G.; Baum, S. M.; Barrett, A. G. M.; Hoffman, B. M. *Dalton Trans*. **2003**, 2093-2102.

(41) Michelsen, U.; Kliesch, H.; Schnurpfeil, G.; Sobbi, A. K.; Wöhrle, D. *Photochem. Photobiol*. **1996**, *64*, 694-701.

(42) Novakova, V.; Morkved, E. H.; Miletin, M.; Zimcik, P. *J. Porphyrins Phthalocyanines*, **2010**, *14*, 582-591

(43) Zimcik, P.; Novakova, V.; Miletin, M.; Kopecky, K. *Macroheterocycles* **2008**, *1*, 21-29 , and refs therein;.

(44) Donzello, M. P.; Viola, E.; Giustini, M.; Monacelli, F.; Ercolani C. *Dalton Trans.*, **2012**, *41*, 6112-6121.

(45) Spiller, W.; Kliesch, H.; Wöhrle, D.; Hackbarth, S.; Röder, B.; Schnurpfeil, G. *J. Porphyrins Phthalocyanines*, **1998**, *2*, 145-158.

(46) Ogunsipe, A.; Maree, D.; Nyokong, T. *J. Mol. Struct*. **2003**, *650*, 131-140.

(47) Musil, Z.; Zimcik, P.; Miletin, M.; Kopecky, K.; Petrik, P.; Lenco, J. *J. Photochem. Photobiol., A* **2007**, *186*, 316-322.

Chapter Five

Tetraanionic and Tetracationic Water-Soluble Manganese Porphyrins: Electrochemical and Spectroelectrochemical Characterization

5.1 Introduction

This chapter reports electrochemical properties of the four water-soluble tetraanionic and tetracationic Mn porphyrins whose structures are shown in Chart 5-1. This project is part of a collaborative study with reseachers in France who synthesized these compounds for use in Magnetic Resonance Imaging (MRI). Hydrophilic moieties (*e.g.*, PEG-chains) were added to two of the compounds to increase water-solubility. Preliminary MRI studies by our collaborators showed that such Mn porphyrins could be used without adverse effects and showed no *in-vivo* toxicity and good solubility at physiological pH.

Our laboratory has long been investigating in the electrochemistry of manganese porphyrins, both compounds with simple structures such as those with TPP macrocycle,[1-5] those with more conjugated macrocycles such as forms with DPP[6,7] and positively charged compound such as TMPyPMn porphyrins.[8,9] We were specifically interested in the manganese porphyrins of Chart 5-1 since more recent studies in literature have described the use of these type compounds in the area of medicine,[10-16] and in the formation of new materials solid state consisting of negatively and positively charged porphyrins with different central metal ions (or metal free), which were combined together in various ratios.[17-22]

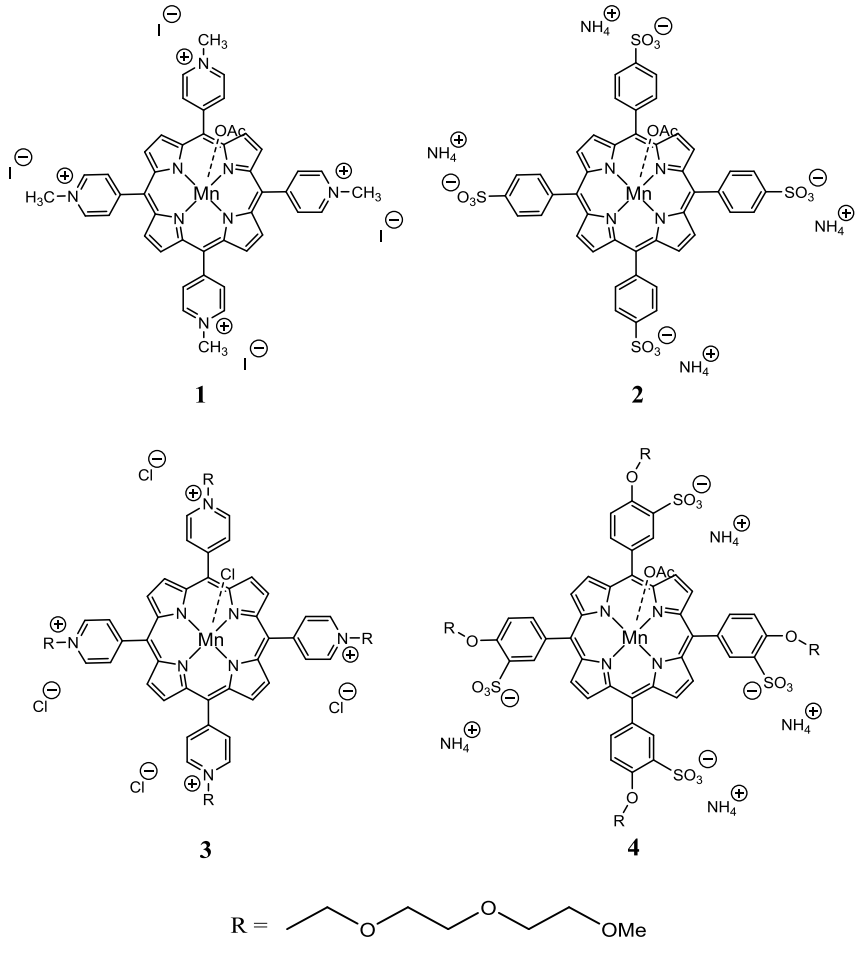

Chart 5-1. Structures of the investigated Manganese TMPyP and TPPS derivatives.

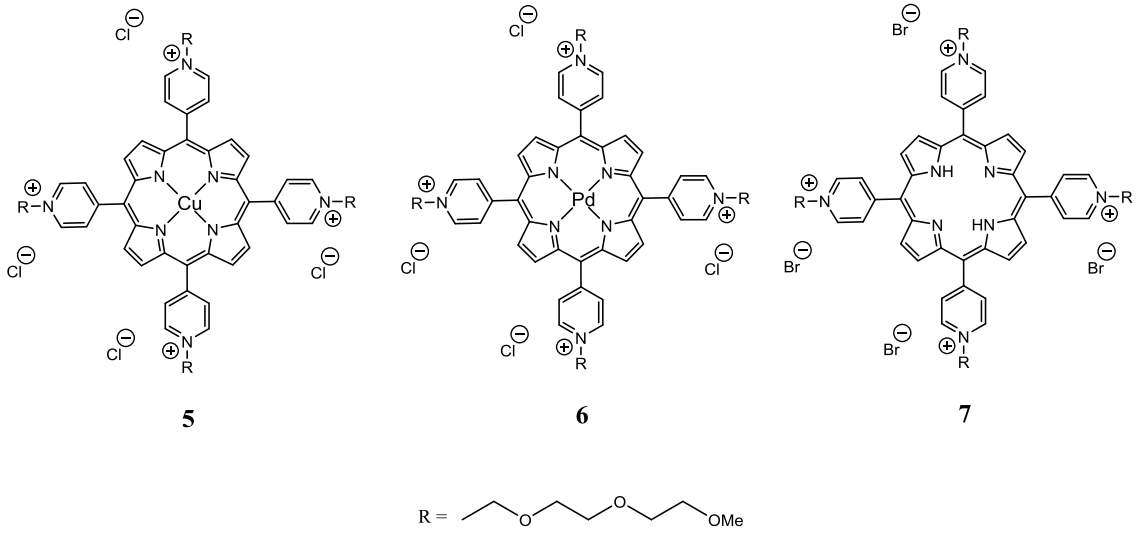

5 **6** **7**

Chart 5-2. Structures of the TMPyP(PEG)M derivatives, M = Cu(II), Pd(II) and 2H.

5.2 Results and Discussion

5.2.1 Synthesis of PEG Derivatives

A one-step procedure was used by our collaborators[23] to prepare the free-base TMPyP(PEG) (Scheme 5-1) starting from tetrapyridyl porphyrin (commercially available). This latter was reacted in DMF in the presence of an excess of the bromo-PEG derivative. The tetra-PEG-derivative was efficiently obtained in 80% yield. The metalation step was carried out in a methanol/water mixture using a large excess of $MnCl_2 \bullet 4H_2O$. The progress of the reaction was monitored by UV-visible spectroscopy by the shift of the Soret band from 427 nm to 463 nm, with complete manganese insertion observed after 1h.

The PEG-tetrasulfonated porphyrin (Scheme 5-2) was prepared in two steps and in good yield starting from the *meso*-tetrakis-(4-hydroxy)porphyrin; the completion of the reaction was monitored by MALDI/TOF mass spectrometry. The four sulfonate groups were introduced at the ortho-position (of the PEG chains) by reaction with $ClSO_3H$. The crude product was purified by chromatography on a C_{18} reverse column with 10% CH_3CN/H_2O as eluent.

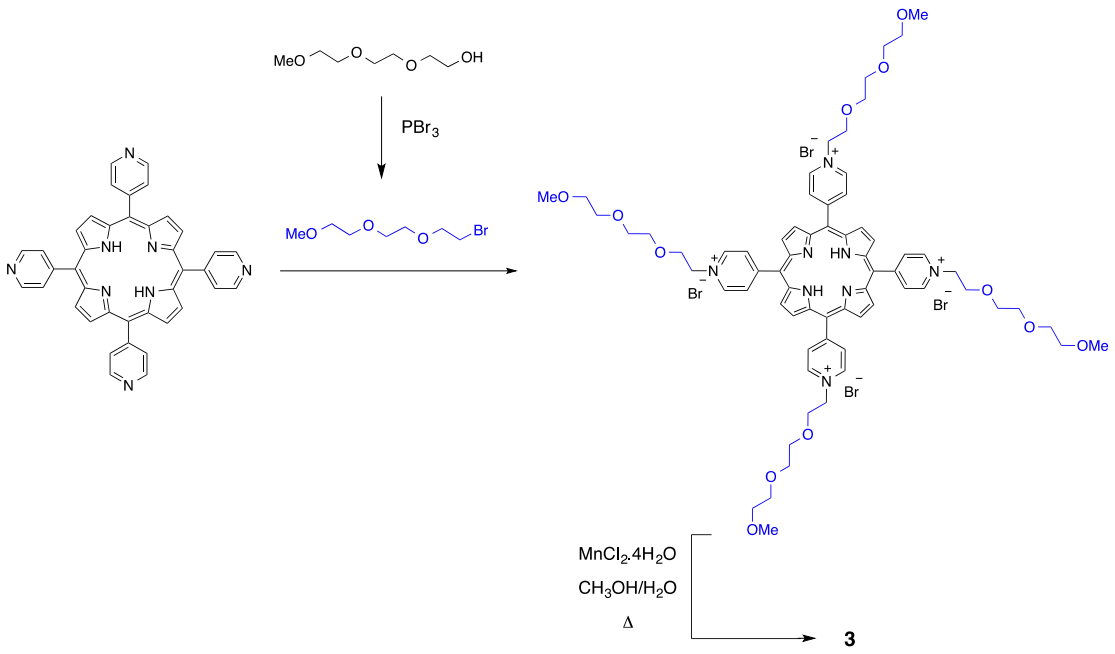

Scheme 5-1. Synthesis route for free-base TMPyP(PEG) complex.

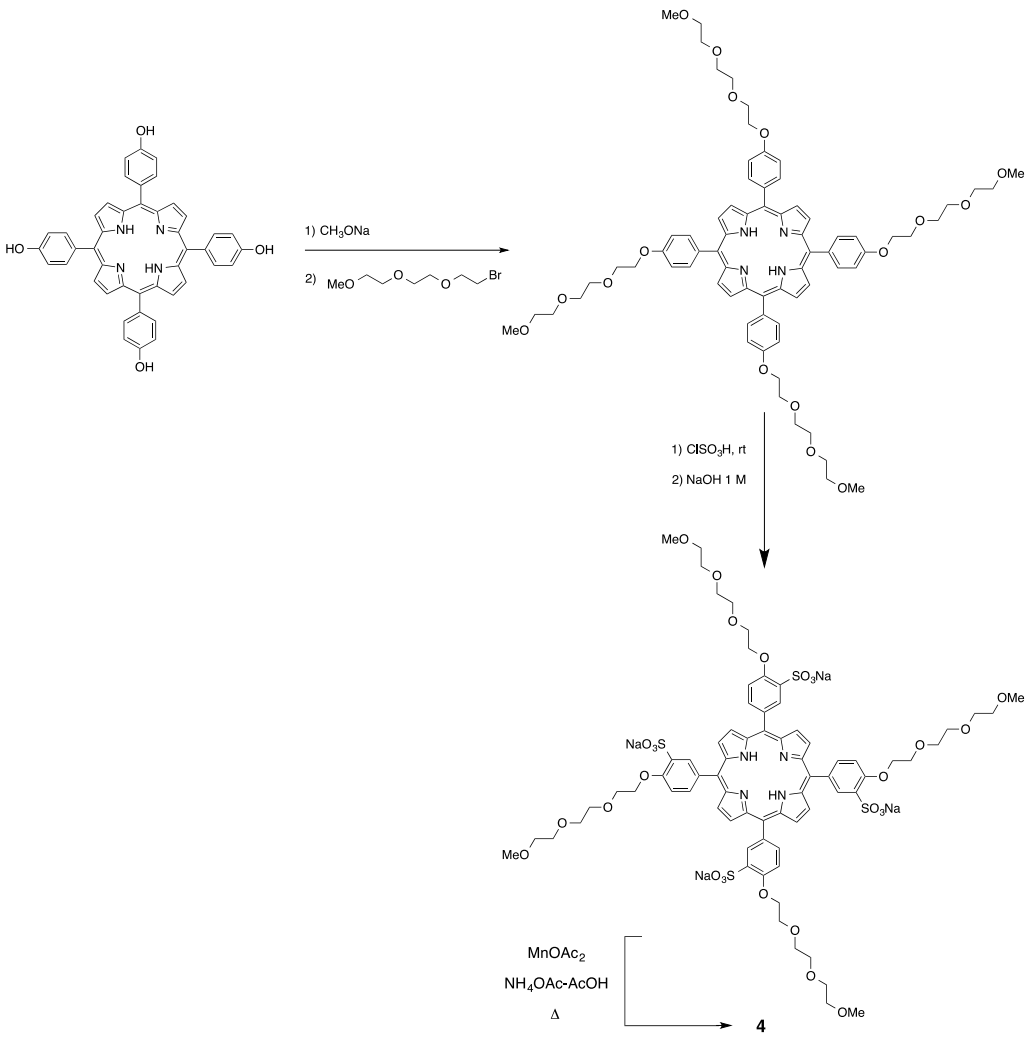

Scheme 5-2. Synthesis route for TPPS(PEG)H_2 complex.

5.2.2 Electrochemical Measurements

The electrochemistry of compounds **1** to **4** was carried out in DMSO and DMF containing 0.1M TBAP. Examples of cyclic voltammograms are illustrated in Figure 5-1 and Figure 5-2 and half-wave potentials for reduction are summarized in Table 5-1. No oxidations could be observed within the positive potential limit of the solvent.

A key difference between the redox behavior of the two series of compounds is the total number of electrons which can be reversibly added to the porphyrin at relatively low potentials. The tetra *N*-alkylpyridyl derivatives, **1** and **3**, can reversibly accept seven electrons at potentials between 0.00 and -1.00 V vs. SCE while the tetrasulfonatoporphyrin complexes, **2** and **4**, are limited to the addition of a single electron in the same range of potential. The first reduction of all four compounds is assigned to a Mn(III)/Mn(II) electron transfer.[3,8,9,20,21,24] This is then followed by two single-electron transfer process at the conjugated macrocycle[9] in the case of **2** and **4**, and two multi-electron transfer processes in the case of **1** and **3** the first of which involves 2e being added to the conjugated macrocycle which is followed by an overall 4e reduction of the four positively charged *N*-alkylpyridyl groups, all of which are reduced at the same halfwave potential of -0.94 to -0.95 V, as shown in Figures 5-1 (DMSO) and Figures 5-2 (DMF) and schematically illustrated in Scheme 5-3.

Although the global electron transfer mechanism for reduction of compound **2** and **4** is the same in DMSO and DMF, some differences exist in the cyclic voltammograms of the two compounds in the two solvents. The first is the electrochemical reversibility of the Mn(III)/(II) processes which is related to the potential difference between the anodic and cathodic peaks of the first reduction. A fast (reversible)

process has a separation between the reduction and oxidation peaks of about 60 mV (the theoretical value is 0.059/n V)[25] while a slow electron transfer process has a much larger peak to peak separation and is generally called quasireversible for E_{pc} - E_{pa} values of 80-600 mV and electrochemically irreversible if there is no return peak at all after an oxidation or reduction. In the case of compound **2**, the peak to peak separation for the first reduction (the Mn(III)/(II) processe) is 220 mV in DMF and 550 mV in DMSO while for compound **4** the separation in these two solvents is 240 mV and 550 mV, respectively. The electrochemical rate of electron transfer , k^o, is directly related to the ΔE_p values for a given scan rate and what this means is that a slower rate of electron transfer is exhibited by compound **4**, the PEG derivative, independent of the solvent.

Compound **4** also differs for compound **2** in DMSO where the PEG porphyrin **4** displays another reversible redox process at $E_{1/2}$ = -0.83 V which is not observed for the structurally related compound **2** in either solvent. This process is assigned to the reduction of free NH_4^+ in solution as determined by independent measurement on the redox properties of NH_4Cl in DMSO, 0.1 M TBAP. (see cyclic voltammogram in Figure 5-3). The absence of this process for compound **4** in DMF or for compound **2** in either solvent indicates that this conversion is more strongly associated with the SO_3^- groups under these solution conditions. This point is not occurred to the chemistry or electrochemistry of the monomeric species reported on the following pages but it may be related to the redox behavior for mixture of the tetracationic and tetraanionic porphyrins described in later sections of this chapter.

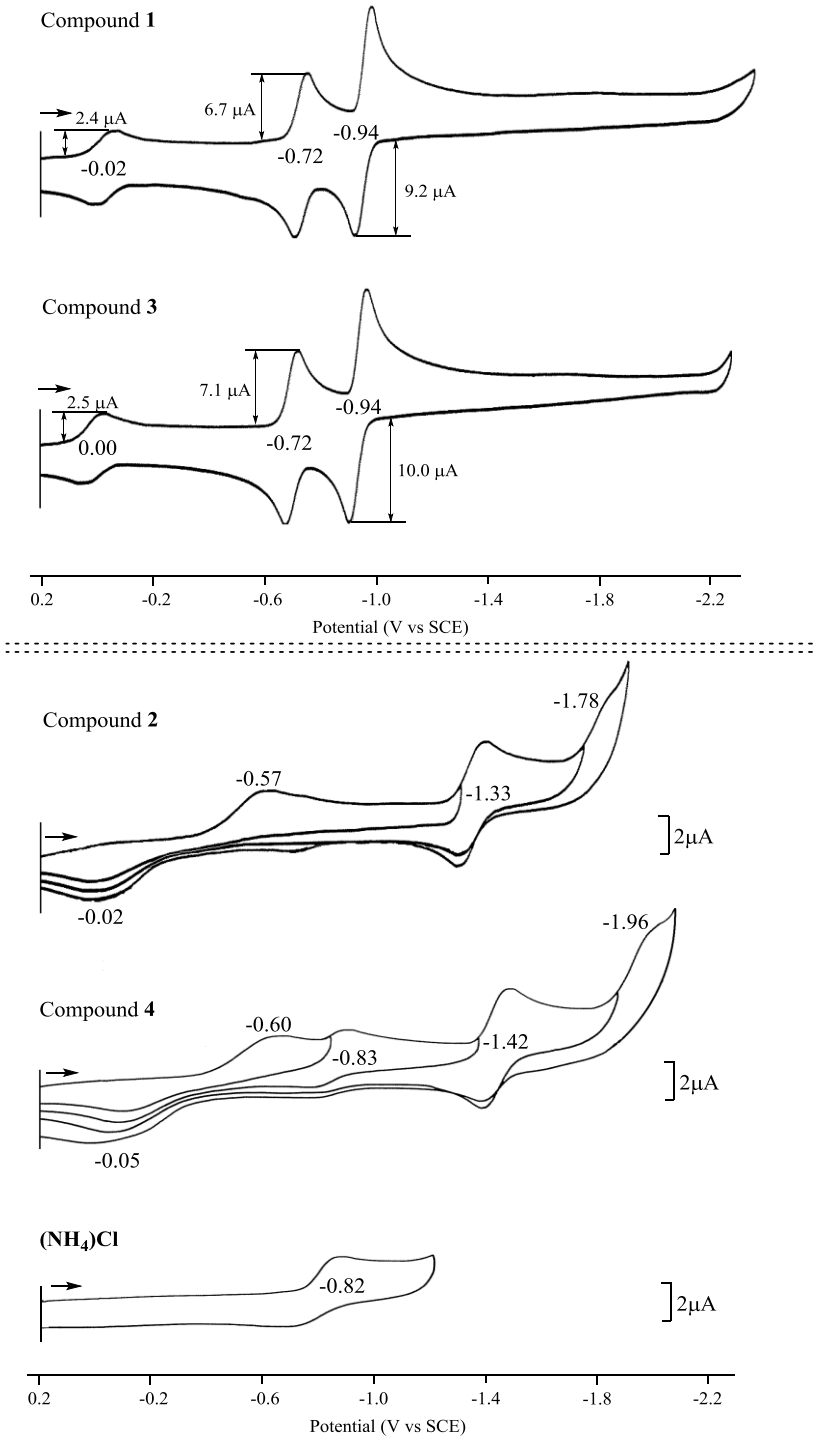

Figure 5-1. Cyclic voltammograms of investigated manganese TMPyP and TPPS derivatives in DMSO, 0.1 M TBAP. Scan rate of 0.1 V/s.

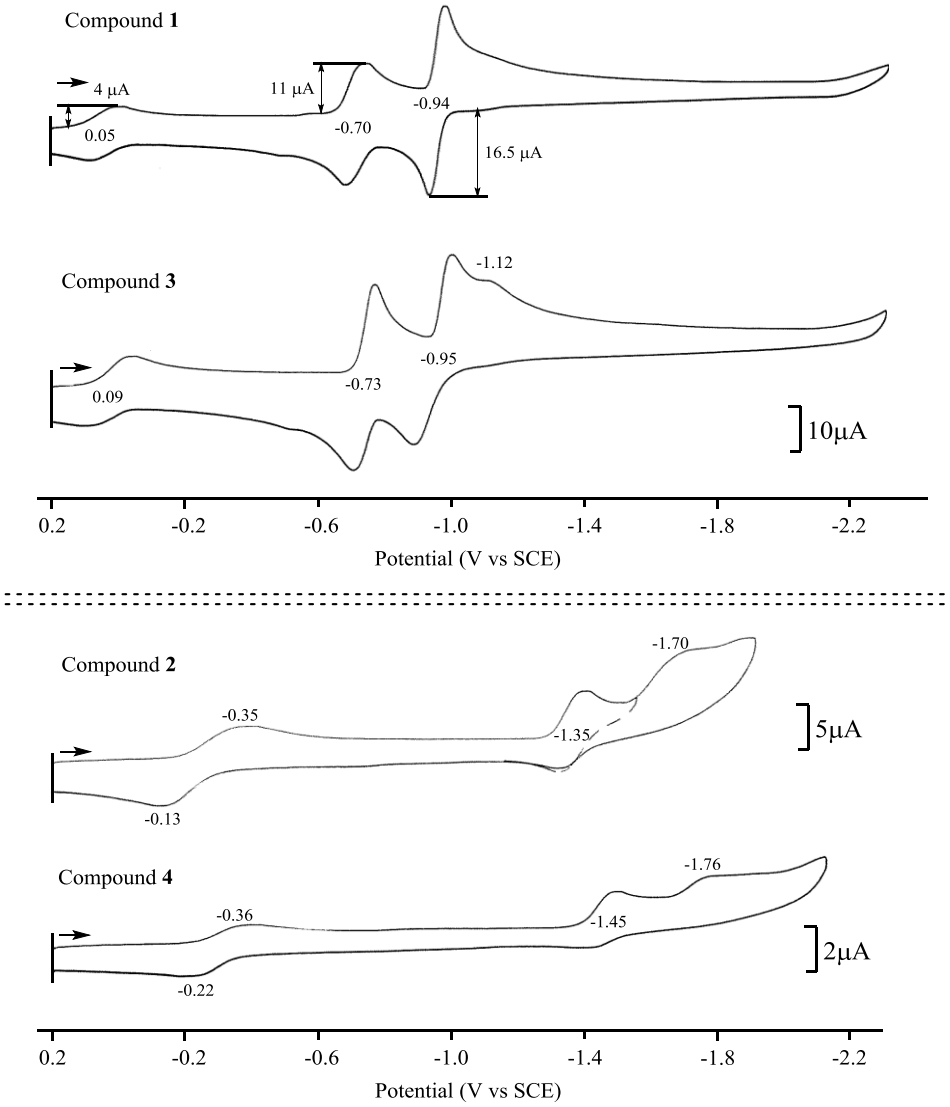

Figure 5-2. Cyclic voltammograms of investigated manganese TMPyP and TPPS derivatives in DMF, 0.1 M TBAP. Scan rate of 0.1 V/s.

Compounds **1** and **3**

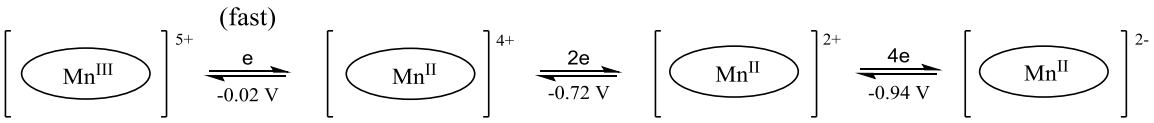

Compounds **2** and **4**

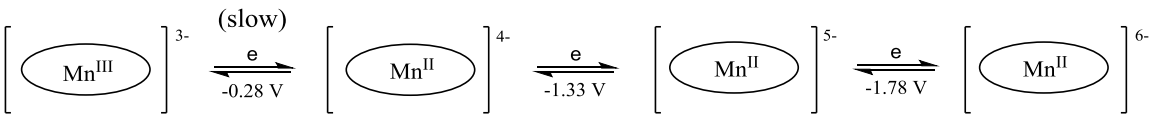

Scheme 5-3. Proposed Reduction mechanism of Compounds **1-4** in DMF or DMSO, containing 0.1 M TBAP. The listed potentials were recorded in DMSO for compounds **1** and **2**.

Table 5-1. Reduction potentials ($E_{1/2}$ V vs SCE) of investigated TMPyP and TPPS complexes in DMF and DMSO, 0.1 M TBAP.

Solvent	Cpd	Reduction (V vs. SCE)		
		Mn^{III}/Mn^{II} (ΔE_p)[a]	2nd[b]	3rd[b]
DMSO	**TMPyPMn 1**	-0.02 (0.08)	-0.72 (2e)	-0.94 (4e)
	TMPyP(PEG)Mn 3	0.00 (0.10)	-0.72 (2e)	-0.94 (4e)
	TPPSMn 2	-0.28 (0.55)	-1.33 (1e)	-1.78 (1e)[c]
	TPPS(PEG)Mn 4	-0.28 (0.55)	-1.42 (1e)	-1.96 (1e)[c]
DMF	**TMPyPMn 1**	0.05 (0.06)	-0.70 (2e)	-0.94 (4e)
	TMPyP(PEG)Mn 3	0.09 (0.06)	-0.73 (2e)	-0.95 (4e)
	TPPSMn 2	-0.24 (0.22)	-1.35 (1e)	-1.70 (1e)[c]
	TPPS(PEG)Mn 4	-0.29 (0.14)	-1.45 (1e)	-1.76 (1e)[c]

[a] the potential difference between the reduction and oxidation peaks of the Mn^{III}/Mn^{II} process are given in parenthesis
[b] number of electron transfer in parenthesis
[c] irreversible peak potential of a scan rate at 0.1 V/s

5.2.3 Reduction of Interacting and Non-Interaction *N*-Alkyl Substituents

Earlier electrochemical studies of $[TMPyPM]^{4+}$, where M = Cu(II), Zn(II) or VO(II), showed reductions in DMF to occur in three two-electron transfer steps,[8,26] the first of which was assigned as involving the porphyrin macrocycle and the later two as reductions at the four external *N*-alkyl groups. The same redox behaviour is observed for the newly synthesized Pd(II) and Cu(II) derivatives whose structures are shown in Chart 5-2 with a tetra- positively charged PEG macrocycle and this is illustrated by the cyclic voltammograms in Figure 5-3

5.2.4 Influence of Central Metal Ion on Ease of Macrocycle and *N*-Alkylpyridyl Reduction

As can be seen in Figure 5-3, the potentials for the first reduction of the macrocycle and the first reduction of *N*-alkylpyridyl groups are both relatively facile in the case of the free-base (metal free) porphyrin and more difficult in the case of the Mn(II) derivative, with the $E_{1/2}$ values for the Cu(II) and Pd(II) complexes being between the two extremes. An early study by Fuhrhop, Kadish, and Davis showed a linear relationship to exist between the potentials for oxidation or reduction of the porphyrin macrocycle and the electronegativity of the central metal ion[27] and this relationship also holds in the case of the *N*-alkylpyridyl porphyrins investigated in the study. Within a series of compounds having the tetraphenylporphyrin (TPP) macrocycle, the most difficult reduction occurs for the Mn(II) complex and the easiest for the VO derivative and the same trend is seen for the TMPyPM complexes. This is seen in Figure 5-5 which plots $E_{1/2}$ value for the macrocycle centered reduction of TMPyPM vs $E_{1/2}$ for the macrocycle centered reduction of TPPM. The plot is linear with a correlation coefficient

of 0.98.

5.2.5 Spectroelectrochemical Measurements

UV-visible spectral changes for the Mn(III)/Mn(II) processes of **1**-**4** in DMSO and DMF were also monitored during controlled potential reduction in a thin-layer cell. Examples of the spectral changes in DMSO are shown in Figure 5-6 and a summary of the spectral data is given in Table 5-2. The spectrum of the neutral compound **1** is characterized by a Soret band at 460 nm and two shoulder bands at 371 and 392 nm. There are also two Q bands at 563 and 598 nm. During the first reduction at -0.50 V, the Soret band at 460 nm shifts to 452 nm and increases in intensity while the two Q bands shift to 575 nm and 617 nm. No new absorptions are observed from 700–900 nm, consistent with a metal-centered electron transfer[1,8] and the conversion of Mn^{III} to Mn^{II}. Similar UV-visible spectral changes are seen for the other three porphyrins but the Mn(III) form of **2** and **4** possesses three rather than two shoulder bands in the two solvents. (see Table 5-2).

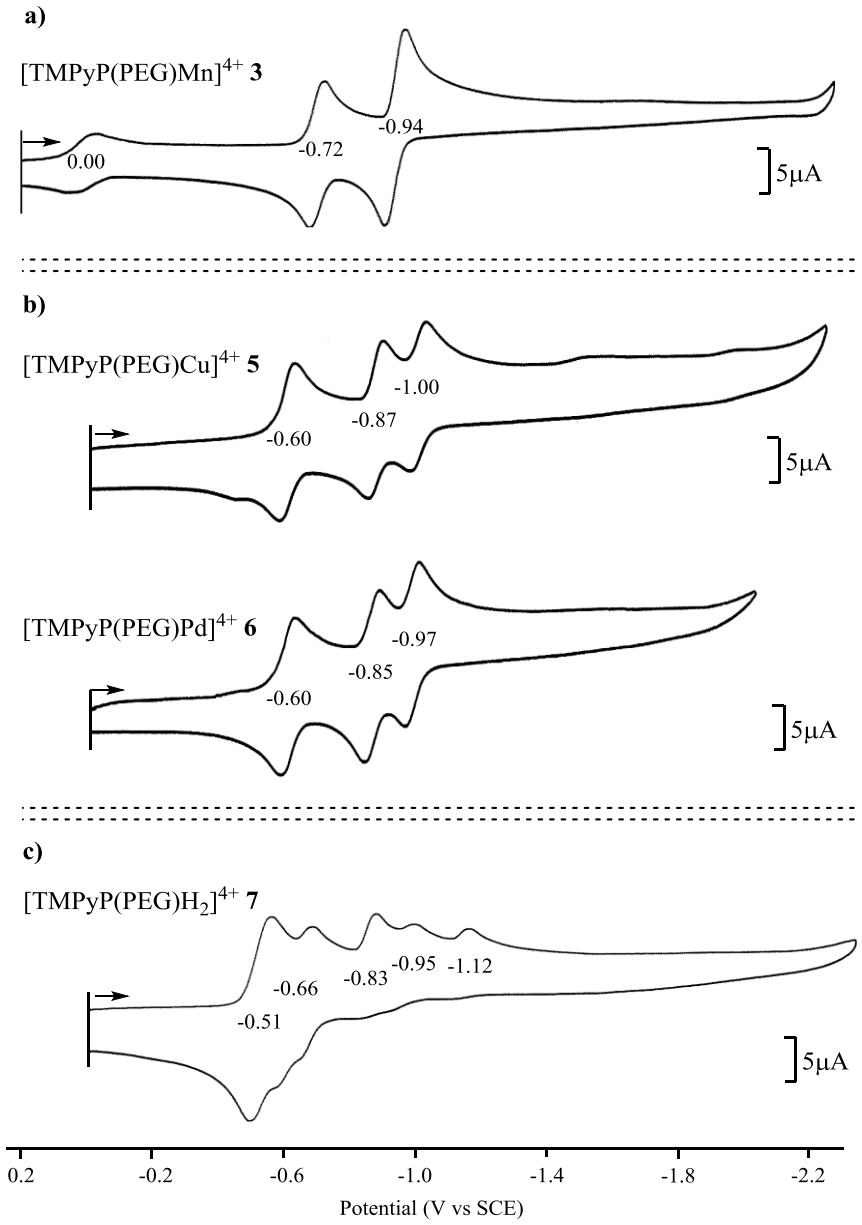

Figure 5-3. Cyclic voltammograms illustrating the three types of redox behaviors for TMPyPM derivatives: a) M = Mn(III), b) M = Cu(II), Pd(II) and c) M= 2H in DMSO, 0.1 M TBAP. Scan rate of 0.1 V/s.

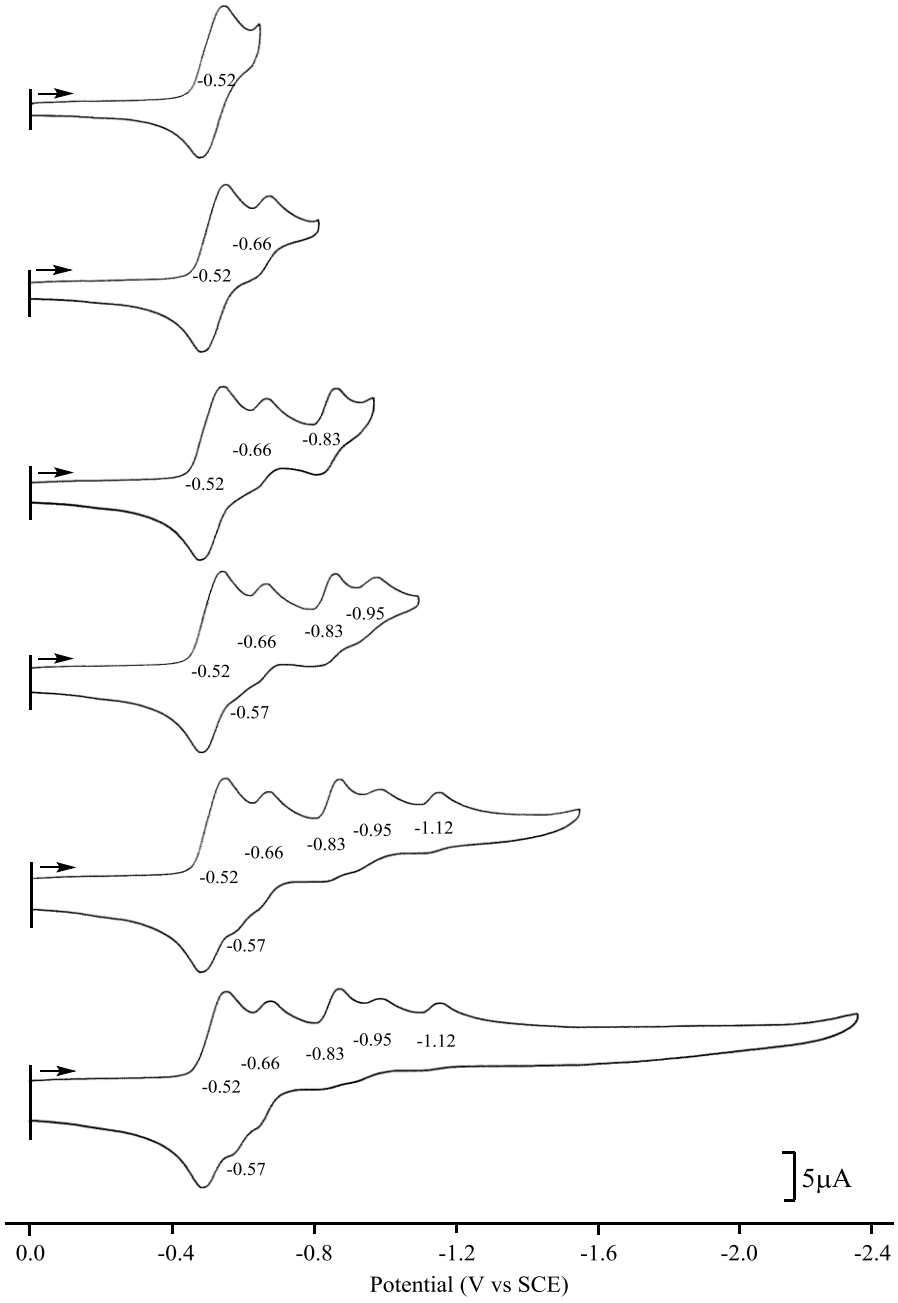

Figure 5-4. Cyclic voltammograms illustrating the stepwise reductions for TMPyP(PEG)H_2 derivative, in DMSO, 0.1 M TBAP. Scan rate of 0.1 V/s.[28]

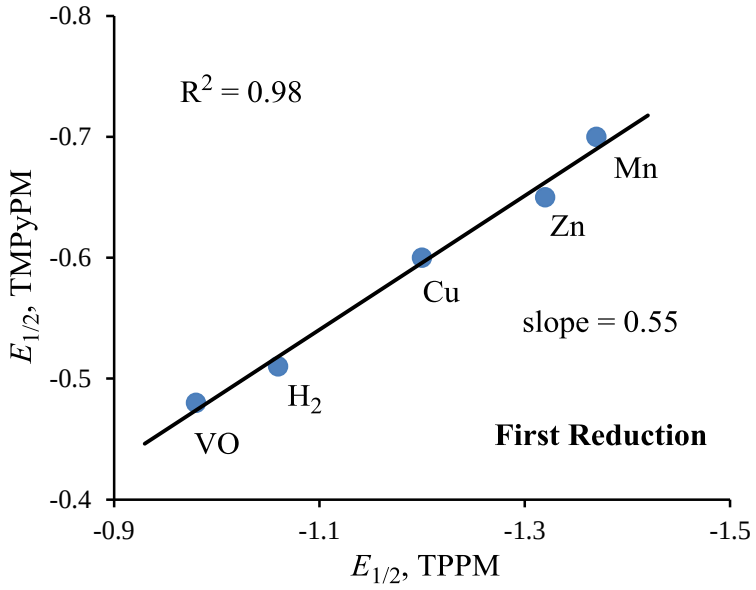

Figure 5-5. Correlation between ring-centered reduction potentials between TPPM and TMPyPM in DMSO, 0.1 M TBAP. The value of $E_{1/2}$ for TPP(VO) were taken from ref 29.

5.2.6 Spectral Properties of Highly Reduced *N*-Alkyl Derivatives

As seen in Figure 5-6 and Table 5-2, UV-visible spectra of the tetra-positively charged compounds **1** and **3** are similar to each other in both their Mn(III) and Mn(II) forms. Both unreduced porphyrins are characterized in DMSO by a sharp Soret band at 460 nm and a single Q band at 563 nm for **1** and 565 nm for **3**. Reduction to Mn(II) leads to a spectrum with a more intense Soret band at 452 nm (**1**) or 457 (**3**) and two Q bands at 575 and 617 nm for **1** or 575 and 621 nm for **3**. Thus, the presence of the PEG groups or a CH_3 group on the tetra- cationic porphyrin has little effect on the UV-visible spectra or on the redox potentials of the Mn(III)/Mn(II) process located at $E_{1/2}$ values of -0.02 to 0.00 V vs. SCE in DMSO (see Figure 5-1).

The second and third reductions of **1** and **3** involve two and four electrons, respectively. The electroreduced Mn(II) porphyrins are also similar to each other as seen by the spectroelectrochemical data in Figure 5-7a. The addition of two electrons to the porphyrins macrocycles of **1** and **3** leads in each case to a decreased intensity Soret band and new bands at 491 and 773 nm for **1** or 507 and 778 nm for **3**. Both spectra are similar to spectra reported for doubly reduced *N*-alkylpyridyl porphyrins containing Cu(II) and Pd(II) central metal ions as shown in Figure 5-7b and Figure 5-7c, respectively. The position of the near-IR band ranges from 778 to 831 nm for the doubly reduced macrocycles depending upon the metal ions. This band disappears upon further reduction of the *N*-alkylpyridyl groups as shown by the spectral change given in Figure 5-7.

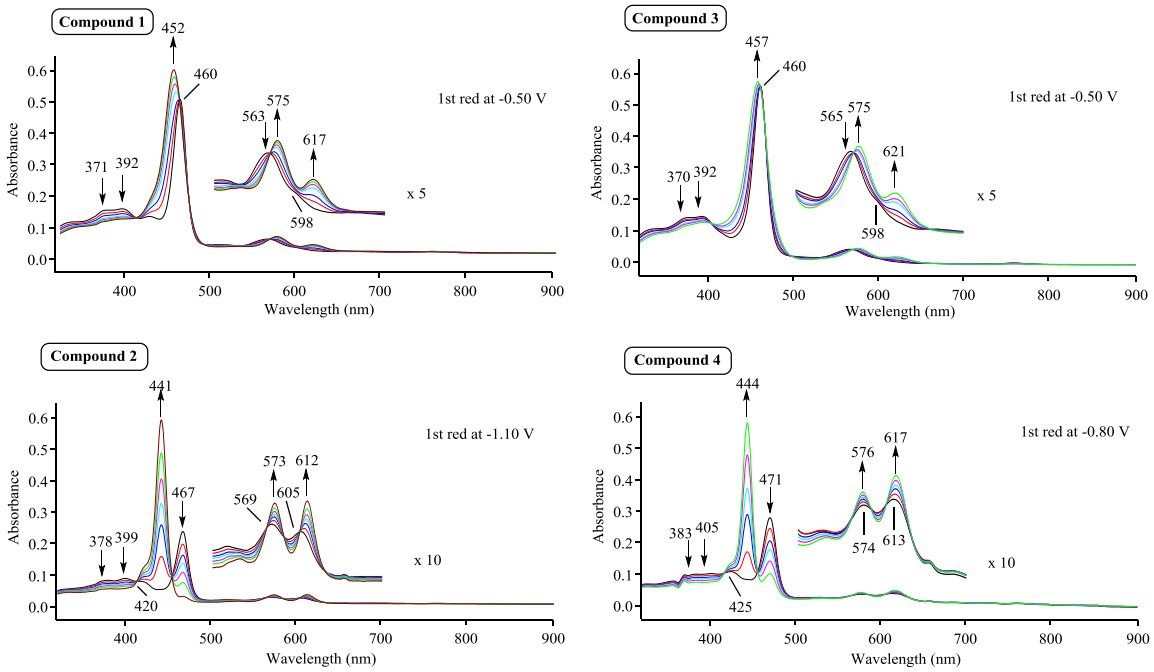

Figure 5-6. UV-visible changes for the Mn^{III}/Mn^{II} process of investigated compounds in DMSO, containing 0.1 M TBAP. A summary of the spectral data is given in Table 5-2.

Table 5-2. UV-visible spectral data λ_{max} (nm) of investigated manganese porphyrins in DMSO and DMF, containing 0.1 M TBAP. Shoulder bands can be seen in Figure 5-3.

Solvent	Cpd	Mn^{III}			Mn^{II}		
		Soret	Q band		Soret	Q band	
DMSO	**TMPyPMn 1**	**460**	563	598	**452**	575	617
	TMPyP(PEG)Mn 3	**460**	565	599	**457**	575	621
	TPPSMn 2	**467**	569	605	**441**	573	612
	TPPS(PEG)Mn 4	**471**	574	613	**444**	576	617
DMF	**TMPyPMn 1**	**460**	571	619	**453**	576	621
	TMPyP(PEG)Mn 3	**466**	582	627	**467**	584	632
	TPPSMn 2	**468**	569	606	**438**	572	611
	TPPS(PEG)Mn 4	**473**	575	615	**441**	576	616

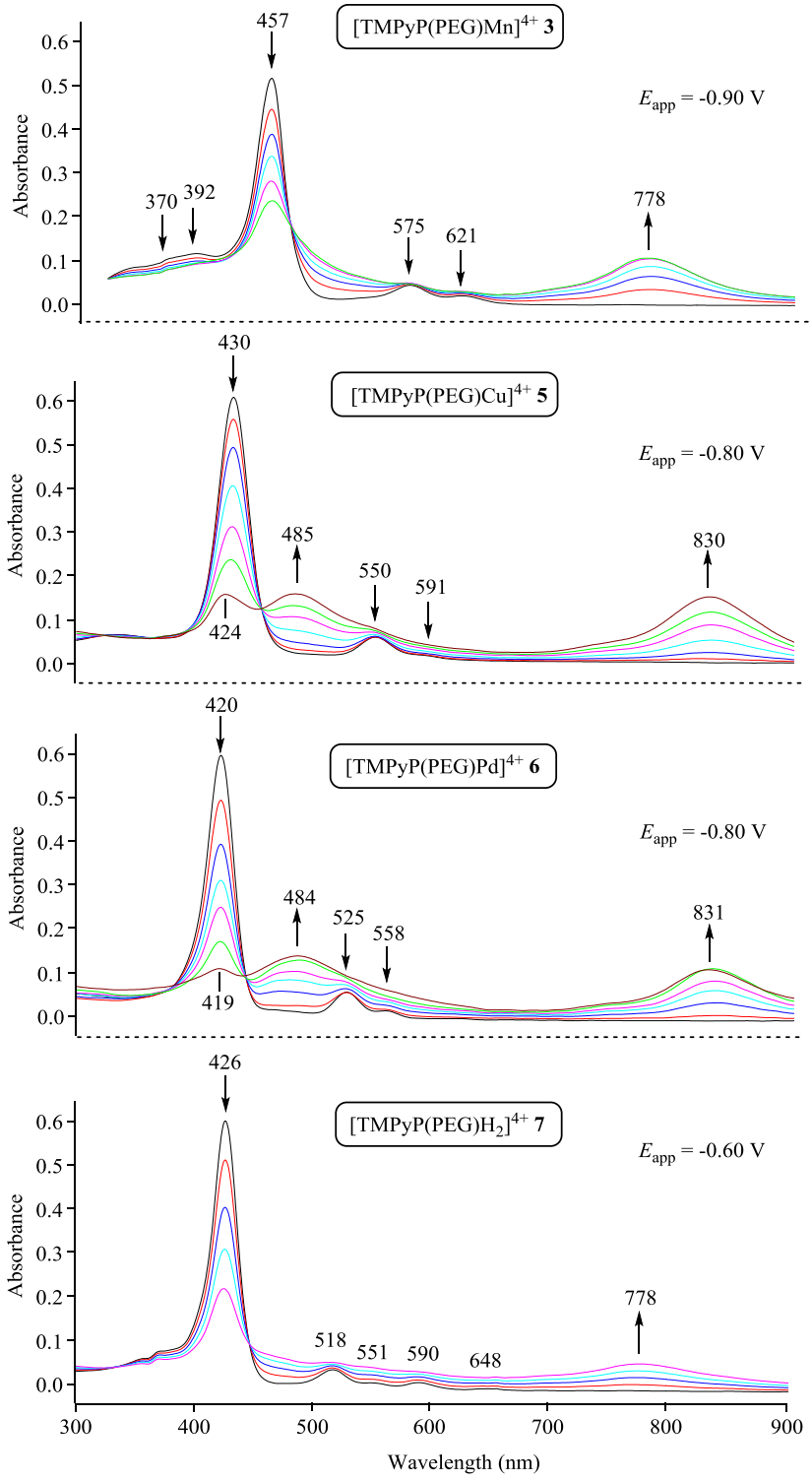

Figure 5-7. UV-visible changes for reductions on the macrocycle of TMPyP(PEG)M where M = Mn(III), Cu(II), Pd(II) or H_2 in DMSO, containing 0.1 M TBAP.

5.2.7 Can Potentials for Reduction of *N*-Alkylpyridyl of Compound 1 Be Changed?

Preliminary studies are carried out on electrochemistry and spectroelectrochemistry of tetracationic and tetraanionic manganese porphyrin "raft", which is the mixture of compounds **1** and **2** with molar ratio being 1:1 in DMF or DMSO solution. According to the previous published literature,[21,22] possible formations of manganese "raft" by compounds **1** and **2** are proposed (but may not be limited to) as shown in Scheme 5-4.

As seen in the cyclic voltammagrams of "raft" in DMF containing 0.1 M TBAP shown in Figure 5-8, during the first scan of "raft", the half-wave potentials for each electron addiction process occurring at compound **1** (or **2**) in the form of "raft" are almost identical to the monomeric form of compound **1** (or **2**) under the same solution condition, whose cyclic voltammograms are also shown in Figure 5-8. The first two reductions at $E_{1/2}$ = -0.04 V and $E_{1/2}$ = -0.24 V are assigned to the conversion of Mn(III) to Mn(II) of compound **1** and compound **2** in the form of "raft", respectively, whose half-wave potentials are same with that of their monomer in DMF (see Figrue 5-8). However, the second reduction at $E_{1/2}$ = -0.24 V in the "raft" is reversible, while the same process corresponding to the central Mn(III) ion reduction of monomeric compound **2** is quasi-reversible, being with a 220 mV peak-peak potential separation. Possible explanations for this better reversibility may either be the loss of axial acetate ligand from compound **2** in the "raft" form or less negative charge effect of peripheral sulfonato groups of compound **2** on its central manganese ion due to neutralization by the four *N*-methylpyridyl groups of compound **1**.

Reductions involving the electron addition processes at porphyrin macrocycles in

the form of "raft" occur at $E_{1/2}$ = -0.68 V for compound **1** and $E_{1/2}$ = -1.38 V compound **2,** which almost identical to the half-wave potentials compound **1** or **2** in their monomeric form (see Figure 5-8).

However, the different electrochemical behaviors are observed for the "raft" of compound **1** and compound **2** as compared to their monomers under the same solution condition. The first is that an extra reduction step is observed for the "raft" at E_{pc} = -0.53 V with less magnitude of current as compared to that of the first two reductions, which is not seen for either monomeric compound **1** or **2**. This extra process is coupled with the re-oxidation peak at E_{pa} = -0.46 V, which is observed on the reverse scan after the irreversible reduction of the four *N*-methylpyridyl groups at $E_{1/2}$ = -0.95 V. These observations may be due to the loss of positive charges on *N*-methylpyridyl groups after reduction leading to the change of orientation of the "raft" as well as the formation of a new redox process E_{pa} = -0.46 V.

As seen in the second scan also shown in the Figure 5-8, this newly formed redox couple of the "raft" is reversible at $E_{1/2}$ = -0.48 V with a two times current height of the first two reductions, indicating two one-electron reduction processes at the same potential. The half-wave potentials and reversibility of all the other redox processes in the second scan occurring at manganese metal centers, porphyrin macrocycles or the peripheral *N*-methylpyridyl groups are same with the corresponding processes in the first scan (see Figure 5-8), with an exception that the current height for the reduction at $E_{1/2}$ = -0.95 V decreases as compared to the same process in the first scan. This also indicates the change of orientation of the "raft" that leads to the electrochemical behavior of the peripheral *N*-methylpyridyl groups.

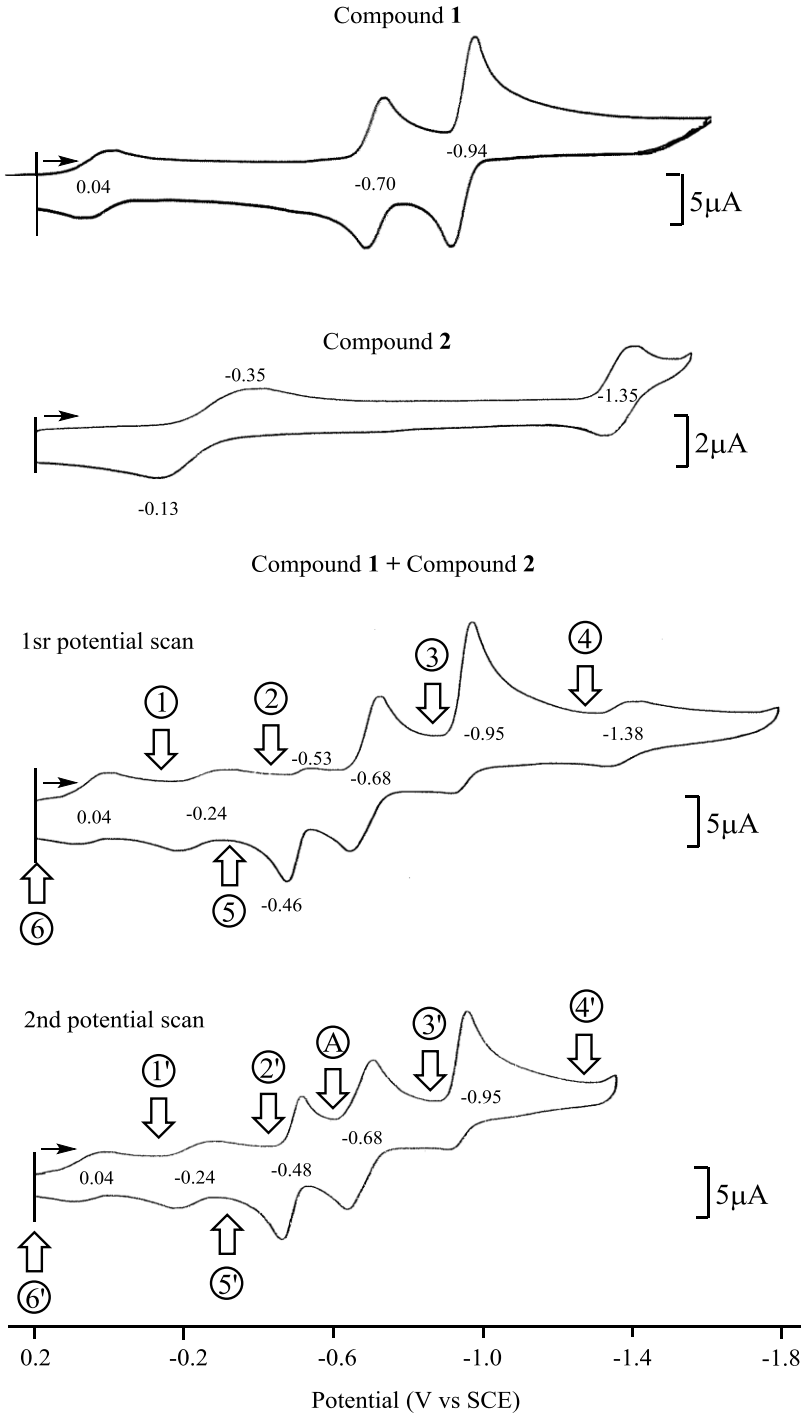

Figure 5-8. Cyclic voltammograms of 1:1 mixture (mole ratio) of compound **1** and compound **2** in DMF, 0.1 M TBAP. Scan rate of 0.1 V/s.

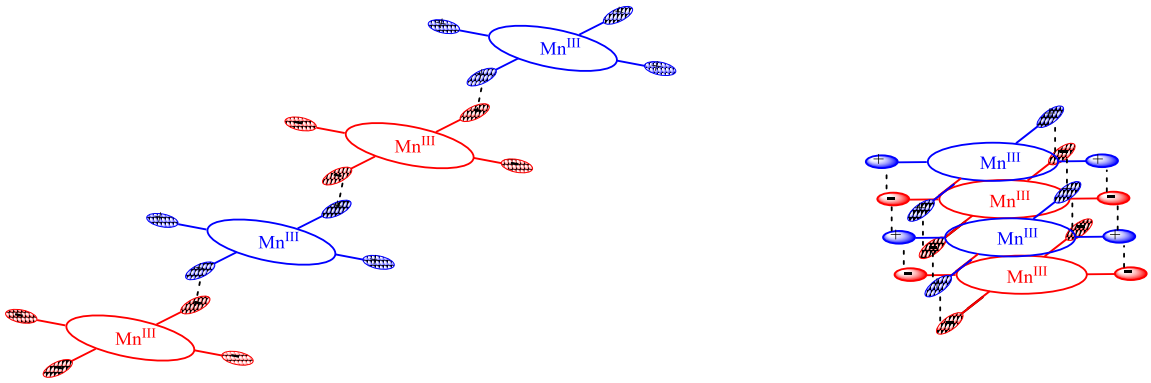

a) Linear b) Stacked

Scheme 5-4. Proposed conformation for the 1:1 mixture of compounds **1** and **2** in DMF or DMSO solution.

Spectroelectrochemistry of the manganese porphyrin "raft" is also investigated in DMF containing 0.1 M TBAP. As shown in Figure 5-9, the UV-visible spectral changes of compound **1** or **2** in the "raft" during step 1 to step 4 (also labeled in Figure 5-8) can resemble the spectral change of monomeric compound **1** or **2** under the same solution condition. Same as the irreversible reduction process at $E_{1/2}$ = -0.95 V in cyclic voltammetry time scale, after the electrolysis at controlled potential at E_{app} = -1.25 V (step 4), the UV-visible spectrum cannot go back to the initial spectrum of the "raft", which has a single Soret band at 461nm, once a controlled potential is applied at E_{app} = 0.20 V (step 6), while a different UV-visible spectrum is observed with split Soret bands at 425 nm and 463 nm as well as a new Q band at 516 nm (see Figure 5-9).

As shown in Figure 5-10, a second scan of spectroelectrochemistry is then carried out to investigate the spectral change of the newly formed UV-visible spectrum with split Soret bands from the first scan. During the first reduction at E_{app} = -0.15 V (step 1'), the band at 463 nm, 516 and 555 nm deceases in intensity with the formation of a new band at 438 nm and with the shift of the bands at 569 nm and 598 nm to 573 nm and 612 nm, respectively. However, no obvious change on the band at 425 nm is observed during the first reduction. In addition, different from the case for monomeric compound **1** or the case in the first scan during the reduction of Mn(III) to Mn(II), the band at 451 nm for monomeric TMPyPMn(II) is not seen in the second scan.

During the second reduction (step 2') at E_{app} = -0.45 V, the band at 463 nm keeps decreasing till total disappearance while the band at 438 nm keeps increasing in intensity, which is consistent with what is observed for the conversion of TPPSMn(III) to TPPSM(II) in the monomeric form of compound **2** or in the form of the "raft" during the

first scan. Again, no obvious change is observed for the band at 425 nm, which is though overlapping with the more intense band at 438 nm. Only during the third reduction at E_{app} = -0.60 V (step A in Figure 5-8) does the band at 425 nm start to decrease with the formation a broad band at 826 nm. The following spectral change from step 3' to 6' are identical to the processes from step 3 to 6 during the first scan.

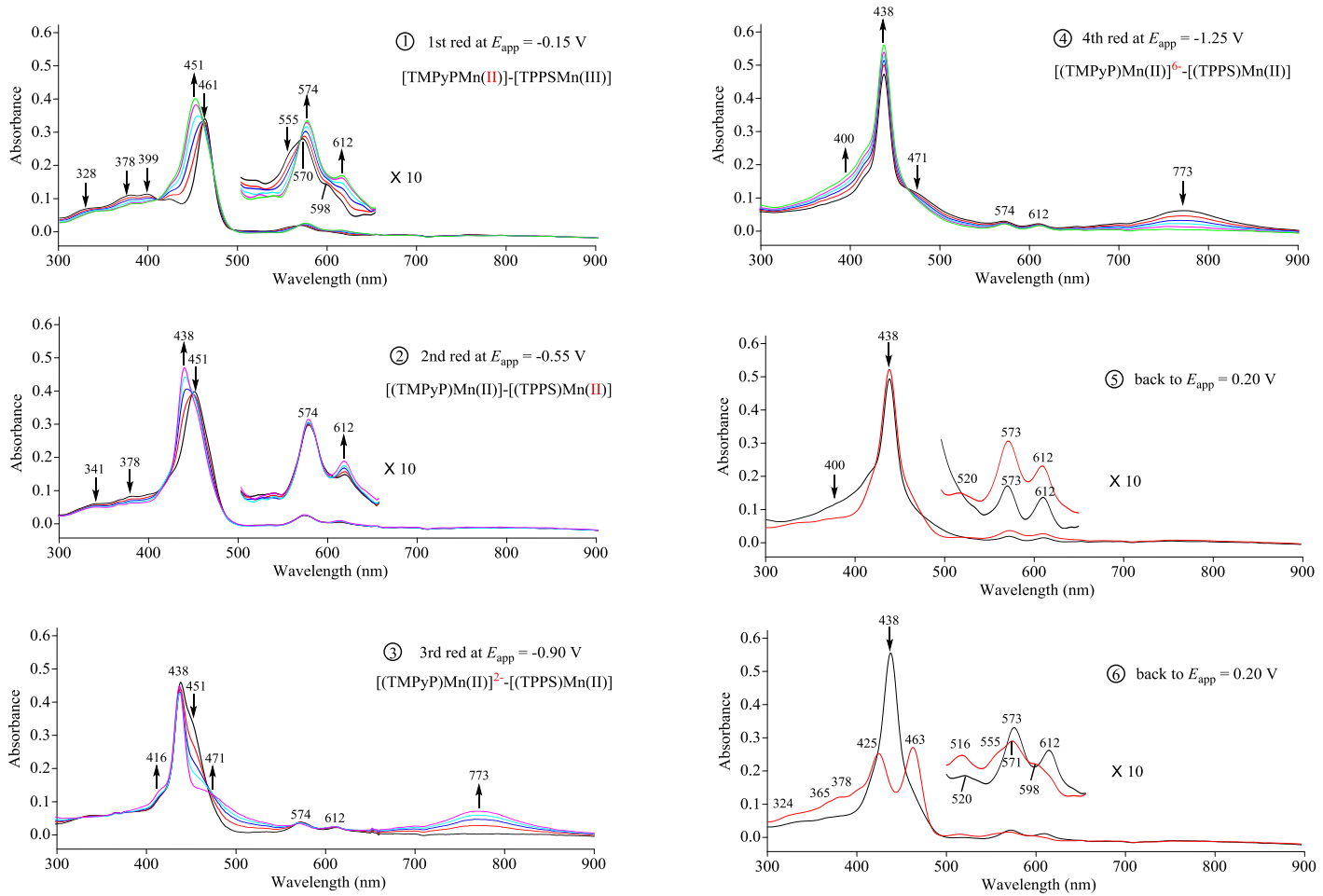

Figure 5-9. First scan of UV-visible spectral changes of 1:1 mixture (mol ratio) of compound **1** and compound **2** during reductions in DMF, 0.1 M TBAP, containing 0.1 M TBAP.

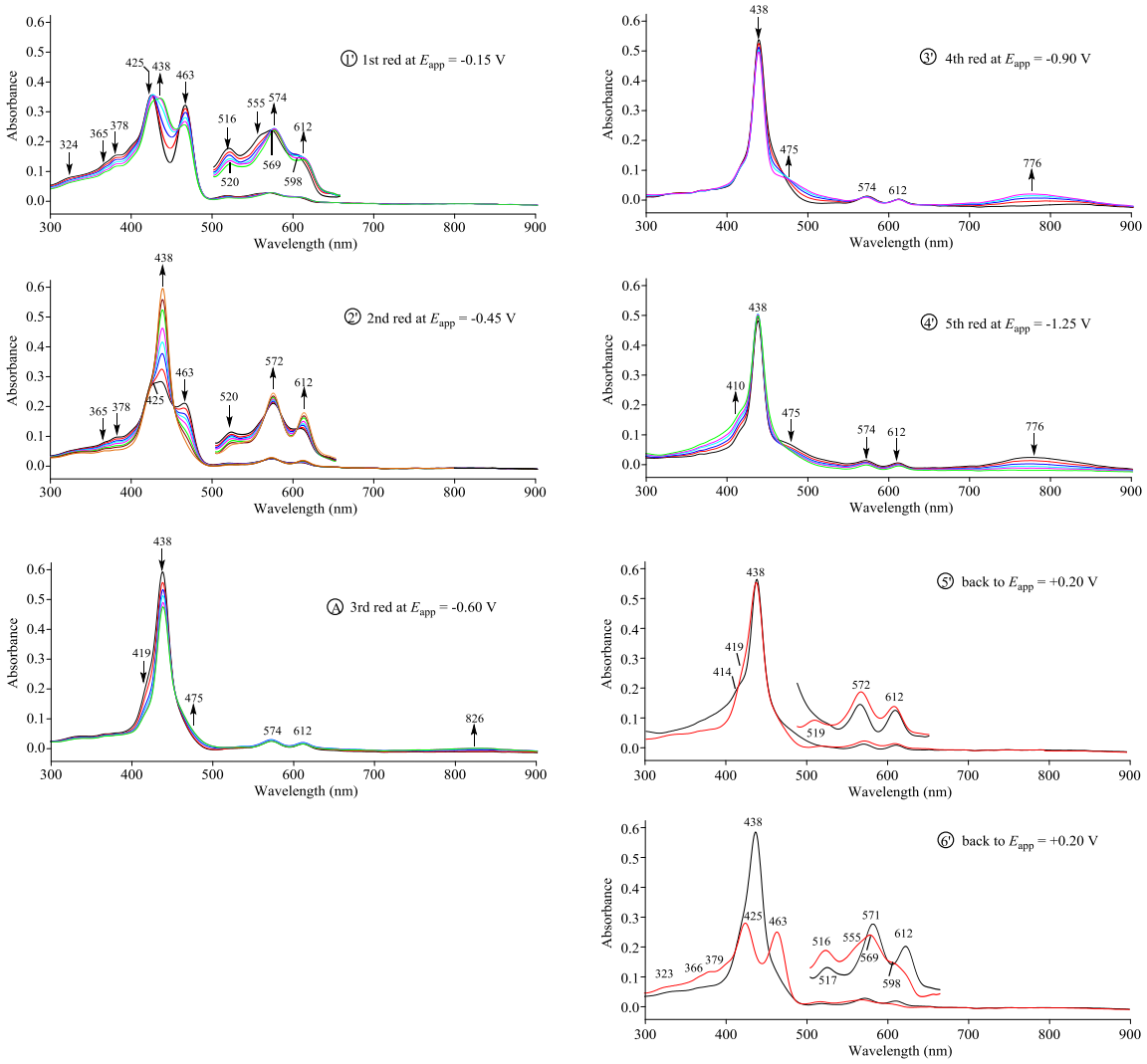

Figure 5-10. Second scan of UV-visible spectral changes of 1:1 mixture (mol ratio) of compound **1** and compound **2** during reductions in DMF, 0.1 M TBAP, containing 0.1 M TBAP.

5.3 Conclusions

Four Mn porphyrin complexes have been prepared and fully characterized as to their redox reactivity and UV-visible spectra in their Mn(III) and Mn(II) forms. The two TMPyP derivatives undergo a rapid and reversible conversion between their Mn(III) and Mn(II) forms while the two TPPSMn(III) complexes are more difficult to reduce and also exhibit slower electron transfer rate as compared to the TMPyP species.

It is observed by spectroelectrochemistry that there is interaction between the porphyrin macrocycle of doubly reduced TMPyP(PEG) complexes and the positive charge on the four *N*-alkypryridyl groups. The number of steps of reduction of the four peripheral *N*-alkypryridyl are dependent upon the central metal ion of the TMPyP(PEG)M. The electrochemical behavior of *N*-alkypryridyl group reduction can also be changed by mixing TMPyMn(III) with TPPSMn(III) in DMF solution and the "raft".

5.4 References

(1) Kadish, K. M.; Van Caemelbecke, E.; Royal, G. In *The Porphyrin Handbook*; Kadish, K. M., Smith, K. M., Guilard, R., Eds.; Academic Press: New York, 2000; Vol. 8, p 1.

(2) Kadish, K. M.; Kelly, S. *Inorg. Chem.* **1979**, *18*, 2968.

(3) Kelly, S. L.; Kadish, K. M. *Inorg. Chem.* **1982**, *21*, 3631.

(4) Kadish, K. M.; Sweetland, M.; Cheng, J. S. *Inorg. Chem.* **1978**, *17*, 2795.

(5) Yang, S.; Sun, B.; Ou, Z.; Meng, D.; Lu, G.; Fang, Y.; Kadish, K. M. *J. Porphyrins Phthalocyanines* **2013**, *17*, 857.

(6) Fukuzumi, S.; Nakanishi, I.; Barbe, J.-M.; Guilard, R.; Van Caemelbecke, E.; Guo, N.; Kadish, K. M. *Angew. Chem., Int. Ed.* **1999**, *38*, 964.

(7) Guilard, R.; Perie, K.; Barbe, J.-M.; Nurco, D. J.; Smith, K. M.; Van Caemelbecke, E.; Kadish, K. M. *Inorg. Chem.* **1998**, *37*, 973.

(8) Van Caemelbecke, E.; Derbin, A.; Hambright, P.; Garcia, R.; Doukkali, A.; Saoiabi, A.; Ohkubo, K.; Fukuzumi, S.; Kadish, K. M. *Inorg. Chem.* **2005**, *44*, 3789.

(9) Van Caemelbecke, E.; Kutner, W.; Kadish, K. M. *Inorg. Chem.* **1993**, *32*, 438.

(10) McCord, J. M.; Fridovich, I. *J. Biol. Chem.* **1969**, *244*, 6049.

(11) Faulkner, K. M.; Liochev, S. I.; Fridovich, I. *J. Biol. Chem.* **1994**, *269*, 23471.

(12) Spasojevic, I.; Batinic-Haberle, I.; Reboucas, J. S.; Idemori, Y. M.; Fridovich, I. *J. Biol. Chem.* **2003**, *278*, 6831.

(13) Reboucas, J. S.; DeFreitas-Silva, G.; Spasojevic, I.; Idemori, Y. M.; Benov, L.; Batinic-Haberle, I. *Free Radical Biol. Med.* **2008**, *45*, 201.

(14) Rabbani, Z. N.; Spasojevic, I.; Zhang, X.; Moeller, B. J.; Haberle, S.; Vasquez-Vivar, J.; Dewhirst, M. W.; Vujaskovic, Z.; Batinic-Haberle, I. *Free Radical Biol. Med.* **2009**, *47*, 992.

(15) Zhao, Y.; Chaiswing, L.; Oberley, T. D.; Batinic-Haberle, I.; St. Clair, W.; Epstein, C. J.; St. Clair, D. *Cancer Res.* **2005**, *65*, 1401.

(16) Piganelli, J. D.; Flores, S. C.; Cruz, C.; Koepp, J.; Batinic-Haberle, I.; Crapo, J.; Day, B.; Kachadourian, R.; Young, R.; Bradley, B.; Haskins, K. *Diabetes* **2002**, *51*, 347.

(17) Adinehnia, M.; Mazur, U.; Hipps, K. W. *Cryst. Growth Des.* **2014**, *14*, 6599.

(18) Eskelsen, J. R.; Qi, Y.; Schneider-Pollack, S.; Schmitt, S.; Hipps, K. W.; Mazur, U. *Nanoscale* **2014**, *6*, 316.

(19) Eskelsen, J. R.; Phillips, K. J.; Hipps, K. W.; Mazur, U. *Chem. Commun. (Cambridge, U. K.)* **2015**, *51*, 2663.

(20) Ruhlmann, L.; Nakamura, A.; Vos, J. G.; Fuhrhop, J.-H. *Inorg. Chem.* **1998**, *37*, 6052.

(21) Ruhlmann, L.; Zimmermann, J.; Fudickar, W.; Siggel, U.; Fuhrhop, J. H. *J. Electroanal. Chem.* **2001**, *503*, 1.

(22) Olaya, A. J.; Schaming, D.; Brevet, P.-F.; Nagatani, H.; Zimmermann, T.; Vanicek, J.; Xu, H.-J.; Gros, C. P.; Barbe, J.-M.; Girault, H. H. *J. Am. Chem. Soc.* **2012**, *134*, 498.

(23) Laguerre, A.; Chang, Y.; Pirrotta, M.; Desbois, N.; Gros, C. P.; Lesniewska, E.; Monchaud, D. *Org. Biomol. Chem.* **2015**, *13*, 7034.

(24) Ramirez-Gutierrez, O.; Claret, J.; Ribo, J. M. *J. Porphyrins Phthalocyanines* **2005**, *9*, 368.

(25) Bard, A. J. In *Electrochemical Methods Fundamentals and Applications*; John Wiley & Sons, Inc.: New York, 2001, p 44.

(26) Kadish, K. M.; Araullo, C.; Maiya, G. B.; Sazou, D.; Barbe, J. M.; Guilard, R. *Inorg. Chem.* **1989**, *28*, 2528.

(27) Fuhrhop, J.-H.; Kadish, K. M.; Davis, D. G. *J Am Chem Soc* **1973**, *95*, 5140.

(28) Cui, Y. Electrochemistry, Acid-Base Properties and Spectroelectrochemistry of Porphyrins, Corroles and Related Molecules (Unpublished doctoral dissertation). University of Houston. 2015, p 115-155.

(29) Kadish, K. M.; Sazou, D.; Araullo, C.; Liu, Y. M.; Saoiabi, A.; Ferhat, M.; Guilard, R. *Inorg. Chem.* **1988**, *27*, 2313.